



저작자표시-비영리-변경금지 2.0 대한민국

이용자는 아래의 조건을 따르는 경우에 한하여 자유롭게

- 이 저작물을 복제, 배포, 전송, 전시, 공연 및 방송할 수 있습니다.

다음과 같은 조건을 따라야 합니다:



저작자표시. 귀하는 원저작자를 표시하여야 합니다.



비영리. 귀하는 이 저작물을 영리 목적으로 이용할 수 없습니다.



변경금지. 귀하는 이 저작물을 개작, 변형 또는 가공할 수 없습니다.

- 귀하는, 이 저작물의 재이용이나 배포의 경우, 이 저작물에 적용된 이용허락조건을 명확하게 나타내어야 합니다.
- 저작권자로부터 별도의 허가를 받으면 이러한 조건들은 적용되지 않습니다.

저작권법에 따른 이용자의 권리는 위의 내용에 의하여 영향을 받지 않습니다.

이것은 [이용허락규약\(Legal Code\)](#)을 이해하기 쉽게 요약한 것입니다.

[Disclaimer](#)

공학박사학위논문

이종 기계 요소를 고려한
기구 위상 최적설계 방법론 개발

Topology Optimization for Mechanism Synthesis Considering
Dissimilar Mechanical Components

2023년 8월

서울대학교 대학원
기계항공공학부
임 능 환

이중 기계 요소를 고려한 기구 위상 최적설계 방법론 개발

Topology Optimization for Mechanism Synthesis Considering
Dissimilar Mechanical Components

지도교수 김 윤 영

이 논문을 공학박사 학위논문으로 제출함
2023년 4월

서울대학교 대학원
기계항공공학부
임 능 환

임능환의 공학박사 학위논문을 인준함
2023년 6월

위 원 장 : 박 종 우

부위원장 : 김 윤 영

위 원 : 김 도 년

위 원 : 장 강 원

위 원 : 김 영 수

ABSTRACT

Topology Optimization for Mechanism Synthesis Considering Dissimilar Mechanical Components

Neung Hwan Yim

School of Mechanical and Aerospace Engineering

The Graduate School

Seoul National University

The mechanism topology optimization design approach offers several advantages, including the ability to synthesize mechanisms of various topologies and dimensions without the need for preliminary design outlines. This approach has been successful in designing innovative general mechanical devices. The majority of general mechanical devices consist of rigid links and joints, whereas robotic mechanisms incorporate dissimilar mechanical components, including elastic components, gear components, and pulley components, to improve performance. Unfortunately, previous mechanism topology optimization approaches have only been capable of synthesizing rigid links and joints, thereby

limiting their applicability to robotic mechanisms. To overcome this limitation, this dissertation proposes an integrated design strategy for rigid-elastic mechanical components, with a focus on a lightweight and cost-effective 1-DOF planar mechanism with a single driving actuator.

This dissertation considers two types of 1-DOF planar mechanisms: 1-DOF fully actuated and 1-DOF underactuated mechanism. The fully actuated mechanism can be synthesized using various dissimilar rigid mechanical components and is ideal for performing precise operations. On the other hand, the underactuated mechanism can be designed by incorporating both elastic and rigid mechanical components, and its underactuated DOF from the elastic components can be utilized to overcome obstacles or adapt to changes in the surrounding environment.

To incorporate dissimilar mechanical components into the mechanism topology optimization approach, the proposed technique utilizes a novel shape spring connected rigid block model (shape-SBM). This model represents the topology and dimensions of diverse mechanisms using fewer design variables and a low discretization resolution. To represent multiple mechanical components, an integrated modeling method is necessary, and the proposed stacking method of the multi-component design space over the shape-SBM serves this purpose. Furthermore, the dissertation suggests new definitions of gear and pulley blocks, which correspond to gear and pulley components, respectively. Additionally, spring components connecting the mass centers of rigid blocks are also taken into consideration for spring components, which provide an elastic force corresponding

to changes in elongations.

To define each component-related design space, we discretize the design domain with gear blocks, pulley blocks, and spring components respectively. These component design spaces are then stacked over the linkage design space, which is the shape SBM with a rigid block. For the component design space, the corresponding rigid block is placed over the gear and pulley blocks with artificial zero-length springs connecting the gear block and pulley block to a rigid block at the four corners, known as gearing springs and pulley springs, respectively. In the case of spring components, we use spring configurations that utilize the stiffness value to represent the spring itself. This modeling method is referred to as multi-stacked SBM. Through this approach, the shape of the blocks and the stiffness values of the various springs can describe the various mechanism topologies and dimensions.

To achieve efficient mechanism topology synthesis, we define an optimization formula based on the integrated mechanical components modeling approach (multi-stacked SBM). Given that the mechanism comprises nonlinearity and many design variables, gradient-based optimization methods are more effective for mechanism topology optimization than global optimization. Accordingly, we formulate new definitions of the objective function and constraint equations to determine the shape of the blocks and the stiffness value of the various springs, thus enabling efficient optimization.

Our proposed method utilizes a multi-stacked SBM and optimization

formulation. In order to validate its effectiveness, we will apply this approach to the synthesis of gear-linkage mechanisms, pulley-linkage mechanisms, and spring-linkage mechanisms, each with varying topologies and dimensions. Although each synthesis problem will be considered with its corresponding stacked-SBM separately in this dissertation, we anticipate that this technology will enable the integration and expansion of rigid-elastic mechanism synthesis and the synthesis method for integrated dissimilar mechanism components. Furthermore, we expect that this technology will encompass not only gear, pulley, and spring components but also other dissimilar mechanism components.

Keywords: Mechanism synthesis, Topology optimization, Dissimilar mechanical component, 1-DOF fully actuated mechanism, 1-DOF underactuated mechanism, Spring-linkage mechanism.

Student Number: 2017-26804

CONTENTS

ABSTRACT	i
CONTENTS.....	v
LIST OF FIGURES.....	ix
CHAPTER 1. INTRODUCTION	1
1.1 Motivation	1
1.2 Previous works	3
1.3 Research objectives	5
1.4 Outline of dissertation	8
CHAPTER 2. Spring connected rigid block model for shape and topology optimization.....	14
2.1 Overview	14
2.2 SBM for unified mechanism modeling	17
2.2.1 Modeling	17
2.2.2 Analysis	19
CHAPTER 3. Topology Optimization of Planar Gear-Linkage Mechanisms .	26
3.1 Overview	26
3.2 Modeling and Analysis.....	32
3.2.1 Modeling	32
3.2.2 Analysis	39
3.3 Gear-linkage mechanism synthesis formulation	49

3.4 Synthesis of various mechanisms by the proposed method	54
3.4.1 Case Study 1 : Gear-linkage mechanisms with a gear of different gear ratios	56
3.4.2 Case Study 2 : Gear-linkage mechanisms with a gear at different locations	60
3.4.3 Case study 3 : Gear-linkage mechanisms having a different number of gears	61
3.5 Synthesis of various mechanisms with shape optimization.	64
3.6 Summary.....	66
CHAPTER 4. Topology Optimization of Planar Pulley-Linkage Mechanisms	86
4.1 Overview	86
4.2 Modeling, analysis and optimization formulation.....	89
4.2.1 Modeling method of multi-stacked SBM.....	89
4.2.2 Analysis method to multi-stacked SBM.....	92
4.2.3 Optimization formulation for stacked SBM.....	94
4.3 Synthesis of various mechanisms by the proposed method	96
4.4 Summary.....	99
CHAPTER 5. Topology Optimization of Planar Spring-Linkage Mechanisms	109
.....	
5.1 Overview	109
5.2 Modeling and Analysis.....	117
5.2.1 Spring-linkage stacked spring connected block model	117

5.2.2 Kinematic analysis of stacked spring-linkage SBM.....	121
5.3 Optimization formulation for synthesizing spring-linkage mechanism ..	125
5.4 Synthesis of various mechanisms by the proposed method	130
5.4.1 Case Study 1: synthesis of various shapes of obstacles	131
5.4.1 Case study 2: Synthesis of the 1-DOF adaptive gripper mechanism	136
5.5 Summary	140
CHAPTER 6. Conclusions.....	157
APPENDIX A. Using mechanism big data to reduce the design variables in mechanism topology optimization.....	161
A.1 Overview	161
A.2 Generation of big data using the SBM for neural network training	166
A.2.1 SBM for unified mechanism modeling	168
A.2.2 Screening for selecting fully rotatable 1-DOF mechanisms.....	169
A.2.3 Representation of the mechanism dataset for the neural network	171
A.3 Mechanism synthesis process.....	176
A.3.1 Topology synthesis step.....	176
A.3.2 Dimensional synthesis step	178
A.4 Mechanism synthesis process.....	181
A.4.1 Test problems.....	182
A.4.2 General mechanism synthesis.....	185

A.4.3 Examination of the performance of the neural network-based approach	186
A.5 Conclusion.....	192
REFERENCES.....	208
ABSTRACT (KOREAN).....	221
ACKNOWLEDGEMENTS.....	226

LIST OF FIGURES

Fig. 1.1 Illustration of dissimilar mechanical components and previous related studies to be covered in this dissertation.	10
Fig. 1.2 (a) a 1-DOF fully actuated linkage mechanism. (b) The 1-DOF underactuated spring-linkage mechanism can overcome obstacles due to deformable spring components.	11
Fig. 1.3 Illustration of key concept of stacking method for dissimilar mechanical components.	12
Fig. 1.4 Illustration of two main class in this dissertation and its corresponding chapter. Firtly, we consider the rigid mechanical components in chapter 3 and 4. Secondly we will consider the rigid and elastic mechanical components in chapter 5.....	13
Fig. 2.1 Representation of general linkage mechanisms using the SBM. (a) The interpretations of two adjacent blocks connected by springs and the effects of the shape-controlling variable ξ_i^x are illustrated. (b) An illustrative example to represent a 4-bar mechanism using the SBM. Blocks of the same color function as a single mega-block (rigidly connected larger component).	24
Fig. 2.2 Configurations of the deformation of the springs. Each configuration consists of (a) $B^{(l)}$, $B^{(m)}$, and the block-connecting spring (k_c), and (b) $B^{(l)}$, the ground, and the anchoring spring (k_{A_j}).	25

Fig. 3.1 (a) A typical geared mechanism we aim to synthesize by the proposed topology optimization method and (b) the proposed block ground model consisting of two design spaces, the linkage design space S_L , and the gear design space ${}^{<r>}S_G$. (The superscript “ r ” in ${}^{<r>}S_G$ denotes the gear ratio.)	68
Fig. 3.2 Representation of various joints in the S_L -based SBM. The stiffness of the block-connecting and anchoring springs take on the bound value (k_{\min} and k_{\max}) to simulate various joint states.	69
Fig. 3.3 Representation of gear and link components in several simple mechanisms using the new notations, ${}^{<>}B^{(l)}$ and ${}^{<r>}B^{(l)}$	70
Fig. 3.4 (a) A geared five-bar mechanism (GFBM). (b) The representation of the GFBM by the developed modeling approach. (c) The representation of the GFBM in terms of M-blocks, a floating block, and a gear block.	71
Fig. 3.5 Various configurations inducing the deformation of springs. Each configuration consisting of : (a) $B^{(l)}$, $B^{(m)}$ (an adjacent block of $B^{(l)}$) and the block-connecting spring k_{C_i} ; (b) $B^{(l)}$, the ground, and the anchoring spring k_{A_j} ; and (c) $B^{(l)}$, ${}^{<r>}G^{(l)}$, and a set of gearing springs denoted by ${}^{<r>}k_{G_w}$	72
Fig. 3.6 The synthesis of a geared five-bar mechanism having an output gear with a gear ratio of 1 by the proposed formulation: (a) The target mechanism, (b) its representation in terms of rigid and gear blocks, (c) the ground model consisting of $S_L \oplus {}^{<l>}S_G \oplus {}^{<0.5>}S_G$ employed for the synthesis, d) the convergence history of	

and $\bar{\eta}$, and $\bar{\psi}_{\max} = \max_{i \in \{1,2,\dots,T\}} \psi_i^*$ (e) the values of the design variables (ξ_i) at

convergence.....73

Fig. 3.7 The synthesis of a geared five-bar mechanism having an output gear with a gear ratio of 0.5 by the proposed formulation: (a) The target mechanism, (b) its representation in terms of rigid and gear blocks, (c) the ground model consisting of $S_L \oplus \langle 1 \rangle S_G \oplus \langle 0.5 \rangle S_G$ employed for the synthesis, d) the convergence history of and $\bar{\eta}$, and $\bar{\psi}_{\max} = \max_{i \in \{1,2,\dots,T\}} \psi_i^*$ (e) the values of the design variables (ξ_i) at

convergence.....74

Fig. 3.8 The evolution history of the synthesized mechanism expressed by the proposed block ground model for the synthesis problem defined in Fig. 6. The numbers in the figure represent the block number.75

Fig. 3.9 The evolution history of the synthesized mechanism expressed by the proposed block ground model for the synthesis problem defined in Fig. 7. The numbers in the figure represent the block number.76

Fig. 3.10 The synthesis of a geared five-bar mechanism having an output gear with the gear ratio of 1 located at the block 2 location. (a) The target mechanism and (b) its representation in terms of rigid and gear blocks.....77

Fig. 3.11 The evolution history of the synthesized mechanism expressed by the proposed block ground model for the synthesis problem defined in Fig. 3.10.78

Fig. 3.12 The synthesis of (a) a linkage-only mechanism and (b) a geared mechanism with two gear trains (i.e. two output gears). The ground model

consisting of $S_L \oplus \langle 1 \rangle S_G \oplus \langle 0.5 \rangle S_G$ is used in applying the proposed topology optimization based synthesis method.....	79
Fig. 3.13 The convergence histories of $\bar{\eta}$ and $\bar{\psi}_{\max} = \max_{t^* \in \{1,2,\dots,T\}} \psi_{t^*}$ and the values of the design variables (ξ_i) at convergence for (a) the problem depicted in Fig. 12(a) and (b) the problem in Fig. 12(b). The design variables having intermediate values are associated with the anchoring springs connected to floating blocks. Therefore, they do not affect the synthesized mechanism configurations.	80
Fig. 3.14 The evolution history of the synthesized mechanism expressed by the proposed block ground model for the synthesis problem defined in Fig. 12(a).....	81
Fig. 3.15 The evolution history of the synthesized mechanism expressed by the proposed block model for the synthesis problem defined in Fig. 12(b).....	82
Fig. 3.16 The shape SBM modeling method with geometric center to represent the block shape and gear components.....	83
Fig. 3.17 The proposed shape Gear SBM with the shape design variables. With shape design variables we can represent the shape of gear-linkage mechanism.....	84
Fig. 3.18 The three synthesis case studies: (a) linkage only mechanism (b) GFBM and (c) two gear linkage mechanism was synthesized.....	85
Fig. 4.1 The main concept of proposed pulley multi-stacked SBM. (a) the previous gear stacked-SBM only stacked one layer. However, the proposed pulley multi-stacked SBM stacked multi design space for rotational relationship with each rigid blocks.	101

Fig. 4.2 The representation of pulley blocks and pulley design space.....	102
Fig. 4.3 The representation of pulley-linkage mechanism with proposed modeling method. (a) the corresponding modeling method can represent the pulley linkage mechanism. (b) the details of linkage design space and (c) pulley design space. .	103
Fig. 4.4 (a) the definition of synthesis problems with 3X3 discretized design space. (b) the results after the optimization process and (c) its corresponding results of pulley-linkage mechanism.....	104
Fig. 4.5 The iteration history (a) and the evolutionary history of the synthesis problem.	105
Fig. 4.6 The synthesis results of different types of mechanism (a) pulley-linkage mechanism, (b) linkage only mechanism, and (c) gear-linkage mechanism (anchored pulley-linkage mechanism).	106
Fig. 4.7 The synthesis results of multi pulley components mechanism.	107
Fig. 4.8 The synthesis results with simultaneously consider the shape of pulley components with its evolutionary history.....	108
Fig. 5.1 Depending on the situation, different mechanisms are needed for a single-driving actuator. (a) If the desired motion is the only consideration, a 1-DOF fully actuated linkage mechanism is required. (b) However, if adaptive motion is necessary, such as overcoming obstacles, a 1-DOF underactuated spring-linkage mechanism is needed.....	142
Fig. 5.2 The proposed method for synthesizing the spring-linkage mechanism involves (a) outlining the topology and dimensions within a stacked block ground	

model. This model includes two design spaces: (b) a link design space (S_L) and (c)	
a spring design space (S_s).	143
Fig. 5.3 In the proposed stacking method, state variables are shared between the linkage and spring design spaces.	144
Fig. 5.4 The stored elastic energy of actual spring components in stacked SBM.	145
Fig. 5.5 (a) Target motion of case study 1 and (b) three different obstacle shape conditions.	146
Fig. 5.6 The results of the first condition of case study 1 include: (a) the synthesized results and their corresponding topology and spring design variables (note that the red ticks in the bar graph represent the dummy block and dummy springs), (b) the convergence history of the constraint equations and objective function, and (c) a comparison between the desired motion and the synthesized motion.	147
Fig. 5.7 The evolutionary history of the synthesized mechanism, as expressed by the proposed block ground model, pertains to the synthesis problem defined in Fig. 6.	148
Fig. 5.8 The synthesized results for the second and third obstacle conditions in Case Study 1 are presented as (a) and (b), respectively. (Note that the red ticks in the bar graph indicate the presence of dummy springs.)	149
Fig. 5.9 (a) The 5-bar underactuated spring-linkage mechanism synthesized for the big obstacle conditions is capable of moving into a perturbed motion. (b) As the corresponding perturbed region is situated over the shape of the big obstacle, the	

synthesized mechanism is able to successfully overcome it.	150
Fig. 5.10 Regarding the synthesized spring-linkage mechanism from the small obstacle condition, (a) the perturbed region is situated over the small obstacle, allowing it to successfully overcome such obstacles. (b) However, it is not capable of overcoming the big obstacle from the second obstacle condition.....	151
Fig. 5.11 The synthesized mechanism and its perturbed domain obtained from different initial design variables. In (a), the initial design variables close to the synthesized results shown in Fig. 5.8(a), while in (b), randomly generated initial design variables are used.....	152
Fig. 5.12 The problem definitions of synthesizing 1-DOF adaptive gripper.	153
Fig. 5.13 The overall results of synthesizing the adaptive gripper include: (a) the successful synthesis of a 1-DOF underactuated 10-bar spring-linkage mechanism, as well as (b) its corresponding design variables (note that the red ticks in the bar graph represent the presence of dummy springs). The success of the overall synthesis can be confirmed by (c) the iteration history of objective functions and constraint equations, as well as (d) its evolutionary history. Furthermore, (e) the synthesized 1-DOF adaptive gripper is capable of generating the desired motions effectively.	154
Fig. 5.14 The overall results of synthesizing the adaptive gripper using the optimization formulations presented in Eq. 17 include: (a) the successful synthesis of a 1-DOF underactuated 7-bar spring-linkage mechanism, along with (b) its corresponding design variables. The success of the overall synthesis can be	

confirmed by (c) the iteration history and (d) the generated motions.	155
Fig. 5.15 (a) the simulation grasping situation for the synthesized adaptive gripper. (b) the simulation results between different sizes.	156
Fig. A.1 (a) The overall process of the proposed method for mechanism synthesis, (b) data generation using the SBM and a method to confirm full rotatability using the work transmittance efficiency ($\bar{\eta}$), and (c) a constructed neural network.	194
Fig. A.2 Examples of the generated mechanisms using randomly generated variables ξ^K , ξ^X and \mathbf{r}_Q based on the SBM. The end-effector locator (\mathbf{P}_E) in the figure is used to indicate the location of the block to which the end-effector is attached.	195
Fig. A.3 Description of a given target path using the Fourier coefficients of the central distance function $f(\tilde{s}_t)$. (a) Analysis needed to calculate the central distance function $f(\tilde{s}_t)$, (b) sketch of the centroid distance function of a typical path using the dimensionless arc length \tilde{s}_t , and (c) Fourier descriptors of the centroid distance function.	196
Fig. A.4 Visualization of the mechanism dataset by dimension reduction by means of a Principal Component Analysis (PCA) using the path data (FFT descriptors) and topology of the mechanism. The spaces of (a) three major component axes and (b) two major component axes are used to visualize. Dots of the same color have an identical $[\xi^K, \mathbf{P}^E]$ in both figures	197
Fig. A.5 Test problems using known mechanisms to generate the target paths: (a)	

Case Study 1 using a 4-bar mechanism and (b) Case Study 2 utilizing a 6-bar mechanism.....	198
Fig. A.6 Detailed procedures of the proposed synthesis method for Case Study 1. (a) Procedure to compute the Fourier descriptor vector \mathbf{C} (with $p=15$) of the target path, (b) topology synthesis step to determine ξ^K and \mathbf{P}^E , (c) dimensional synthesis step to determine ξ^X , and (d) the synthesized mechanism with the generated path.	199
Fig. A.7 Evolution history of the dimensional synthesis step for Case Study 1. ...	200
Fig. A.8 Paths considered for general mechanism synthesis: (a) Target path 1 (the path describing the trajectory of a finger in the reference frame of a swimmer over his/her full stroke cycle), (b) target path 2 (the path describing the anteroposterior and dorsoventral motion relative to a turtle's body throughout the limb cycle), and (c) target path 3	201
Fig. A.9 (a) Procedure to synthesize a mechanism generating Target path 1, (b) the synthesized mechanism (its end-effector location is indicated by the red square) and (c) comparison of the target path and the path generated by the synthesized mechanism.....	202
Fig. A.10 (a) Procedure to synthesize a mechanism generating Target path 2, (b) the synthesized mechanism (its end-effector location is indicated by the red square), and (c) comparison of the target path and the path generated by the synthesized mechanism.....	203

Fig. A.11 (a) Procedure to synthesize a mechanism generating Target path 3, (b) the synthesized mechanism (its end-effector location is indicated by the red square), and (c) comparison of the target path and the path generated by the synthesized mechanism.....204

Fig. A.12 An illustrative example to show that (nearly) the same path can be obtained with different values of (ξ^K, \mathbf{P}^E) . The path generated by a reference mechanism is (nearly) recovered by a synthesized mechanism (having a different (ξ^K, \mathbf{P}^E) from that of the reference mechanism) with the developed approach...205

Fig. A.13 Mechanism data plotted on the three major principal axes used in Fig. 6. Blue filled dots: mechanisms having $({}^R\xi^K, {}^R\mathbf{P}^E)$ with various values of ξ^X . Orange open dots: mechanisms having $({}^S\xi^K, {}^S\mathbf{P}^E)$ with various values of ξ^X .206

Fig. A.14 (a) The target mechanism and the generated path at its end-effector (this problem is taken from Ref.) and (b) comparison of the proposed big data approach and the gradient-based method given in Ref. in terms of computational cost.....207

CHAPTER 1.

INTRODUCTION

1.1 Motivation

As technology evolves rapidly, new hardware systems need to be developed, often requiring complex synthesis conditions. For example, electric cars' suspension and steering systems must be designed to minimize space and make room for battery storage, and highly adaptive robots must be able to adjust to environmental changes. To meet these new design challenges, novel mechanism configurations and various mechanical components are necessary. However, traditional mechanism design approaches heavily rely on the designer's experience and intuitional knowledge. These approaches typically start with the conceptual design stage, where the mechanism's topology is determined based on the designer's prior knowledge, followed by the detailed design stage, which determines the specific mechanism dimensions. Unfortunately, this approach can result in trial-and-error design processes and limit creative results, making it unsuitable for designing novel hardware systems that require complex design

conditions.

Keeping up with above rapidly evolving technology and complex design conditions requires a new approach to mechanism design. Mechanism topology optimization is a promising method that simultaneously determines a mechanism's topology and dimensions, without relying on reference baseline information, by using mathematically defined mechanism design problems. Recently, this method has gained significant attentions due to its successful applications in various fields, including electric vehicle suspension, transformable wheels, and exoskeletons. However, current mechanism topology optimization design methods are limited to linkage mechanisms and cannot consider dissimilar mechanical components.

To overcome this limitation, we propose a novel mechanism topology optimization approach that considers dissimilar mechanical components, including gear components, pulley components, and spring components, in addition to the linkage mechanism. However, previous researches have relied on trial-and-error-based design methods to incorporate various dissimilar mechanical components. As a result, in this dissertation, we will discuss a mechanism topology optimization method that considers dissimilar mechanical components, which has the potential to produce more diverse and efficient mechanism designs.

1.2 Previous works

The optimization of mechanism topology began with Felter's dissertation [1], which introduced a modeling method and energy formulation. Kawamoto and his colleague [2] then built on this work, advancing the field through the development of a nonlinear bar modeling and a formulation for controlling the degree of freedom of the mechanism. These developments resulted in the successful resolution of converter problems and path generation problems using global optimization algorithms [3, 4]. However, despite these successes, limitations existed for the application of mechanism topology optimization to real-world problems. This was because the nonlinear bar model was restricted to linkage-only mechanisms with revolute joints, and optimization formulations based on global optimization methods were not suitable for highly nonlinear mechanisms due to the high time costs and local optimization issues.

In order to overcome these limitations, researchers have investigated alternative modeling techniques to describe diverse mechanisms and control the degree of freedom (DOF) [5, 6]. For example, Kim et al. [7] introduced a spring-connected rigid block model (SBM) to model linkage mechanisms, indirectly representing them through the stiffness of artificial zero-length springs. This approach allowed for the incorporation of various joint types, expanding the scope of the model. Building on this, Kang et al. [8, 9] further developed the SBM by connecting blocks with double artificial zero-length springs, successfully addressing a wider range of joint types in mechanism topology optimization.

The control of DOF in mechanism synthesis is a significant challenge, and researchers have employed various techniques to address it, such as adjacent matrix, graph theory, and numbering methods. However, as DOF cannot be represented by continuous design variables, global optimization was usually used. To tackle this challenge, physical quality-based approaches have been proposed by Nam et al. [10], Osaki and Nishiwaki [4], and Sedlachek and Eberhardt [3]. Additionally, Kim and Kim [11] also developed a physics-based work transmittance efficiency function for DOF control, enabling the use of gradient-based optimization algorithms. Consequently, mechanism topology optimization has been successful in addressing various mechanism synthesis issues, including mobile robots and exoskeletons, using the work transmittance efficiency function and SBM modeling. Nevertheless, these approaches are restricted to linkage mechanisms with rigid links and joints. To overcome this limitation, the proposed stacked-SBM can express dissimilar components, and a new physics-based optimization formula will be presented in the following dissertation.

1.3 Research objectives

This dissertation proposes an integrated design strategy for dissimilar rigid-elastic mechanical components using topology optimization. The focus is on developing a novel approach to topology optimization for 1-DOF planar mechanisms that incorporate dissimilar mechanical components, such as gear, pulley, and spring components with linkage mechanisms. The main proposed approach involves stacking dissimilar mechanical component design spaces over the existing spring-connected rigid block model of the linkage mechanism. However, to reduce the complexity of optimization caused by the increasing number of design variables, the proposed approach considers only rigid links and revolute joints in this dissertation.

To optimize mechanisms with low discretization resolutions, we can simultaneously optimize the block shape and the stiffness of artificial springs in SBM. However, when synthesizing dissimilar mechanical components, it becomes challenging to consider dimensions of both the dissimilar components and the linkage mechanism together. This is because the addition of more design variables makes the optimization process more time-consuming and difficult. To address this issue, we propose a new shape SBM modeling approach in our mechanism topology optimization design method. This approach utilizes the geometric center, in addition to the block's shape, to determine the topology and dimensions of different mechanical components. This novel modeling method eliminates the need for extra design variables. And this technique will be presented in Chapter 2.

Moreover, we can modify the SBM into JBM and DSBM to reflect the linkage mechanism. This modification will allow us to theoretically consider prismatic joints or other joint types. However, as part of our all proposed design process in this dissertation, we will apply the newly proposed shape SBM to represent the mechanism topology and dimensions.

This dissertation proposes a synthesis approach that can be divided into two parts. The first part involves integrating dissimilar rigid mechanical components, such as pulley and gear components, to the linkage mechanism using a stacking design technique. With these components, we can design a 1-DOF fully actuated mechanism that can repeatedly and precisely generate the desired motion at the end-effector, as shown in Fig. 1.2(a). Furthermore, we can synthesize the 1-DOF fully actuated mechanism more effectively and compactly with dissimilar components. To achieve this, we propose a mechanism topology optimization approach for synthesizing the 1-DOF fully actuated mechanism with gear and pulley components. Therefore, we propose a new gear block and pulley block in Chapters 3 and 4, respectively to consider these components with a linkage mechanism using SBM. The stacking method is a crucial technique for integrating dissimilar rigid mechanical components simultaneously in topology optimization. We stack the design space for mechanical components with the corresponding rigid block over the linkage design space (SBM). Additionally, the configuration of mechanical components should be represented by the stiffness of newly proposed connected artificial springs. After proposing the multi-stacked SBM modeling

methods, we present a new optimization formulation with a physics-based function to carry out gradient-based optimization. This is a critical step in achieving optimal synthesis results, and we will discuss it further in this dissertation.

The second part of our design technique involves the consideration of rigid-elastic mechanisms, which allow for the incorporation of 1-DOF underactuated mechanisms using spring components and a linkage mechanism, as shown in Fig. 1.2(b). These mechanisms can adapt to environmental changes by using spring components to provide underactuated DOF, which is particularly useful for adaptive mechanisms like grippers and gait robots. To address this, we propose a topology optimization approach for synthesizing the 1-DOF underactuated spring-linkage mechanism while taking environmental variables into account. We stack the spring components over the linkage SBM and consider the necessary design requirements for environmental changes. Consequently, we offer analytical techniques and optimization formulations with new physical quality in this second stage, which will be detailed in Chapter 5.

For mechanism synthesis through topology optimization with dissimilar components, the multi-stacked SBM method can be utilized, as shown in Fig. 1.3, which stacks the SBM to represent different components. This approach has the potential to be used for all types of components in theory, and the proposed optimization formulation can also be expanded accordingly. However, in this dissertation, we will focus only on a single dissimilar component with a linkage mechanism.

1.4 Outline of dissertation

The dissertation is organized as follows.

In Chapter 2, we will introduce the ground modeling methods for linkage mechanisms used throughout the dissertation, including the novel shape spring connected rigid block model (shape SBM). The design domain is discretized by rigid blocks connected by artificial zero length springs, and the combinations of stiffness of these artificial springs can represent the topology of a mechanism. Moreover, the geometric center of rigid blocks can be used to represent the dimensions of dissimilar mechanical components, which is the key improvement of this shape SBM over previous models. This novel approach allows for a reduction in the number of design variables, leading to a more efficient optimization process.

Chapter 3 will describe the topology optimization method for developing gear-linkage mechanisms. We propose a new gear block and its gear design space to represent the gear components, and we stack the SBM in the gear design space with four gearing springs at each node. This enables us to use the stiffness of gearing springs to represent the gear components. Additionally, this chapter provides a formulation and analysis approach for optimization.

In Chapter 4, we will introduce the topology optimization method for synthesizing pulley-linkage mechanisms, building upon the gear optimization

method proposed in Chapter 3. Specifically, we will propose the use of a pulley block and multi-stacked SBM approach to represent pulley-linkage mechanisms, with the potential for expansion to include gear blocks. This approach will offer a new method for optimizing topology and expanding the range of mechanisms that can be synthesized.

In Chapter 5, we will present the topology optimization method for developing spring-linkage mechanisms. These mechanisms can overcome environmental changes due to the presence of spring components, making them underactuated. We propose a stacked spring SBM along with a novel optimization formulation that considers the target motions and environmental changes simultaneously.

In chapter 6, the conclusion of paper is presented.

In Appendix A, we propose a method to streamline the optimization process by minimizing the number of design variables involved. Specifically, we explore how to simplify the gradient-based mechanism topology optimization process by utilizing mechanism big data to pre-determine the mechanism's topology design variables.

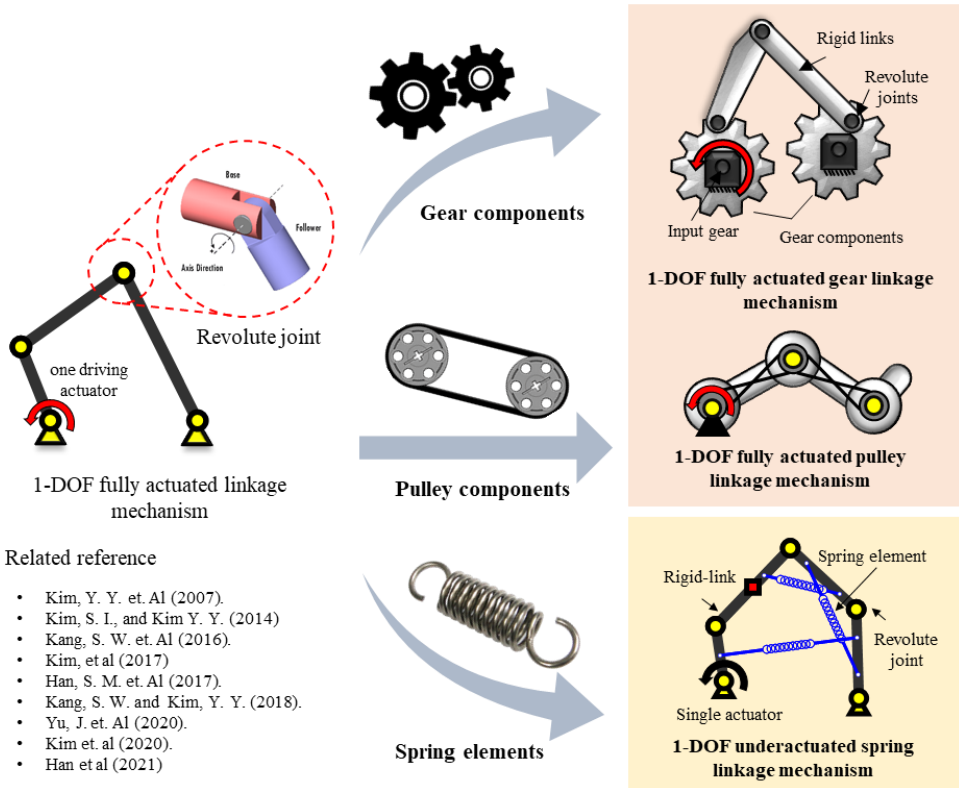


Fig. 1.1 Illustration of dissimilar mechanical components and previous related studies to be covered in this dissertation.

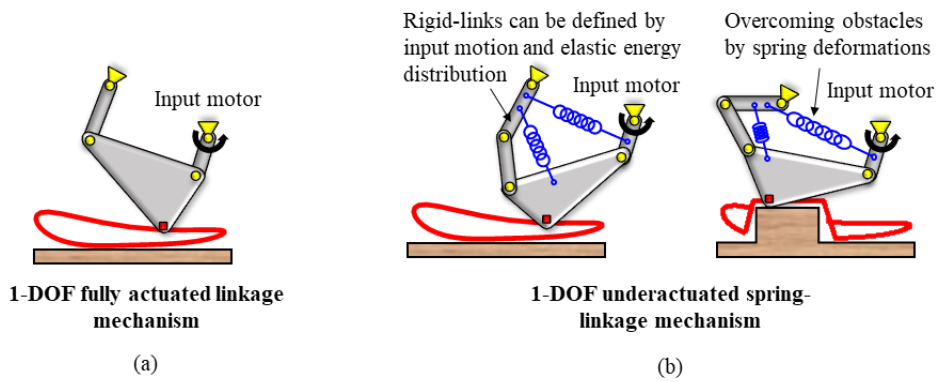


Fig. 1.2 (a) a 1-DOF fully actuated linkage mechanism. (b) The 1-DOF underactuated spring-linkage mechanism can overcome obstacles due to deformable spring components.

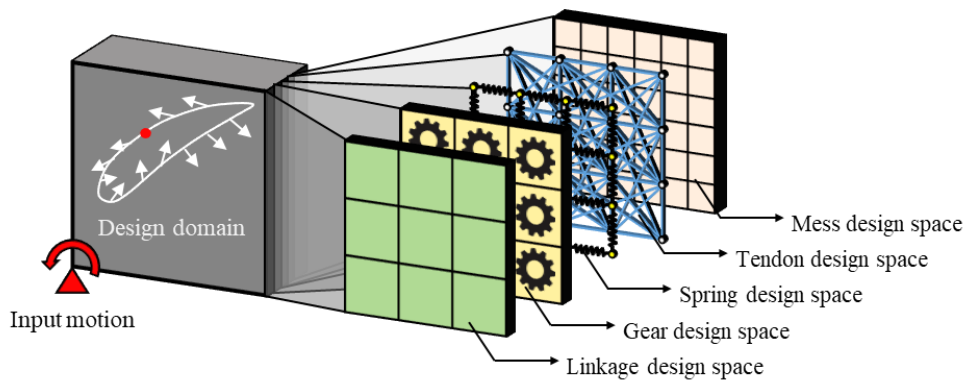
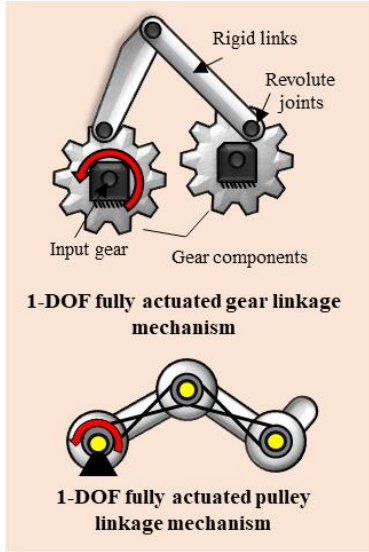
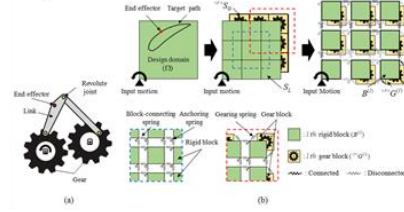


Fig. 1.3 Illustration of key concept of stacking method for dissimilar mechanical components.

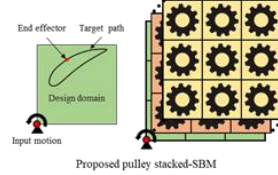
Class 1 : rigid mechanical components



Chapter 3

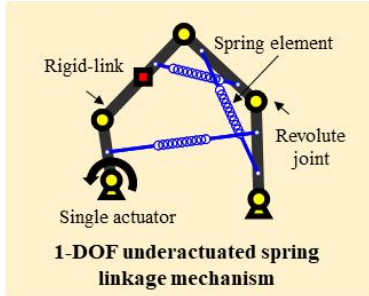


Chapter 4



$$\Omega = S_z \oplus \begin{matrix} <-1> \\ (1) \end{matrix} S_x \oplus \begin{matrix} <-1> \\ (2) \end{matrix} S_x \cdots \begin{matrix} <-1> \\ (13) \end{matrix} S_x$$

Class 2 : rigid and elastic mechanical components



Chapter 5

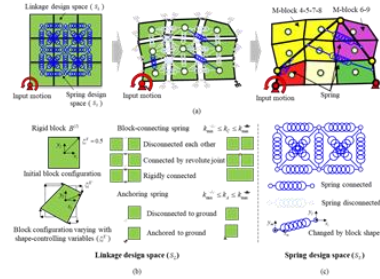


Fig. 1.4 Illustration of two main class in this dissertation and its corresponding chapter. Firtly, we consider the rigid mechanical components in chapter 3 and 4. Secondly we will consider the rigid and elastic mechanical components in chapter 5.

CHAPTER 2.

Spring connected rigid block model for shape and topology optimization

2.1 Overview

In order to proceed with the mechanism synthesis by topology optimization, a ground model that can represent various topology and the dimensions of the mechanism in one manner is required. This ground model discretizes the design area into various components, representing the topology and dimensions of various mechanisms through connectivity and shapes of components. The ground structure models used for mechanism topology optimization were mainly nonlinear-bar model [11] and spring connected rigid block model (SBM) [7-9, 12-14]. Because it can express the topology and dimensions of various mechanisms using the shape of blocks and stiffness of artificial zero length springs rather than the topology of the mechanism itself, SBM is known to be more expandable than the nonlinear bar model. For this reason, it was possible to simultaneously consider various joint types such as revolute joint, prismatic joint and pin in slot joint in mechanisms

topology optimization through SBM [8, 9]. In this dissertation, we hope to expand the range of mechanism topology optimization with various types of mechanical components, SBM will be used to represent the mechanism.

However, in the case of using such a ground structure, complicated mechanisms can be expressed through high resolution design domain. And these high resolutions increase the difficulty of mechanism synthesis. But in the case of SBM, as the shape of the block is also altered, a mechanism synthesis result from high resolution design domain is obtained even in low resolution design domain. In addition, when the mechanical component is included in the mechanism topology optimization, new dimension design variables should be added in order to synthesize the dimensions of each mechanical components. However, previous shape SBM only change the four nodes of each rigid block and it can only affect the dimension of linkage mechanism. Therefore, we suggest a new SBM modeling method which consider the geometric center of rigid block. When the four nodes of each rigid block are changed with the shape design variables, the geometric center of rigid block is also changed with the relationship between four nodes. And this geometric center can be used to synthesize other mechanical components. In this dissertation, we will use this geometric center of rigid block to represent the dimensions of gear components and initial lengths of spring components.

This chapter proceeds as follows. Because this proposed shape spring-connected rigid block model (shape SBM) is used to model mechanisms with various mechanical types, this Section 2.2 presents a brief description of the shape SBM

and its kinematic analysis.

2.2 SBM for unified mechanism modeling

2.2.1 Modeling

Fig. 2.1(a) shows the novel SBM [15] employed to represent the diverse mechanisms of different configurations (including topologies) in this dissertation. The design domain of linkage mechanism synthesis is discretized into N_b rigid blocks that are inter-connected by zero-length block-connecting springs of variable stiffnesses. Each of the rigid blocks is also connected to the ground by zero-length anchoring springs of variable stiffnesses. The SBM in the section is discretized into 3×3 rigid blocks. Clearly, the use of a more refined block discretization can represent more complicated mechanisms, though it also incurs a higher computational cost. A recent study [12], showed that if a low-resolution mesh yields a mechanism within an allowable error bound, the use of a high-resolution mesh can yield the same mechanism. It has also been demonstrated [12] that a large class of 4-bar, 6-bar and other multi-links mechanisms can be represented by an SBM using 3×3 rigid blocks. While this work considers revolute joints only, an extended SBM version [8, 9] capable of representing prismatic and general joints. Although the use of an SBM with more than 3×3 blocks allows the synthesis of more complicated mechanisms than those mentioned above, a 3×3 SBM will be used here to avoid excessive computational time for the generation of the mechanism configuration data.

To explain how the SBM represents a linkage mechanism, first we note that two adjacent blocks (a rigid block and the ground) can represent different linkage components depending on the stiffness values of the block-connecting springs (the anchoring springs). If the stiffness of a block-connecting spring is denoted by \mathbf{k}_c , it is set to vary between its lower bound $k_c = 0$ (numerically, $k_c = \varepsilon \approx 0$) and upper bound $k_c = k_{\max}$ (k_{\max} : a pre-selected value). The anchoring spring stiffness \mathbf{k}_A also varies between $k_A = 0$ and $k_A = k_{\max}$. Different connection states of a linkage mechanism can be realized when block-connecting or anchoring springs take on their lower or upper bound stiffness values, as illustrated on the right side of Fig. 2.1(a). Instead of using $0 < \xi_c \leq 1$ and $0 < \xi_A \leq 1$ directly as the independent variables, it is more convenient to use normalized design variables $0 < \xi_c \leq 1$ and $0 < \xi_A \leq 1$ such that $\mathbf{k}_c = k_{\max} \cdot (\xi_c)^3$ and $\mathbf{k}_A = k_{\max} \cdot (\xi_A)^3$, as in earlier studies [12, 13]. We will use the vector symbol ξ^K to represent a set of variables determining the stiffness values of all springs (block-connecting and anchoring). These are henceforth referred to here as the topology variables. indicated real-valued variables, however, ξ^K has to represent integer variables taking on either their lower (0) or upper (1) bound values, which corresponds to a disconnected or connected state between two adjacent rigid blocks when the optimization process is over. These spring values are used to identify the connectivity of rigid blocks and thus the mechanism topology these blocks represent. Another set of variables used to generate various mechanisms is denoted

by the vector symbol ξ^x , which determines the coordinates of the grid points used to discretize a given design domain into rigid blocks and thus to determine the dimensions of the rigid blocks.

2.2.2 Analysis

The generating path at the end effector \mathbf{r}_{Q,t^*} at time step t^* can be expressed in terms of the global Cartesian coordinates (X, Y) . This can be expressed as $\mathbf{r}_{Q,t^*} = [X_{t^*}^{(l)}, Y_{t^*}^{(l)}]$. On the hand, the state vector $\mathbf{q}_{t^*}^{(l)}$ of the l -th rigid block at time step t^* in the SBM is expressed using its center coordinates $[X_{t^*}^{(l)}, Y_{t^*}^{(l)}]$ and rotation angle $(\phi_{t^*}^{(l)})$ with respect to the global coordinate system:

$$\mathbf{q}_{t^*}^{(l)} = [X_{t^*}^{(l)}, Y_{t^*}^{(l)}, \phi_{t^*}^{(l)}]^T \quad (2.1)$$

Note that the connectivity between the end-effector block and the adjacent blocks by the block-connecting spring determine where the end-effector is located (which link is the coupler link). Moreover, the center coordinates will vary if the shape design variables ξ^x vary (the relative dimensions of the end-effector in the coupler link are determined). The input link, which is assumed to provide simple rotation, can be associated with any block. However, Block $B^{(1)}$ is chosen so as to make full use of the design domain. Regarding the selected values of ξ^K , ξ^x , and \mathbf{r}_Q , the movements of all blocks for a prescribed input rotation motion can be determined by a quasi-static force equilibrium state. If the states of all rigid blocks

except for input block 1 are denoted by the state variable vector \mathbf{v}_{t^*} at time step t^* , this can be expressed as

$$\mathbf{v}_{t^*} = [(\mathbf{q}_{t^*}^{(2)})^T, (\mathbf{q}_{t^*}^{(3)})^T, \dots, (\mathbf{q}_{t^*}^{(N_B)})^T]^T \quad (2.2)$$

In terms of \mathbf{v}_{t^*} , the quasi-static force equilibrium can be written as [11, 12]:

$$\mathbf{F}_{\text{int},t^*}(\mathbf{v}_{t^*}) - \mathbf{F}_{\text{ext},t^*} = 0 \text{ for } (t^* = 1, 2, 3, \dots, T; \text{ where } T \text{ is the total time step}) \quad (2.3)$$

where $\mathbf{F}_{\text{int},t^*}$ and $\mathbf{F}_{\text{ext},t^*}$ are the internal and external force, respectively. The external force ($\mathbf{F}_{\text{ext},t^*}$) is intentionally introduced to facilitate the subsequent analysis, which is defined as (see [11, 12])

$$\mathbf{F}_{\text{ext},t^*} = F_0 \frac{\mathbf{r}_{Q,t^*} - \mathbf{r}_{Q,t^*-1}}{\|\mathbf{r}_{Q,t^*} - \mathbf{r}_{Q,t^*-1}\|}, \quad (F_0 = 1) \quad (2.4)$$

where F_0 is the magnitude of the force applied at the end-effector. As Eq. (2.4) indicates, the external force acts in the opposite direction relative to the motion of the end-effector.

The internal force $\mathbf{F}_{\text{int},t^*}$ is caused by the elastic deformation of the block-connecting and anchoring springs and is calculated as $dU_{t^*}/d\mathbf{v}_{t^*}$, where U_{t^*} denotes the total elastic energy stored in the springs. The state variable vector for each time step (\mathbf{v}_{t^*}) can be obtained through the quasi-static equilibrium of Eq. (2.2), and the path generated by the end-effector ($\mathbf{r}_{Q,t^*} = [X_{t^*}^{(l)}, Y_{t^*}^{(l)}]$) can be obtained through the state vector $\mathbf{q}_{t^*}^{(l)}$ of the l th rigid block at time step t^* through the relationship expressed as Eq. 2.2.

$\mathbf{F}_{\text{int},t^*}$ is the internal force caused by the stretched artificial springs in the design domain. In Eq. (2.3), $\mathbf{F}_{\text{int},t^*}$ can be determined as the differential value for the state variables (\mathbf{v}_{t^*}) of the elastic energy from the stretched spring (U_{t^*}) stemming from the input motion and external force ($\mathbf{F}_{\text{ext},t^*}$) in the design domain,

$$\frac{dU_{t^*}}{d\mathbf{v}_{t^*}} = \left\{ \left(\frac{dU_{t^*}}{d\mathbf{q}_{t^*}^{(2)}} \right)^T, \left(\frac{dU_{t^*}}{d\mathbf{q}_{t^*}^{(3)}} \right)^T, \left(\frac{dU_{t^*}}{d\mathbf{q}_{t^*}^{(4)}} \right)^T, \dots, \left(\frac{dU_{t^*}}{d\mathbf{q}_{t^*}^{(N_B)}} \right)^T \right\}^T \quad (2.5)$$

where

$$\frac{dU_{t^*}}{d\mathbf{q}_{t^*}^{(l)}} = \left\{ \frac{dU_{t^*}}{dX_{t^*}^{(l)}}, \frac{dU_{t^*}}{dY_{t^*}^{(l)}}, \frac{dU_{t^*}}{d\phi_{t^*}^{(l)}} \right\}^T \quad (2.6)$$

The total elastic energy (U_{t^*}) from the springs in the design domain can be obtained from the summation of block-connecting springs which connect the blocks and the anchoring springs which connect the block to the ground.

Here, we assume that the corner node ($N_{C_i,1}$) of rigid block $B^{(l)}$ is connected by block-connecting spring (k_{C_i}) at the corner node ($N_{C_i,2}$) of rigid block $B^{(m)}$ in Fig. 2.2(a) and anchoring spring (k_{A_j}) at the ground in Fig. 2.2(b). The corner nodes ($N_{C_i,1}, N_{C_i,2}$) attached to blocks $B^{(l)}$ and $B^{(m)}$ are expressed by subscripts 1 and 2, respectively. From the global coordinate system (X, Y), the position vectors to the geometric center of blocks $B^{(l)}$ and $B^{(m)}$ (i.e., the X, Y values of $q_{t^*}^{(l)}$ and $q_{t^*}^{(m)}$), which are connected by the block-connecting spring (k_{C_i}), are correspondingly denoted as $\mathbf{r}_{C_i}^{(l)}$ and $\mathbf{r}_{C_i}^{(m)}$. The position vector from the geometric center of block

$B^{(l)} (B^{(m)})$ to corner node $N_{C_i,1} (N_{C_i,2})$ from the block fixed local coordinate is denoted by $\mathbf{s}_{C_i,1}^{(l)} (\mathbf{s}_{C_i,2}^{(m)})$. The coordinate transformation matrix from the global coordinates of $B^{(l)} (B^{(m)})$ is denoted by $\mathbf{T}_{C_i}^{(l)} (\mathbf{T}_{C_i}^{(m)})$. Hence, the position vectors of each of the corner nodes $(N_{C_i,1}, N_{C_i,2})$ attached to blocks $B^{(l)}$ and $B^{(m)}$ in the global coordinates can be correspondingly expressed as $\mathbf{r}_{C_i}^{(l)} + (\mathbf{T}_{C_i}^{(l)})^{-1} \mathbf{s}_{C_i,1}^{(l)}$ and $\mathbf{r}_{C_i}^{(m)} + (\mathbf{T}_{C_i}^{(m)})^{-1} \mathbf{s}_{C_i,2}^{(m)}$. The stretched length of the block-connecting spring (k_{C_i}) can be considered as the displacement of the stretched block-connecting spring \mathbf{u}_{C_i} . The displacement of the stretched block-connecting spring is determined using the equation below.

$$\mathbf{u}_{C_i} = (\mathbf{r}_{C_i}^{(l)} + (\mathbf{T}_{C_i}^{(l)})^{-1} \mathbf{s}_{C_i,1}^{(l)}) - (\mathbf{r}_{C_i}^{(m)} + (\mathbf{T}_{C_i}^{(m)})^{-1} \mathbf{s}_{C_i,2}^{(m)}) \quad (2.7)$$

Therefore, the elastic energy U_{C_i} from block-connecting spring k_{C_i} , which is stretched about \mathbf{u}_{C_i} , is expressed as shown below.

$$U_{C_i} = \frac{1}{2} k_{C_i} (\mathbf{u}_{C_i})^T (\mathbf{u}_{C_i}) \quad (2.8)$$

The elastic energy U_{A_j} from anchoring spring (k_{A_j}) in Fig. 2.2(b) which connects corner node $(N_{A_j,1})$ of rigid block $B^{(l)}$ and the ground (block 0), can be expressed by the stretched displacement \mathbf{u}_{A_j} . The stretched displacement \mathbf{u}_{A_j} is determined as follows:

$$\mathbf{u}_{A_j} = (\mathbf{r}_{A_j}^{(l)} + (\mathbf{T}_{A_j}^{(l)})^{-1} \mathbf{s}_{A_j,1}^{(l)}) - (\mathbf{r}_{A_j}^{(0)}) \quad (2.9)$$

Therefore, the stored elastic energy U_{A_j} in anchoring spring k_{A_j} is expressed as follows:

$$U_{A_j} = \frac{1}{2} k_{A_j} (\mathbf{u}_{A_j})^T (\mathbf{u}_{A_j}) \quad (2.10)$$

The total elastic energy U_{t^*} in the design domain at the certain time t^* is the sum of the elastic energy from the N_C number of block-connecting springs and the N_A number of anchoring springs.

$$\frac{d\mathbf{F}_{\text{int},t^*}(\mathbf{v}_{t^*})}{d\mathbf{v}_{t^*}} = \frac{d^2 U_{t^*}}{d\mathbf{v}_{t^*} d\mathbf{v}_{t^*}} \triangleq \mathbf{J}_{t^*} \quad (2.11)$$

The Jacobian matrix \mathbf{J}_{t^*} can also be obtained from the union set of Jacobian matrix (\mathbf{J}_{C_i,t^*}) from block-connecting spring (k_{C_i}) and Jacobian matrix (\mathbf{J}_{A_j,t^*}) from anchoring spring (k_{A_j}) .

Using a number of randomly generated variables ξ^K , ξ^X and \mathbf{r}_Q based on the SBM, we can obtain the paths of the end-effectors of the generated mechanisms using the quasi-static analysis described above. Accordingly, we can build the data needed to train a neural network for mechanism synthesis determining M_T and \mathbf{r}_Q for a given end-effector path.

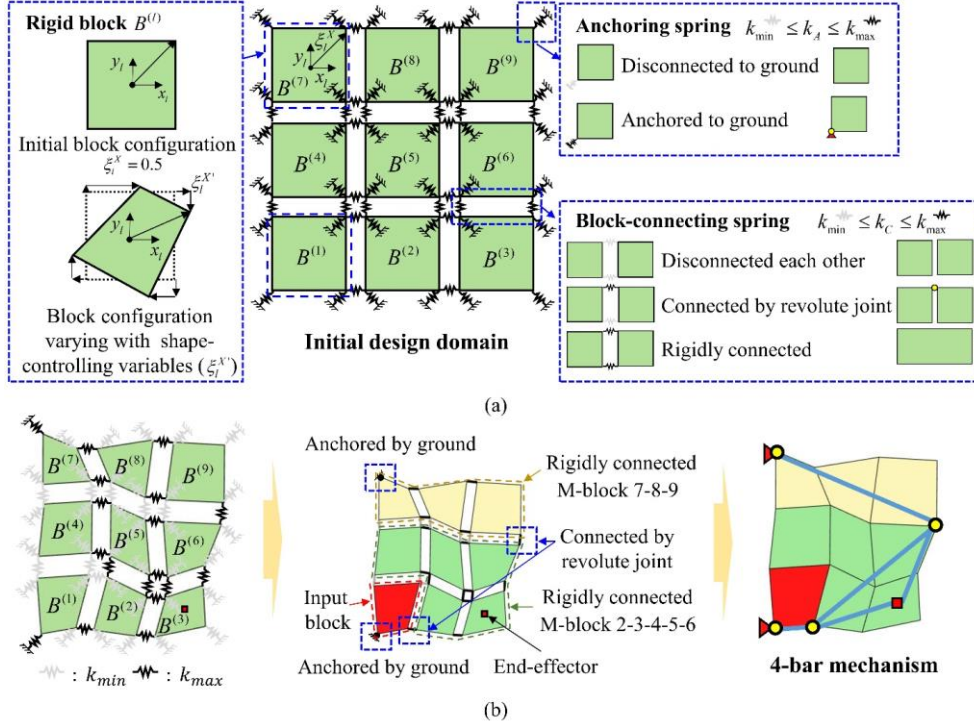


Fig. 2.1 Representation of general linkage mechanisms using the SBM. (a) The interpretations of two adjacent blocks connected by springs and the effects of the shape-controlling variable ξ_i^X are illustrated. (b) An illustrative example to represent a 4-bar mechanism using the SBM. Blocks of the same color function as a single mega-block (rigidly connected larger component).

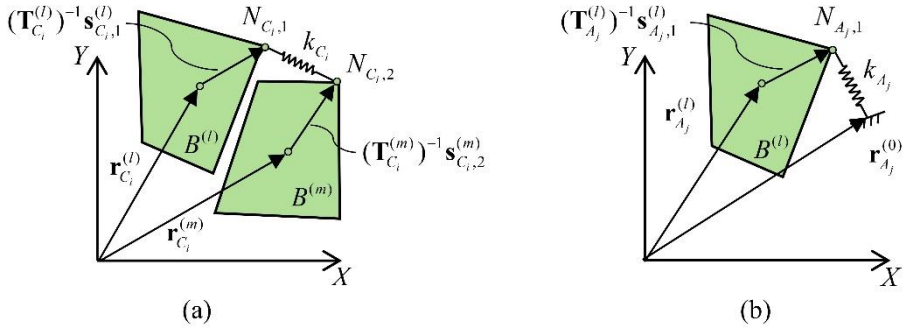


Fig. 2.2 Configurations of the deformation of the springs. Each configuration consists of (a) $B^{(l)}$, $B^{(m)}$, and the block-connecting spring (k_{C_i}), and (b) $B^{(l)}$, the ground, and the anchoring spring (k_{A_j}).

CHAPTER 3.

Topology Optimization of Planar Gear-Linkage Mechanisms

3.1 Overview

Mechanism synthesis refers to a method used to find a mechanism that produces desired motion at its end effector for a given input motion. With linkage-only mechanisms consisting of link and joint components alone, diverse output motions cannot be generated. Accordingly, the synthesis of gear-linkage mechanisms including non-circular gears for exact path generation has been investigated as an important research subject [16-27]. In these earlier studies, sequential approaches were mainly used, i.e., with the type, number, and dimension of the mechanisms determined in sequence. Type synthesis determines whether a linkage-only mechanism or a gear-linkage mechanism is to be used. The number of links and joints in the mechanism is then determined by means of a number synthesis approach, and the locations of gears and the sizes of the links are determined by dimensional synthesis. Only with the sequential approach, however, it is difficult to

find new mechanisms beyond the designer's intuition. To overcome this limitation, we aim to develop a new systematic method based on topology optimization for the synthesis of gear-linkage mechanisms by which type, number, and dimensional synthesis methods can be simultaneously performed. To the best of the authors' knowledge, the synthesis of gear-linkage mechanisms using a topology optimization method has not been explored or attempted thus far. Therefore, several unexplored issues, such as the simultaneous handling of dissimilar mechanism types in the context of topology optimization, must be newly addressed.

Because no baseline design is required, the methods based on topology optimization have received much attention. With these methods, number and dimensional synthesis can be so far conducted simultaneously [2-8, 10, 11, 13, 28-32]. However, a method of topology-optimization based synthesis covering up to type synthesis has not been proposed or attempted so far. Here we note that for efficient mechanism synthesis by topology optimization, a gradient-based method is undoubtedly preferred [2, 7, 8, 11, 13, 28, 30, 31]. A gradient-based method requires the use of continuous design variables, calling for ground models that can be used to generate various mechanisms when the design variables take on upper or lower bound values. Currently, two major ground models, the nonlinear elastic bar model [2, 11, 28, 30] and the SBM (spring-connected rigid block model) [7, 8, 13] have been used for the synthesis of linkage-only mechanisms. The nonlinear elastic bar model discretizes the design domain with nonlinear bars connecting pre-defined grid nodes and controls their existence to configure the desired linkage

mechanism. On the other hand, the SBM discretizes the design domain with rigid blocks that are connected by artificial zero-length translational elastic springs, the stiffness levels of which are varied as a function of the design variables. In the SBM approach, the existence and types of joints can be determined by the values of the spring stiffness. The issue here is that none of the earlier methods can be directly used to synthesize mechanisms consisting of both linkages and gears because they are of different types; the existing topology-optimization-based synthesis methods cannot deal with type synthesis of mechanisms. Therefore, a new topology optimization formulation is needed to perform type, number and dimensional synthesis simultaneously.

Before presenting our method to synthesize gear-linkage mechanisms, it is important to pinpoint several major issues that need to be addressed in developing a topology optimization-based synthesis of linkage-gear mechanisms. First, we should develop a new ground model that can represent not only the existence of link and joint components but also the existence of gear components. Second, the synthesis method should allow the use of continuous design variables so that a numerically efficient gradient-based optimizer can be incorporated. Third, it should be equally applicable to the synthesis of not only gear-linkage mechanisms but also linkage-only mechanisms; this means that a type synthesis involving linkages and gears should be also possible. To resolve these critical issues, we propose to extend the SBM. As the connectivity between domain-discretizing blocks can be controlled by zero-length springs in the SBM, the SBM may be better suited to

determine the connectivity between gears and linkages in the synthesis of gear-linkage mechanisms. To accommodate additional gear components in the model, we introduce a new type of zero-length springs to represent the existence of a gear. Below, we briefly explain how this new concept is realized. A more detailed account of it will be presented in Sec. 3.2.

To handle both linkages and gears simultaneously in our topology-optimization-based synthesis approach, we propose to introduce two design spaces occupying the same physical domain, one design space (S_L) for the linkage synthesis ground model and the other design space (S_G) for the gear synthesis ground model, as presented in Fig. 3.1. The linkage design space S_L is identical to that used in the earlier SBM [7] where the design domain is discretized by rigid blocks that are connected by zero-length springs with variable degrees of stiffness. In the linkage design space S_L , a linkage mechanism can be represented if the stiffnesses of the zero-length springs take on upper and lower bound values (more precisely, the stiffness is interpolated as a function of the design variable). On the other hand, the gear design space S_G is a space discretized by gear blocks, which are blocks representing output gears. The gear design space will be elaborated below in more detail.

The gear design space is assumed to occupy the same physical space as the linkage design space. The number and size of the gear blocks are identical to those of the rigid blocks used in the linkage design space. Each gear block is assumed to

be always connected to an input gear which rotates according to a prescribed input motion. However, gear blocks rotate independently of each other at a specified gear ratio. If any gear block in S_G is not connected to a rigid block in S_L , the corresponding gear block does not contribute to the output motion at the end effector. In order to make an output gear contribute to the output motion, we connect a gear block in S_G by a set of zero-length springs, which will be referred to as “gearing springs,” to its counterpart rigid block that occupies the same location occupied by the gear block.

Therefore, the synthesis of gear-linkage mechanisms by the proposed approach is to determine the distribution of the stiffness values of the two sets of springs, one set connecting the rigid blocks of S_L to each other and the other set connecting the gear blocks of S_G and the rigid blocks of S_L . If the stiffness of the spring connecting a gear block and its counterpart rigid block takes on the upper (lower) bound value, a gear is regarded to appear (disappear) in the synthesized mechanism. The details of the proposed approach are also explained in Sec. 3.2.

Because no earlier topology-optimization-based methods consider both linkages and gears simultaneously, Sec. 3.2 is entirely devoted to the modeling technique, which is followed by a kinematic analysis procedure. Sec. 3.3 presents a gradient-based mechanism synthesis formulation in the framework of topology optimization and the sensitivity analysis needed to update the design variables. Numerical case studies are presented in Sec. 3.4, where the synthesis of both gear-linkage

mechanisms and linkage-only mechanisms are considered. The main reason to consider the synthesis of linkage-only mechanisms is to show that a mechanism of different type can be synthesized; if a gear is needed to yield the desired mechanism, a gear component will automatically be included in the synthesis process. Otherwise, no gear will appear in the synthesized mechanism.

3.2 Modeling and Analysis

3.2.1 Modeling

Figure 3.1(a) shows a typical gear-linkage mechanism (which will also be referred to as a geared mechanism) that we aim to synthesize by topology optimization. To carry out mechanism synthesis in the framework of topology optimization, the design domain for mechanism synthesis should be discretized into several components, the combination of which should be able to represent the desired mechanism. Unlike in any of earlier topology-optimization-based mechanism synthesis methods that are applicable to the synthesis of linkage-only mechanisms, both linkages and gears should be simultaneously synthesized for the problem under consideration. In what follows, we will explain how the proposed modeling technique is suitable for the simultaneous synthesis of linkages and gears.

Figure 3.1(b) shows the proposed block ground model, in which the design domain Ω is treated as a superposition of two design spaces, S_L and $\langle r \rangle S_G$. The symbol S_L represents the linkage design space discretized by rigid blocks $B^{(l)}$ ($l=1, \dots, N_B$), while $\langle r \rangle S_G$ represents the gear design space discretized by gear blocks $\langle r \rangle G^{(l)}$ ($l=1, \dots, N_B$) having a gear ratio of r . Here, $N_B = N_X \times N_Y$ is the total number of the rigid blocks, where N_X and N_Y denote the numbers of the blocks in the horizontal (X) and vertical (Y) directions, respectively. Note that the number and size of the rigid blocks in S_L are identical to those of the gear blocks

in $\langle r \rangle S_G$. To consider gears having different gear ratios simultaneously, such as r_1 and r_2 , multiple gear spaces $\langle r_1 \rangle S_G$, $\langle r_2 \rangle S_G$, for instance, can be introduced. Therefore, the design domain Ω can be interpreted as a superposition of S_L , $\langle r_1 \rangle S_G$, $\langle r_2 \rangle S_G, \dots$, which can be symbolically expressed as

$$\Omega \equiv S_L \oplus \langle r_1 \rangle S_G \oplus \langle r_2 \rangle S_G \dots \quad (3.1)$$

The notion of S_L consisting of $B^{(l)}$ has been used in earlier studies [7], but the notion of $\langle r \rangle S_G$ consisting of $\langle r \rangle G^{(l)}$ is newly proposed here to accommodate gears. To facilitate the subsequent discussion, we will use simply $\langle r \rangle S_G$ to denote the gear design spaces to represent any one or all instances of $\langle r_1 \rangle S_G$, $\langle r_2 \rangle S_G$, \dots . After a brief review of the modeling technique used in S_L , a detailed account of our new modeling technique using $\langle r \rangle S_G$ and $\langle r \rangle G^{(l)}$ will be presented.

Figure 3.2 illustrates how two adjacent rigid blocks $B^{(l)}$ and $B^{(m)}$ are connected to each other in the design space of S_L . It also explains how various joint states can be represented by the stiffness values of block-connecting springs when they take on the upper (k_{\max}) and lower (k_{\min}) bound values. As illustrated in Fig. 3.2, two adjacent rigid blocks are assumed to be connected by zero-length springs, denoted by k_{c_1} and k_{c_2} . These springs are called block-connecting springs because they control the connectivity between adjacent blocks. Moreover, the corner nodes of the rigid blocks are connected to the ground by zero-length springs denoted by k_{A_1} , k_{A_2} , k_{A_3} , and k_{A_4} , referred to here as anchoring springs.

These springs are needed in order to fix a revolute joint to the ground.

The symbols k_C and k_A will also be used to represent the stiffness values of springs. Because the stiffness values can vary between k_{\min} and k_{\max} as functions of the design variables, various joint states can be represented when k_C and k_A take on k_{\min} or k_{\max} values. (When the stiffness takes on an intermediate value between k_{\min} and k_{\max} , the situation corresponds to an artificial joint state that is needed only to allow the use of continuous design variables. Therefore, the synthesis method should be so formulated as to avoid these intermediate states.) The second to fourth columns in Fig. 3.2 illustrate how various joint states in a linkage mechanism can be represented by block-connecting and anchoring springs taking on their bound values. For instance, a revolute joint can be simulated if $k_{C_1} = k_{\max}$ and $k_{C_2} = k_{A_1} = k_{A_2} = k_{A_3} = k_{A_4} = k_{\min}$. Similarly, other joint states can be represented as illustrated in Fig. 3.2.

At this point, it will be worth to explain how DOFs can be estimated when two rigid blocks shown in Fig. 3.2 are connected by block-connecting springs when their stiffness values take on their bound values. Clearly, each of the rigid blocks in Fig. 3.2 has 3 DOFs (two rigid-body translations and one rotation). If $k_{C_1} = k_{\max}$ and $k_{C_2} = k_{A_1} = k_{A_2} = k_{A_3} = k_{A_4} = k_{\min}$ between $B^{(l)}$ and $B^{(m)}$, the connection implies the state of revolute joint connection at one of their common corner nodes. Because the revolute joint limits the translation motion between two blocks, the system DOF of the two blocks connected by the block-connecting springs is (3+3-

2)=4. On the other hand, $k_{A_1} = k_{\max}$ and $k_{C_1} = k_{C_2} = k_{A_2} = k_{A_3} = k_{A_4} = k_{\min}$

(corresponding the configuration shown in the bottom of Fig. 3.2), $B^{(l)}$ has (3-2) DOF while $B^{(m)}$ has 3 DOFs. However, $B^{(m)}$ is completely disconnected from other block or the ground, $B^{(m)}$ is ignored in counting the actual DOF of the synthesized mechanism. However, there is no need to explicitly calculate the DOF because an indirect energy based formulation [11] will be employed to ensure that the synthesized mechanism has the correct DOF. This will be discussed in Sec. 3.

To facilitate the subsequent discussion, we will introduce what is termed a megablock, denoted by M-block l - m . It consists of multiple rigid blocks ($B^{(l)}$ and $B^{(m)}$ in Fig. 3.2) that are rigidly connected to each other through zero-length springs with $k_{C_1} = k_{C_2} = k_{\max}$. As illustrated in the second row in Fig. 3.2, the megablock actually simulates a long link component. We often use the terminology of a floating block to indicate a rigid block that is not connected to any other rigid block. Because floating blocks do not contribute to the motion of a mechanism to be synthesized, they can be ignored in the synthesized mechanism. More details pertaining to the spring connected rigid block model can be found in the literature [8].

At this point, we explain the role of the ${}^{<r>}S_G$ design space, which is newly introduced to synthesize gear components in gear-linkage mechanisms. First, all of the gear blocks ${}^{<r>}G^{(l)}$ ($l=1, \dots, N_B$) used to discretize ${}^{<r>}S_G$ are connected by zero-length gearing springs ${}^{<r>}k_{G_i}$ to their counterpart rigid blocks

$B^{(l)}$ ($l=1, \dots, N_B$), as shown in Fig. 3.1(b). The gear block $\langle r \rangle G^{(l)}$ is an output gear having the gear ratio of r . It occupies precisely the same location as the rigid block $B^{(l)}$ before an input motion takes place. Note that the four gearing springs shown in Fig. 3.1(b) are controlled by the same stiffness value of $\langle r \rangle k_{G_l}$.

To facilitate the explanation of the block ground model technique, we pinpoint the key features of the gear block $\langle r \rangle G^{(l)}$ as follows.

KF 1) The center of the gear block $\langle r \rangle G^{(l)}$ is assumed to be fixed in space, but it is connected to an input block in such a way that it rotates by θ/r as the input block rotates by θ . The input block is a block to which an input rotational motion is prescribed. Although no explicit connection is drawn in Fig. 3.1(b), all of the gear blocks $\langle r \rangle G^{(l)}$ ($l=1, \dots, N_B$) are assumed to work as output gears that are connected to the input block. (In Fig. 3.1(b), the design domain is discretized by 3×3 blocks in which one block located at the lower left corner serves as the input block. Therefore, the remaining eight blocks serve as gear blocks.)

KF 2) Referring to Fig. 3.1(b), the gear block $\langle r \rangle G^{(l)}$ is connected to the rigid block $B^{(l)}$ by four springs at their four corner nodes. The stiffnesses of the four springs are controlled by a single stiffness value denoted by $\langle r \rangle k_{G_l}$. If $\langle r \rangle k_{G_l} = k_{\max}$, $B^{(l)}$ behaves as if it is rigidly connected to $\langle r \rangle G^{(l)}$. In this case, $B^{(l)}$ follows precisely the motion of $\langle r \rangle G^{(l)}$, allowing one to set $B^{(l)}$

$\equiv \langle r \rangle G^{(l)}$. If $\langle r \rangle k_{G_i} = k_{\min}$, on the other hand, $B^{(l)}$ is disconnected from $\langle r \rangle G^{(l)}$. In this case, $\langle r \rangle G^{(l)}$ does not contribute to the output motion. (However, the gear block $\langle r \rangle G^{(l)}$ always rotates by θ/r regardless of the value of $\langle r \rangle k_{G_i}$ because an input block rotates by θ). Because $\langle r \rangle G^{(l)}$ contributes to the actual motion as a gear component only when $\langle r \rangle k_{G_i} = k_{\max}$, the design space $\langle r \rangle S_G$ can be viewed as a background space affecting the motion of the rigid blocks in S_L .

From the key features discussed above, it is clear that $\langle r \rangle G^{(l)}$ meaningfully contributes to the output motion when $B^{(l)}$ rotates identically to $\langle r \rangle G^{(l)}$ under the condition of $\langle r \rangle k_{G_i} = k_{\max}$. Based on this observation, we introduce a symbol $\langle r \rangle B^{(l)}$ to indicate $B^{(l)}$ that rotates identically to $\langle r \rangle G^{(l)}$. If this notation is used, we can also define $\langle > B^{(l)}$ to represent a rigid block $B^{(l)}$ that is disconnected from $\langle r \rangle G^{(l)}$ for which $\langle r \rangle k_{G_i} = k_{\min}$. Using these notations, gear and link components in certain mechanisms can be represented in terms of $\langle > B^{(l)}$ and $\langle r \rangle B^{(l)}$, as illustrated in Fig. 3.3.

Figure 3.4(a) shows a more realistic mechanism. It is a geared five-bar linkage mechanism (GFBM) which consists of two links and one pair of gears having a gear ratio of 1. Fig. 3.4(b) illustrates how the GFBM can be represented in terms of $\langle l \rangle B^{(l)}$, $\langle > B^{(l)}$, and the block-connecting springs having bound stiffness values. The blocks of the same color in Fig. 3.4(b) (and in Fig. 3.4(c)) are supposed to behave

as a single rigid body. For instance, the system of $\diamond B^{(5)}$, $\diamond B^{(6)}$, $\diamond B^{(8)}$ and $\diamond B^{(9)}$ behaves as a single rigid body and likewise, the system of $\diamond B^{(4)}$ and $\diamond B^{(7)}$ also behaves as another single rigid body. Each of the remaining blocks $\diamond B^{(1)}$, $\diamond B^{(2)}$, and $\diamond B^{(3)}$ behaves as a single rigid body, respectively. Two design spaces S_L and ${}^{<1>}S_G$ are needed to represent the given GFBM. Because the linkage design space is discretized by nine blocks in the illustration, the superscript l in $B^{(l)}$ varies from 1 to 9. The gear design space ${}^{<1>}S_G$ is discretized also by nine blocks ${}^{<1>}G^{(l)}$ ($l=1,2,\dots,9$). The output gear having the gear ratio of one in the given GFBM in Fig. 3.4(a) is represented by ${}^{<1>}B^{(3)}$.

Although not shown explicitly, $\diamond B^{(4)}$ and $\diamond B^{(7)}$ are connected to each other by block-connecting springs with $k_c = k_{\max}$. Moreover, four adjacent blocks $\diamond B^{(5)}$, $\diamond B^{(6)}$, $\diamond B^{(8)}$, and $\diamond B^{(9)}$ are connected to each other by block-connecting springs with $k_c = k_{\max}$. Fig. 3.4(c) shows the representation of the GFBM in terms of M-blocks, a floating block and a gear block where M-block 4-7 and M-block 5-6-8-9 serve correspondingly as link 1 and link 2. Revolute joint 1 is represented through a block-connecting spring of $k_c = k_{\max}$ between $\diamond B^{(1)}$ and $\diamond B^{(4)}$ (of M-block 4-7). Likewise, revolute joint 2 is represented by a block-connecting spring between $\diamond B^{(7)}$ (of M-block 4-7) and $\diamond B^{(8)}$ (of M-block 5-6-8-9) while revolute joint 3 is symbolized by a block-connecting spring between ${}^{<1>}B^{(3)}$ and $\diamond B^{(6)}$ (of M-block 5-6-8-9). Block $\diamond B^{(2)}$ is a floating block which does not contribute to the motion

of the GFBM. Although only one mechanism example is considered here, Fig. 3.4 suggests that a mechanism consisting of linkage and gear components can be represented by the proposed ground model. In the next section, the procedure of kinematic analysis will be given before the topology-optimization-based mechanism synthesis formulation is presented in Sec. 3.3.

3.2.2 Analysis

The kinematic analysis of the block-model-based mechanism can be performed through a quasi-static nonlinear analysis. If the position of an input block is specified in each time step, the position of other driven blocks should be determined by the analysis. Here, we use the principle of total elastic energy minimization for the analysis, where the elastic energy is stored in all of springs employed in our model. When calculating the elastic energy, we need to consider three configurations in which block-connecting springs, anchoring springs, and gearing springs are stretched independently.

Let us consider a rigid block $B^{(l)}$ that is connected to an adjacent rigid block $B^{(m)}$ by a i^{th} block-connecting spring k_{C_i} to the ground by an j^{th} anchoring spring k_{A_j} and to the gear block ${}^{<r>G^{(l)}}$ by a set of w^{th} gearing springs denoted by ${}^{<r>k_{G_w}}$, as shown in Fig. 3.5. The deformed configurations are illustrated in Fig. 3.5.

The coordinates of the centers of $B^{(l)}$ and $B^{(m)}$ are denoted by $\mathbf{r}_{C_i}^{(l)}$ and $\mathbf{r}_{C_i}^{(m)}$, which are expressed in the global coordinate system (X, Y) . The two corner nodes

connected by k_{C_i} occupy the same spatial position before the spring k_{C_i} is stretched. Their positions during motion become $\mathbf{r}_{C_i}^{(l)} + (\mathbf{T}_{C_i}^{(l)})^{-1} \mathbf{s}_{C_i,1}^{(l)}$ and $\mathbf{r}_{C_i}^{(m)} + (\mathbf{T}_{C_i}^{(m)})^{-1} \mathbf{s}_{C_i,2}^{(m)}$, respectively. The corner nodes $(N_{C_i,1}, N_{C_i,2})$ attached to blocks $B^{(l)}$ and $B^{(m)}$ are denoted by the subscripts 1 and 2, respectively. The position vector from the center of block $B^{(l)}$ ($B^{(m)}$) to corner node $N_{C_i,1}$ ($N_{C_i,2}$) in the block-fixed local coordinate system is denoted by $\mathbf{s}_{C_i,1}^{(l)}$ ($\mathbf{s}_{C_i,2}^{(m)}$). The coordinate transformation matrices from the global to the block-fixed local coordinate systems are denoted by $\mathbf{T}_{C_i}^{(l)}$ for block $B^{(l)}$ and $\mathbf{T}_{C_i}^{(m)}$ for $B^{(m)}$. Therefore, the block-connecting spring k_{C_i} during motion is stretched by the displacement \mathbf{u}_{C_i} :

$$\mathbf{u}_{C_i} = (\mathbf{r}_{C_i}^{(l)} + (\mathbf{T}_{C_i}^{(l)})^{-1} \mathbf{s}_{C_i,1}^{(l)}) - (\mathbf{r}_{C_i}^{(m)} + (\mathbf{T}_{C_i}^{(m)})^{-1} \mathbf{s}_{C_i,2}^{(m)}) \quad (3.2)$$

The transformation matrices $\mathbf{T}_{C_i}^{(l)}$ and $\mathbf{T}_{C_i}^{(m)}$ are defined as

$$\mathbf{T}_{C_i}^{(l)} = \begin{bmatrix} \cos \phi_{C_i}^{(l)} & \sin \phi_{C_i}^{(l)} \\ -\sin \phi_{C_i}^{(l)} & \cos \phi_{C_i}^{(l)} \end{bmatrix}; \quad \mathbf{T}_{C_i}^{(m)} = \begin{bmatrix} \cos \phi_{C_i}^{(m)} & \sin \phi_{C_i}^{(m)} \\ -\sin \phi_{C_i}^{(m)} & \cos \phi_{C_i}^{(m)} \end{bmatrix} \quad (3.3)$$

where $\phi_{C_i}^{(l)}$ ($\phi_{C_i}^{(m)}$) is the angle between the global coordinate system (X, Y) and the block-fixed local coordinate system of $B^{(l)}$ ($B^{(m)}$). The elastic energy U_{C_i} stored by the block-connecting spring k_{C_i} is therefore written as follows:

$$U_{C_i} = \frac{1}{2} k_{C_i} (\mathbf{u}_{C_i})^T (\mathbf{u}_{C_i}) \quad (3.4)$$

Figure 3.5(b) illustrates that corner node 1 ($N_{A_j,1}$) of the rigid block $B^{(l)}$ is

connected to the ground (block 0) through the j^{th} anchoring spring k_{A_j} . The stretch

\mathbf{u}_{A_j} of the spring is expressed as

$$\mathbf{u}_{A_j} = (\mathbf{r}_{A_j}^{(l)} + (\mathbf{T}_{A_j}^{(l)})^{-1} \mathbf{s}_{A_j,1}^{(l)}) - (\mathbf{r}_{A_j}^{(0)}) \quad (3.5)$$

where $\mathbf{r}_{A_j}^{(0)}$ is the position vector of the ground node connected to corner node 1 of

$B^{(l)}$. The transformation matrix $\mathbf{T}_{A_j}^{(l)}$ is given by

$$\mathbf{T}_{A_j}^{(l)} = \begin{bmatrix} \cos \phi_{A_j}^{(l)} & \sin \phi_{A_j}^{(l)} \\ -\sin \phi_{A_j}^{(l)} & \cos \phi_{A_j}^{(l)} \end{bmatrix} \quad (3.6)$$

The stored elastic energy U_{A_j} in the anchoring spring k_{A_j} is simply expressed as follows:

$$U_{A_j} = \frac{1}{2} k_{A_j} (\mathbf{u}_{A_j})^T (\mathbf{u}_{A_j}) \quad (3.7)$$

In Fig. 3.5(c), rigid block $B^{(l)}$ and gear block ${}^{<r>G^{(l)}}$ are connected by a set of four gearing springs denoted by a single stiffness, ${}^{<r>k_{G_w}}$. The subscript w in ${}^{<r>k_{G_w}}$ denotes the w^{th} set of gearing springs. It is emphasized that the gearing springs connecting each of the four corner nodes of the rigid block and their counterparts in the gear block are varied by the single spring stiffness ${}^{<r>k_{G_w}}$. The deformation of the gearing spring attached to the a^{th} corner node ($N_{G_w,a}$) can be described by the relative displacement between the rigid block and the gear block, as

$$\mathbf{u}_{G_w,a} = (\mathbf{r}_{G_w}^{(l)} + (\mathbf{T}_{G_w}^{(l)})^{-1} \mathbf{s}_{G_w,a}^{(l)}) - (\mathbf{r}_{G_w}^{(0)} + (\mathbf{T}_{G_w}^{(0)})^{-1} \mathbf{s}_{G_w,a}^{(0)}) \quad (a=1,2,3,4) \quad (3.8)$$

where $\mathbf{r}_{G_w}^{(0)}$ denotes the center position vector of gear block ${}^{<r>G^{(l)}}$. The

superscript 0 is used to indicate that the center of the gear block is always attached to the ground. The symbol $\mathbf{s}_{G_w,a}^{(0)}$ denotes the relative distance vector from $\mathbf{r}_{G_w}^{(0)}$ to the a^{th} corner node of the gear block ${}^{<r>G^{(l)}}$ in the gear block-fixed local coordinate system. The transformation matrices $\mathbf{T}_{G_w}^{(l)}$ and $\mathbf{T}_{G_w}^{(0)}$ are written as

$$\mathbf{T}_{G_w}^{(l)} = \begin{bmatrix} \cos \phi_{G_w}^{(l)} & \sin \phi_{G_w}^{(l)} \\ -\sin \phi_{G_w}^{(l)} & \cos \phi_{G_w}^{(l)} \end{bmatrix}; \quad \mathbf{T}_{G_w}^{(0)} = \begin{bmatrix} \cos \phi_{G_w}^{(0)} & \sin \phi_{G_w}^{(0)} \\ -\sin \phi_{G_w}^{(0)} & \cos \phi_{G_w}^{(0)} \end{bmatrix} \quad (3.9)$$

where $\phi_{G_w}^{(l)}$ ($\phi_{G_w}^{(0)}$) is the angle between the gear block-fixed local coordinate system of $B^{(l)}$ (${}^{<r>G^{(l)}}$) and the global coordinate system. The stored elastic energy U_{G_w} in the four gearing springs is written as

$$U_{G_w} = \sum_{a=1}^4 \frac{1}{2} k_{G_w} (\mathbf{u}_{G_w,a})^T (\mathbf{u}_{G_w,a}) \quad (3.10)$$

By summing up the elastic energy expressions for all spring components, the total elastic energy U_{t^*} stored in the design domain Ω at a certain time t^* is given by

$$U_{t^*}(\mathbf{q}_{t^*}) = \sum_{i=1}^{N_c} U_{C_i,t^*}(\mathbf{q}_{t^*}) + \sum_{j=1}^{N_a} U_{A_j,t^*}(\mathbf{q}_{t^*}) + \sum_{w=1}^{N_g} U_{G_w,t^*}(\mathbf{q}_{t^*}) \quad (3.11)$$

where N_c , N_a and N_g denote the total numbers of block-connecting, anchoring, and gearing springs, respectively. The symbol \mathbf{q}_{t^*} is defined as

$$\mathbf{q}_{t^*} = [(\mathbf{q}_{t^*}^{(1)})^T, (\mathbf{q}_{t^*}^{(2)})^T, \dots, (\mathbf{q}_{t^*}^{(l)})^T, \dots, (\mathbf{q}_{t^*}^{(N_B)})^T]^T \quad (3.12)$$

with

$$\mathbf{q}_{t^*}^{(l)} = [(\mathbf{r}_{t^*}^{(l)})^T, \phi_{t^*}^{(l)}]^T = [X_{t^*}^{(l)}, Y_{t^*}^{(l)}, \phi_{t^*}^{(l)}]^T \quad (3.13)$$

where $\mathbf{r}_{t^*}^{(l)} = [X_{t^*}^{(l)}, Y_{t^*}^{(l)}]^T$ represents the position vector of the center of $B^{(l)}$ and $\phi_{t^*}^{(l)}$, the orientation angle of $B^{(l)}$ with respect to the global coordinate system at the time t^* . Because rigid block 1 is reserved to denote the input block, $\mathbf{q}_{t^*}^{(1)}$ should be excluded in the definition of the state variable vector \mathbf{v}_{t^*} defined at time step t^* :

$$\mathbf{v}_{t^*} = [(\mathbf{q}_{t^*}^{(2)})^T, (\mathbf{q}_{t^*}^{(3)})^T, \dots, (\mathbf{q}_{t^*}^{(N_B)})^T]^T \quad (3.14)$$

To find the state variable vector \mathbf{v}_{t^*} , the following force equilibrium is solved for a given input motion prescribed at t^* .

$$\text{Solve } F_{\text{int},t^*}(\mathbf{v}_{t^*}) = F_{\text{ext},t^*} \text{ for } (t^* = 1, 2, 3, \dots, T) \quad (3.15)$$

Here, F_{ext,t^*} is the prescribed external force and F_{int,t^*} is the internal force generated by the stretched zero-length springs in the design domain. The external force F_{ext,t^*} is needed to set up the topology optimization, as proposed in [11]. The specific form of F_{ext,t^*} will be given in the next section.

The internal force F_{int,t^*} can be obtained by $F_{\text{int},t^*} = dU_{t^*} / d\mathbf{v}_{t^*}$ as

$$\frac{dU_{t^*}}{d\mathbf{v}_{t^*}} = \left\{ \left(\frac{dU_{t^*}}{d\mathbf{q}_{t^*}^{(2)}} \right)^T, \left(\frac{dU_{t^*}}{d\mathbf{q}_{t^*}^{(3)}} \right)^T, \left(\frac{dU_{t^*}}{d\mathbf{q}_{t^*}^{(4)}} \right)^T, \dots, \left(\frac{dU_{t^*}}{d\mathbf{q}_{t^*}^{(N_B)}} \right)^T \right\}^T \quad (3.16)$$

where

$$\frac{dU_{t^*}}{d\mathbf{q}_{t^*}^{(l)}} = \left\{ \left(\frac{dU_{t^*}}{d\mathbf{r}_{t^*}^{(l)}} \right)^T, \frac{dU_{t^*}}{d\phi_{t^*}^{(l)}} \right\}^T = \left\{ \frac{dU_{t^*}}{dx_{t^*}^{(l)}}, \frac{dU_{t^*}}{dy_{t^*}^{(l)}}, \frac{dU_{t^*}}{d\phi_{t^*}^{(l)}} \right\}^T \quad (3.17)$$

Because the total elastic energy can be divided into three expressions contributed by the block-connecting, anchoring, and gearing springs, one can write

$$\frac{dU_{t^*}}{d\mathbf{r}_{t^*}^{(l)}} = \sum_{i \in S_C^{(l)}} k_{C_i, t^*} (\mathbf{u}_{C_i, t^*}) + \sum_{j \in S_A^{(l)}} k_{A_j, t^*} (\mathbf{u}_{A_j, t^*}) + \sum_{w \in S_G^{(l)}} \left(\sum_{a=1}^4 k_{G_w, t^*} (\mathbf{u}_{G_w, a, t^*}) \right) \quad (3.18)$$

and

$$\begin{aligned} \frac{dU_{t^*}}{d\phi_{t^*}^{(l)}} = & \sum_{i \in S_C^{(l)}} \left\{ k_{C_i, t^*} \left(\frac{d\{(\mathbf{T}_{C_i}^{(l)})^{-1}\}}{d\phi_{t^*}^{(l)}} \mathbf{s}_{C_i}^{(l)} \right)^T (\mathbf{u}_{C_i, t^*}) \right\} \\ & + \sum_{j \in S_A^{(l)}} \left\{ k_{A_j, t^*} \left(\frac{d\{(\mathbf{T}_{A_j}^{(l)})^{-1}\}}{d\phi_{t^*}^{(l)}} \mathbf{s}_{A_j}^{(l)} \right)^T (\mathbf{u}_{A_j, t^*}) \right\} \\ & + \sum_{w \in S_G^{(l)}} \sum_{a=1}^4 \left\{ k_{G_w, t^*} \left(\frac{d\{(\mathbf{T}_{G_w}^{(l)})^{-1}\}}{d\phi_{t^*}^{(l)}} \mathbf{s}_{G_w}^{(l)} \right)^T (\mathbf{u}_{G_w, a, t^*}) \right\} \end{aligned} \quad (3.19)$$

where $S_C^{(l)}$, $S_A^{(l)}$ and $S_G^{(l)}$ correspondingly represent the sets of block-connecting, anchoring, and gearing springs connected to $B^{(l)}$.

As a gradient-based optimization algorithm is to be employed for the gear-linkage mechanism synthesis, an expression for the gradient of the internal force is needed. For later use, it is derived explicitly here as

$$\frac{d\mathbf{F}_{\text{int}, t^*}(\mathbf{v}_{t^*})}{d\mathbf{v}_{t^*}} = \frac{d^2 U_{t^*}}{d\mathbf{v}_{t^*} d\mathbf{v}_{t^*}} \triangleq \mathbf{J}_{t^*} \quad (3.20)$$

where the Jacobian matrix \mathbf{J}_{t^*} can be expressed in terms of \mathbf{J}_{C_i, t^*} , \mathbf{J}_{A_j, t^*} , and \mathbf{J}_{G_w, t^*} related to the block-connecting, anchoring, and gearing springs, respectively.

The Jacobean matrix $\mathbf{J}_{t^*} = d^2 U_{t^*} / d\mathbf{v}_{t^*} d\mathbf{v}_{t^*}$ for the kinematic and sensitivity analyses will be derived in this section. When calculating the elastic energy U_{t^*}

stored in the design domain, the deformations of block-connecting, anchoring, and gearing springs will be considered independently. To simplify the expressions below, however, we do not explicitly write corner. Hence, $\mathbf{s}_{C_i,1}^{(l)} (\mathbf{s}_{A_j,2}^{(l)})$ is denoted by $\mathbf{s}_{C_i}^{(l)} (\mathbf{s}_{A_j}^{(l)})$.

If the block-connecting spring k_{C_i} connects block l and block m , the Jacobean matrix \mathbf{J}_{C_i,t^*} for k_{C_i} can be expressed as

$$\mathbf{J}_{C_i,t^*} = \frac{d}{d\mathbf{q}_{t^*}^{(l,m)}} \left(\frac{dU_{C_i,t^*}}{d\mathbf{q}_{t^*}^{(l,m)}} \right) = \begin{bmatrix} \frac{d}{d\mathbf{q}_t^{(l)}} \left(\frac{dU_{C_i,t^*}}{d\mathbf{q}_t^{(l)}} \right) & \frac{d}{d\mathbf{q}_t^{(m)}} \left(\frac{dU_{C_i,t^*}}{d\mathbf{q}_t^{(l)}} \right) \\ \frac{d}{d\mathbf{q}_t^{(l)}} \left(\frac{dU_{C_i,t^*}}{d\mathbf{q}_t^{(m)}} \right) & \frac{d}{d\mathbf{q}_t^{(m)}} \left(\frac{dU_{C_i,t^*}}{d\mathbf{q}_t^{(m)}} \right) \end{bmatrix}$$

$$= \begin{bmatrix} \frac{d}{d\mathbf{r}_t^{(l)}} \left(\frac{dU_{C_i,t^*}}{d\mathbf{r}_t^{(l)}} \right) & \frac{d}{d\phi_t^{(l)}} \left(\frac{dU_{C_i,t^*}}{d\mathbf{r}_t^{(l)}} \right) & \frac{d}{d\mathbf{r}_t^{(m)}} \left(\frac{dU_{C_i,t^*}}{d\mathbf{r}_t^{(l)}} \right) & \frac{d}{d\phi_t^{(m)}} \left(\frac{dU_{C_i,t^*}}{d\mathbf{r}_t^{(l)}} \right) \\ \left(\frac{d}{d\mathbf{r}_t^{(l)}} \left(\frac{dU_{C_i,t^*}}{d\phi_t^{(l)}} \right) \right)^T & \frac{d}{d\phi_t^{(l)}} \left(\frac{dU_{C_i,t^*}}{d\phi_t^{(l)}} \right) & \left(\frac{d}{d\mathbf{r}_t^{(m)}} \left(\frac{dU_{C_i,t^*}}{d\phi_t^{(l)}} \right) \right)^T & \frac{d}{d\phi_t^{(m)}} \left(\frac{dU_{C_i,t^*}}{d\phi_t^{(l)}} \right) \\ \frac{d}{d\mathbf{r}_t^{(l)}} \left(\frac{dU_{C_i,t^*}}{d\mathbf{r}_t^{(m)}} \right) & \frac{d}{d\phi_t^{(l)}} \left(\frac{dU_{C_i,t^*}}{d\mathbf{r}_t^{(m)}} \right) & \frac{d}{d\mathbf{r}_t^{(m)}} \left(\frac{dU_{C_i,t^*}}{d\mathbf{r}_t^{(m)}} \right) & \frac{d}{d\phi_t^{(m)}} \left(\frac{dU_{C_i,t^*}}{d\mathbf{r}_t^{(m)}} \right) \\ \left(\frac{d}{d\mathbf{r}_t^{(l)}} \left(\frac{dU_{C_i,t^*}}{d\phi_t^{(m)}} \right) \right)^T & \frac{d}{d\phi_t^{(l)}} \left(\frac{dU_{C_i,t^*}}{d\phi_t^{(m)}} \right) & \left(\frac{d}{d\mathbf{r}_t^{(m)}} \left(\frac{dU_{C_i,t^*}}{d\phi_t^{(m)}} \right) \right)^T & \frac{d}{d\phi_t^{(m)}} \left(\frac{dU_{C_i,t^*}}{d\phi_t^{(m)}} \right) \end{bmatrix}$$

(3.21)

The submatrices in Eq. (3.21) can be calculated as

$$\frac{d}{d\mathbf{r}_t^{(l)}} \left(\frac{dU_{C_i,t^*}}{d\mathbf{r}_t^{(m)}} \right) = M \begin{bmatrix} k_{C_i} & k_{C_i} \\ k_{C_i} & k_{C_i} \end{bmatrix}$$

($M = 1$ if $l = m$, $M = -1$ else)

(3.22)

$$\frac{d}{d\phi_i^{(l)}} \left(\frac{dU_{C_i,t^*}}{d\mathbf{r}_i^{(l)}} \right) = k_{C_i} \left(\frac{d\{\mathbf{T}_{C_i,t^*}^{(l)}\}^{-1}}{d\phi_i^{(l)}} \mathbf{s}_{C_i,t^*}^{(l)} \right); \quad \frac{d}{d\phi_i^{(l)}} \left(\frac{dU_{C_i,t^*}}{d\mathbf{r}_i^{(m)}} \right) = -k_{C_i} \left(\frac{d\{\mathbf{T}_{C_i,t^*}^{(l)}\}^{-1}}{d\phi_i^{(l)}} \mathbf{s}_{C_i,t^*}^{(l)} \right) \quad (3.23)$$

$$\frac{d}{d\phi_i^{(m)}} \left(\frac{dU_{C_i,t^*}}{d\mathbf{r}_i^{(l)}} \right) = -k_{C_i} \left(\frac{d\{\mathbf{T}_{C_i,t^*}^{(m)}\}^{-1}}{d\phi_i^{(m)}} \mathbf{s}_{C_i,t^*}^{(m)} \right); \quad \frac{d}{d\phi_i^{(m)}} \left(\frac{dU_{C_i,t^*}}{d\mathbf{r}_i^{(m)}} \right) = k_{C_i} \left(\frac{d\{\mathbf{T}_{C_i,t^*}^{(m)}\}^{-1}}{d\phi_i^{(m)}} \mathbf{s}_{C_i,t^*}^{(m)} \right) \quad (3.24)$$

$$\frac{d}{d\phi_i^{(l)}} \left(\frac{dU_{C_i,t^*}}{d\phi_i^{(l)}} \right) = k_{C_i} \left(\frac{d\{\mathbf{T}_{C_i,t^*}^{(l)}\}^{-1}}{d\phi_i^{(l)}} \mathbf{s}_{C_i,t^*}^{(l)} \right)^T \left(\frac{d\{\mathbf{T}_{C_i,t^*}^{(l)}\}^{-1}}{d\phi_i^{(l)}} \mathbf{s}_{C_i,t^*}^{(l)} \right) + k_{C_i} \left(\frac{d}{d\phi_i^{(l)}} \left(\frac{d\{\mathbf{T}_{C_i,t^*}^{(l)}\}^{-1}}{d\phi_i^{(l)}} \mathbf{s}_{C_i,t^*}^{(l)} \right)^T \right) \left(\mathbf{u}_{C_i,t^*} \right) \quad (3.25)$$

$$\frac{d}{d\phi_i^{(m)}} \left(\frac{dU_{C_i,t^*}}{d\phi_i^{(m)}} \right) = k_{C_i} \left(\frac{d\{\mathbf{T}_{C_i,t^*}^{(m)}\}^{-1}}{d\phi_i^{(m)}} \mathbf{s}_{C_i,t^*}^{(m)} \right)^T \left(\frac{d\{\mathbf{T}_{C_i,t^*}^{(m)}\}^{-1}}{d\phi_i^{(m)}} \mathbf{s}_{C_i,t^*}^{(m)} \right) + k_{C_i} \left(\frac{d}{d\phi_i^{(m)}} \left(\frac{d\{\mathbf{T}_{C_i,t^*}^{(m)}\}^{-1}}{d\phi_i^{(m)}} \mathbf{s}_{C_i,t^*}^{(m)} \right)^T \right) \left(\mathbf{u}_{C_i,t^*} \right) \quad (3.26)$$

$$\frac{d}{d\phi_i^{(m)}} \left(\frac{dU_{C_i,t^*}}{d\phi_i^{(l)}} \right) = -k_{C_i} \left(\frac{d\{\mathbf{T}_{C_i,t^*}^{(l)}\}^{-1}}{d\phi_i^{(l)}} \mathbf{s}_{C_i,t^*}^{(l)} \right)^T \left(\frac{d\{\mathbf{T}_{C_i,t^*}^{(m)}\}^{-1}}{d\phi_i^{(m)}} \mathbf{s}_{C_i,t^*}^{(m)} \right) \quad (3.27)$$

Similarly, the Jacobean matrix \mathbf{J}_{A_j,t^*} for the anchoring spring k_{A_j} connecting block l and ground is given by

$$\mathbf{J}_{A_j,t^*} = \frac{d}{d\mathbf{q}_i^{(l)}} \left(\frac{dU_{A_j,t^*}}{d\mathbf{q}_i^{(l)}} \right) = \begin{bmatrix} \frac{d}{d\mathbf{r}_i^{(l)}} \left(\frac{dU_{A_j,t^*}}{d\mathbf{r}_i^{(l)}} \right) & \frac{d}{d\phi_i^{(l)}} \left(\frac{dU_{A_j,t^*}}{d\mathbf{r}_i^{(l)}} \right) \\ \left(\frac{d}{d\mathbf{r}_i^{(l)}} \left(\frac{dU_{A_j,t^*}}{d\phi_i^{(l)}} \right) \right)^T & \frac{d}{d\phi_i^{(l)}} \left(\frac{dU_{A_j,t^*}}{d\phi_i^{(l)}} \right) \end{bmatrix} \quad (3.28)$$

The components of the submatrices in Eq. (3.28) can be calculated as

$$\frac{d}{d\mathbf{r}_i^{(l)*}} \left(\frac{dU_{A_j, i^*}}{d\mathbf{r}_i^{(l)*}} \right) = \begin{bmatrix} k_{A_j} & k_{A_j} \\ k_{A_j} & k_{A_j} \end{bmatrix} \quad (3.29)$$

$$\frac{d}{d\phi_i^{(l)*}} \left(\frac{dU_{A_j, i^*}}{d\mathbf{r}_i^{(l)*}} \right) = k_{A_j} \left(\frac{d \left\{ \mathbf{T}_{A_j, i^*}^{(l)} \right\}^{-1}}{d\phi_i^{(l)*}} \mathbf{s}_{A_j, i^*}^{(l)} \right) \quad (3.30)$$

$$\frac{d}{d\phi_i^{(l)*}} \left(\frac{dU_{A_j, i^*}}{d\phi_i^{(l)*}} \right) = k_{A_j} \left(\frac{d \left\{ \mathbf{T}_{A_j, i^*}^{(l)} \right\}^{-1}}{d\phi_i^{(l)*}} \mathbf{s}_{A_j, i^*}^{(l)} \right)^T \left(\frac{d \left\{ \mathbf{T}_{A_j, i^*}^{(l)} \right\}^{-1}}{d\phi_i^{(l)*}} \mathbf{s}_{A_j, i^*}^{(l)} \right) + k_{A_j} \left(\frac{d}{d\phi_i^{(l)*}} \left(\frac{d \left\{ \mathbf{T}_{A_j, i^*}^{(l)} \right\}^{-1}}{d\phi_i^{(l)*}} \right) \mathbf{s}_{A_j, i^*}^{(l)} \right)^T \left(\mathbf{u}_{A_j, i^*} \right) \quad (3.31)$$

The Jacobean matrix \mathbf{J}_{G_w, i^*} for the gearing spring k_{G_w} that connects block l and gear block l is given by

$$\mathbf{J}_{G_w, i^*} = \frac{d}{d\mathbf{q}_i^{(l)*}} \left(\frac{dU_{G_w, i^*}}{d\mathbf{q}_i^{(l)*}} \right) = \begin{bmatrix} \frac{d}{d\mathbf{r}_i^{(l)*}} \left(\frac{dU_{G_w, i^*}}{d\mathbf{r}_i^{(l)*}} \right) & \frac{d}{d\phi_i^{(l)*}} \left(\frac{dU_{G_w, i^*}}{d\mathbf{r}_i^{(l)*}} \right) \\ \left(\frac{d}{d\mathbf{r}_i^{(l)*}} \left(\frac{dU_{G_w, i^*}}{d\phi_i^{(l)*}} \right) \right)^T & \frac{d}{d\phi_i^{(l)*}} \left(\frac{dU_{G_w, i^*}}{d\phi_i^{(l)*}} \right) \end{bmatrix} \quad (3.32)$$

The components of the submatrices in Eq. (3.32) are

$$\frac{d}{d\mathbf{r}_i^{(l)*}} \left(\frac{dU_{G_w, i^*}}{d\mathbf{r}_i^{(l)*}} \right) = \begin{bmatrix} 4k_{G_w} & 4k_{G_w} \\ 4k_{G_w} & 4k_{G_w} \end{bmatrix} \quad (3.33)$$

$$\frac{d}{d\phi_i^{(l)*}} \left(\frac{dU_{G_w, i^*}}{d\mathbf{r}_i^{(l)*}} \right) = \left(\frac{d}{d\mathbf{r}_i^{(l)*}} \left(\frac{dU_{G_w, i^*}}{d\phi_i^{(l)*}} \right) \right)^T = \sum_{a=1}^4 k_{G_w} \left(\frac{d \left\{ \mathbf{T}_{G_w, i^*}^{(l)} \right\}^{-1}}{d\phi_i^{(l)*}} \mathbf{s}_{G_w, i^*}^{(l)} \right) \quad (3.34)$$

$$\begin{aligned}
\frac{d}{d\phi_i^{(l)}} \left(\frac{dU_{G_w, t^*}}{d\phi_i^{(l)}} \right) &= \sum_{a=1}^4 k_{G_w} \left(\frac{d \left\{ \mathbf{T}_{G_w, t^*}^{(l)} \right\}^{-1}}{d\phi_i^{(l)}} \mathbf{s}_{G_w, a, t^*}^{(l)} \right)^T \left(\frac{d \left\{ \mathbf{T}_{G_w, t^*}^{(l)} \right\}^{-1}}{d\phi_i^{(l)}} \mathbf{s}_{G_w, a, t^*}^{(l)} \right) \\
&\quad + \sum_{a=1}^4 k_{G_w} \left(\frac{d}{d\phi_i^{(l)}} \left(\frac{d \left\{ \mathbf{T}_{G_w, t^*}^{(l)} \right\}^{-1}}{d\phi_i^{(l)}} \right) \mathbf{s}_{G_w, a, t^*}^{(l)} \right)^T \left(\mathbf{u}_{G_w, a, t^*} \right)
\end{aligned} \tag{3.35}$$

3.3 Gear-linkage mechanism synthesis formulation

Section 3.2 described the modeling method and the analysis procedure to determine the state variables. In this section, we present a topology optimization formulation to synthesize gear-linkage mechanisms. For the optimization formulation, the objective function and constraint equations are expressed in terms of continuous design variables, allowing the use of numerically efficient gradient-based optimization to update the design variables. The sensitivities of the objective function and constraint equations will also be derived.

Note that the key variables to determine the mechanism configuration are the stiffness of the springs. Because they should reach their bound values upon convergence, they are interpolated as functions of the design variables (ξ_i):

$$k_i = k_{\max} \times (\xi_i)^p \quad \text{for } 0 < \xi_{\min} \leq \xi_i \leq 1; \quad i = 1, 2, \dots, N_t; \quad N_t = N_c + N_a + N_g \quad (3.36)$$

As ξ_i approaches ξ_{\min} and ξ_{\max} , k_i approaches its lower (k_{\min}) and upper (k_{\max}) bounds. The springs having lower and upper bound values represent disconnected and connected states, between two adjacent blocks. Moreover, to avoid a numerical singularity, ξ_{\min} is assigned a small non-zero number (here, ξ_{\min} is set to 10^{-3}). The symbol p denotes a penalization factor (here, p is set to 3), which is introduced to move k_i towards its bound values. The penalization technique has been a standard method for structural optimization [33], and it has also been found to be effective when used in conjunction with topology-optimization-based mechanism synthesis [8, 13]

Employing the work-transmittance efficiency formulation developed in earlier work [11], the following optimization formulation is established for the synthesis of gear-linkage mechanisms:

$$\begin{aligned}
& \underset{\xi \in R^{N_t}}{\text{Minimize}} && 1 - \bar{\eta} \\
& \text{Subject to} && \psi_{t^*}(\xi) \leq \varepsilon \quad (t^* = 1, 2, \dots, T) \\
& && (\varepsilon: \text{a small value of tolerance})
\end{aligned} \tag{3.37}$$

Here, T is the total time step needed to complete the input motion. The symbol $\bar{\eta}$ denotes the mean value of the work transmittance efficiency (η_{t^*}) over the total time step of the input motion. It is defined as follows:

$$\bar{\eta} = \frac{1}{T} \sum_{t^*=1}^T \eta_{t^*} \quad (0 = \bar{\eta}_{\min} \leq \bar{\eta} \leq \bar{\eta}_{\max} = 1) \tag{3.38}$$

The explicit expression of η_{t^*} is given as [11]

$$\eta_{t^*} = \frac{W_{out,t^*}}{W_{inp,t^*}} = \frac{W_{out,t^*}}{W_{out,t^*} + U_{t^*}} \quad (t^* = 1, 2, \dots, T) \tag{3.39}$$

In Eq. (3.39), the work transmittance efficiency η_{t^*} represents the ratio of the output work W_{out,t^*} to the input work W_{inp,t^*} . The last expression in Eq. (3.39) is obtained by means of $W_{inp,t^*} = W_{out,t^*} + U_{t^*}$. When defining W_{out,t^*} , the following form of the external force \mathbf{F}_{ext,t^*} is assumed to be applied at the end effector:

$$\mathbf{F}_{ext,t^*} = F_0 \frac{\hat{\mathbf{r}}_{Q,t^*-1} - \hat{\mathbf{r}}_{Q,t^*}}{\|\hat{\mathbf{r}}_{Q,t^*-1} - \hat{\mathbf{r}}_{Q,t^*}\|} \tag{3.40}$$

The expression in Eq. (3.40) represents a force of constant magnitude F_0 acting

against the motion of the end effector. Once \mathbf{F}_{ext,t^*} is given, W_{out,t^*} can be calculated as

$$W_{out,t^*} = \sum_{t=1}^{t^*} \mathbf{F}_{ext,t} \cdot (\mathbf{r}_{Q,t-1} - \mathbf{r}_{Q,t}) \quad (3.41)$$

The constraint equation is used to ensure that the target path $\hat{\mathbf{r}}_{Q,t^*}$ is correctly traced by and the actual path \mathbf{r}_{Q,t^*} of the end effector of the synthesized mechanism. Therefore, we introduce the Euclidean error ψ_{t^*} to measure the distance between $\hat{\mathbf{r}}_{Q,t^*}$ and \mathbf{r}_{Q,t^*} at every time step t^* , as

$$\psi_{t^*}(\xi) = \|\mathbf{r}_{Q,t^*}(\xi) - \hat{\mathbf{r}}_{Q,t^*}\| \quad (t^* = 1, 2, \dots, T) \quad (3.42)$$

The significance of using the formulation (3.39) which minimizes $1 - \bar{\eta}$, equivalently, maximizes $\bar{\eta}$ ensures that the correct kinematic degree of freedom (DOF) is obtained. The target path is to be traced by satisfying the constraint equations.

Accordingly, the sensitivity of the objective function with respect to the design variable (ξ) is written as

$$\frac{d(1 - \bar{\eta})}{d\xi} = -\frac{d\bar{\eta}}{d\xi} = -\frac{1}{T} \sum_{t^*=1}^T \frac{d\eta_{t^*}}{d\xi} \quad (3.43)$$

The sensitivity of the work transmittance efficiency η_{t^*} at time step t^* is

$$\begin{aligned}
\frac{d\eta_{t^*}}{d\xi} &= \frac{d\mathbf{k}}{d\xi} \frac{d\eta_{t^*}}{d\mathbf{k}} \\
&= \frac{d\mathbf{k}}{d\xi} \left(\frac{dW_{out,t^*}}{d\mathbf{k}} \frac{\partial}{\partial W_{out,t^*}} \left(\frac{W_{out,t^*}}{W_{out,t^*} + U_{t^*}} \right) + \frac{dU_{t^*}}{d\mathbf{k}} \frac{\partial}{\partial U_{t^*}} \left(\frac{W_{out,t^*}}{W_{out,t^*} + U_{t^*}} \right) \right) \\
&= \frac{d\mathbf{k}}{d\xi} \left(\frac{dW_{out,t^*}}{d\mathbf{k}} \frac{U_{t^*}}{(W_{out,t^*} + U_{t^*})^2} - \frac{dU_{t^*}}{d\mathbf{k}} \frac{W_{out,t^*}}{(W_{out,t^*} + U_{t^*})^2} \right)
\end{aligned} \tag{3.44}$$

where the vector \mathbf{k} consists of the spring stiffness:

$$\begin{aligned}
\mathbf{k} &= \{k_1, k_2, \dots, k_{N_t}\}^T \\
&= \{k_{C_1}, k_{C_2}, \dots, k_{C_{N_c}}, k_{A_1}, k_{A_2}, \dots, k_{A_{N_a}}, k_{G_1}, k_{G_2}, \dots, k_{G_{N_g}}\}^T
\end{aligned} \tag{3.45}$$

By using Eq. (3.36), $d\mathbf{k}/d\xi$ can be explicitly given as

$$\frac{d\mathbf{k}}{d\xi} = \text{diag}(p \times k_{\max} \times (\xi_1)^{p-1}, p \times k_{\max} \times (\xi_2)^{p-1}, \dots, p \times k_{\max} \times (\xi_{N_t})^{p-1}) \tag{3.46}$$

To obtain $dW_{out,t^*}/d\mathbf{k}$, Eq. (3.41) is used:

$$\frac{dW_{out,t^*}}{d\mathbf{k}} = \sum_{t=1}^{t^*} \mathbf{F}_{ext,t} \cdot \frac{d}{d\mathbf{k}} (\mathbf{r}_{Q,t-1} - \mathbf{r}_{Q,t}) \tag{3.47}$$

and $dU_{t^*}/d\mathbf{k}$ is expressed as

$$\frac{dU_{t^*}}{d\mathbf{k}} = \frac{\partial U_{t^*}}{\partial \mathbf{k}} + \frac{d\mathbf{v}_{t^*}}{d\mathbf{k}} \frac{\partial U_{t^*}}{\partial \mathbf{v}_{t^*}} \tag{3.48}$$

To calculate $d\mathbf{v}_{t^*}/d\mathbf{k}$, we use $dF_{int,t^*}/d\mathbf{k} = 0$ given the fact that Eq. (3.15) and

$dF_{ext,t^*}/d\mathbf{k} = 0$. Accordingly, we have

$$0 = \frac{dF_{int,t^*}}{d\mathbf{k}} = \frac{\partial F_{int,t^*}}{\partial \mathbf{k}} + \frac{d\mathbf{v}_{t^*}}{d\mathbf{k}} \frac{\partial F_{int,t^*}}{\partial \mathbf{v}_{t^*}} = \frac{\partial^2 U_{t^*}}{\partial \mathbf{v}_{t^*} \partial \mathbf{k}} + \frac{d\mathbf{v}_{t^*}}{d\mathbf{k}} \frac{\partial^2 U_{t^*}}{\partial \mathbf{v}_{t^*} \partial \mathbf{v}_{t^*}} = \frac{\partial^2 U_{t^*}}{\partial \mathbf{v}_{t^*} \partial \mathbf{k}} + \frac{d\mathbf{v}_{t^*}}{d\mathbf{k}} \mathbf{J}_{t^*} \tag{3.49}$$

where $F_{int,t^*} = \partial U_{t^*} / \partial \mathbf{v}_{t^*}$ is used. From Eq. (3.48),

$$\frac{d\mathbf{v}_{i^*}}{d\mathbf{k}} = -\frac{\partial^2 U_{i^*}}{\partial \mathbf{v}_{i^*} \partial \mathbf{k}} [\mathbf{J}_{i^*}]^{-1} \quad (3.50)$$

Because all necessary expressions to calculate $d\eta_{i^*}/d\xi$ and $d\mathbf{k}/d\xi$ are determined, the sensitivity of the objective function can now be explicitly evaluated. Correspondingly, the sensitivity of the constraint equation is expressed as follows:

$$\frac{d\psi_{i^*}}{d\xi} = \frac{d\mathbf{k}}{d\xi} \frac{d\psi_{i^*}}{d\mathbf{k}} = \frac{d\mathbf{k}}{d\xi} \frac{d}{d\mathbf{k}} \left(\left\| \mathbf{r}_{\varrho, i^*}(\xi) - \hat{\mathbf{r}}_{\varrho, i^*} \right\| \right) = \frac{d\mathbf{k}}{d\xi} \frac{d\mathbf{v}_{i^*}}{d\mathbf{k}} \frac{\partial}{\partial \mathbf{v}_{i^*}} \left(\left\| \mathbf{r}_{\varrho, i^*}(\xi) - \hat{\mathbf{r}}_{\varrho, i^*} \right\| \right) \quad (3.51)$$

The sensitivity of the objective function and the constraint equations derived above are used to update the design variable ξ . In this paper, the update of the design variables is done using the method of moving asymptotes [34], an efficient gradient-based optimization approach. Introducing heterogeneous design variables significantly increases the difficulty of optimization. From this perspective, replacing the presence of gear elements with four translational springs instead of torsional springs is highly efficient. Similarly, when it comes to gear ratios, stacking gear blocks of various ratios proved to be more efficient in terms of optimization convergence, rather than introducing the gear ratio itself as a design variable.

3.4 Synthesis of various mechanisms by the proposed method

This section aims to investigate the validity and effectiveness of the proposed method for synthesizing various mechanisms involving link and gear components. Specifically, the following three case studies are considered using the same modeling and formulation:

Case Study 1 to investigate if geared mechanisms having a different gear ratio can be synthesized. Specifically, the synthesis of geared five-bar mechanisms (GFBMs) with an output gear having a gear ratio of 1 or 0.5 are considered.

Case Study 2 to investigate if GFBMs with an output gear having the gear ratio of 1 located at different positions can be synthesized.

Case Study 3 to investigate if the developed formulation can be uniformly applied to linkage-only mechanisms and gear-linkage mechanisms having a different number of gears.

To solve the synthesis problems considered in Case Studies 1, 2 and 3, the design domain Ω is assumed to be superposed of one linkage design space S_L and two gear design spaces consisting of discretized gear blocks having gear ratios of 1 and 0.5. Accordingly, the design domain Ω for all case studies is defined as:

$$\Omega = S_L \oplus {}^{<1>}S_G \oplus {}^{<0.5>}S_G \quad (3.52)$$

Each of the three design spaces is discretized by 3×3 rigid or gear blocks for the present analysis. More blocks may be used to find more complicated

mechanisms, but it was demonstrated that quite general mechanisms can be synthesized with the 3×3 discretization in the synthesis of linkage-only mechanisms [8, 13]. Accordingly, we will mainly work with the 3×3 discretization. Because nine blocks are used to discretize S_L , $^{<1>}S_G$, and $^{<0.5>}S_G$ ($N_B = 9$), $2 \times 2 \times 3 + 2 \times 3 \times 2 = 24$ block-connecting springs ($N_c = 24$) and $4 \times 8 = 32$ anchoring springs ($N_a = 32$) are used in S_L . The anchoring springs are used to connect four corner nodes of eight blocks, excluding input block 1. Also except for input block 1, each of the remaining eight rigid blocks in S_L is connected to its counterpart gear blocks of $^{<1>}S_G$ and $^{<0.5>}S_G$. Therefore, there are $8 \times 2 = 16$ independent sets of gearing springs ($N_g = 16$) in the gear design spaces. Altogether, 72 design variables are used to solve the mechanism synthesis problems by formulation (3.22). Here, it is remarked that even the relatively coarse 3×3 discretization model can produce numerical candidate mechanisms when 72 design variables take on their lower or upper bound values. To test the validity of the proposed method, the target mechanisms in all examples belong the space of the candidate mechanisms. (After verifying the validity of the method, we, in the future, aim to synthesize a mechanism that does not belong to the space of candidate mechanisms by incorporating shape optimization in which the

nodal coordinates of the discretizing blocks can be also varied.)

To synthesize a mechanism using formulation (3.22), the initial values of the design variables (ξ) should be provided. For all case studies considered here, the initial values of the design variables controlling block-connecting and anchoring springs were set to $0.5 \approx (\xi_{\min} + \xi_{\max})/2$ in order to start with unbiased intermediate states. On the other hand, the initial values of the design variables controlling the gearing springs were set to ξ_{\min} to allow the rigid blocks to move freely upon the initial iterations. The values of the other parameters used for the optimization are as follows:

$$\begin{aligned} k_{\max} &= 10^4 & \varepsilon &= 0.005 \\ F_0 &= 1 & \xi_{\min} &= 10^{-3} & T &= 36 \end{aligned} \quad (3.53)$$

These values were shown be effective in earlier instances of block-based topology optimization for mechanism synthesis [8, 13].

3.4.1 Case Study 1 : Gear-linkage mechanisms with a gear of different gear ratios

With Case Study 1, we aim to investigate if gear-linkage mechanisms can be successfully synthesized by the proposed formulation. Specifically, we attempt to recover the geared five-bar mechanisms (GFBM) shown in Figs. 3.6(a) and 3.7(a) by the developed block model. The GFBM in Fig. 3.6(a) includes an output gear with a gear ratio of 1, while the GFBM in Fig. 3.7(a) includes an output gear with a

gear ratio of 0.5. The equivalent block models of the GFBMs in Figs. 3.6(a) and 3.7(a) are shown in Figs. 3.6(b) and 3.7(b), respectively. As illustrated in Figs. 3.6(b) and 3.7(b), gears in the target mechanisms are located at block 3. Therefore, the corresponding blocks working as gears are indicated by $\langle 1 \rangle B^{(3)}$ for the problem in Fig. 3.6(b) and $\langle 0.5 \rangle B^{(3)}$ for the problem in Fig. 3.7(b). Other blocks are gearless rigid blocks denoted by $\langle l \rangle B^{(l)}$ ($l=1, \dots, 9; l \neq 3$). The locations of the end effector are also illustrated in Figs. 3.6(b) and 3.7(b). They are located at the center of block 7. The output paths illustrated in Figs. 3.6(b) and 3.7(b) represent the loci of the end effectors as the input blocks are rotated by 360° . To synthesize the target mechanisms shown in Figs. 3.6(b) and 3.7(b), the target output paths are depicted in the ground model shown in Figs. 3.6(c) and 3.7(c). Although not explicitly sketched in these figures, the ground model consists of three design spaces $S_L \oplus \langle 1 \rangle S_G \oplus \langle 0.5 \rangle S_G$. Because a gear having a gear ratio of 1 (0.5) is needed for the problem shown in Fig. 3.6 (Fig. 3.7), a ground model consisting only of $S_L \oplus \langle 1 \rangle S_G$ ($S_L \oplus \langle 0.5 \rangle S_G$) may be needed. However, we used $S_L \oplus \langle 1 \rangle S_G \oplus \langle 0.5 \rangle S_G$ intentionally to demonstrate that the developed method can successfully find a gear having the required gear ratio only.

As mentioned earlier, 72 design variables were used to solve this mechanism synthesis problem using the initial values and the optimization parameters given above. The convergence histories of the objective function ($\bar{\eta}$ is plotted instead of $1-\bar{\eta}$) and the maximum value of the constraint equation $\bar{\psi}_{\max} = \max_{i^* \in \{1, 2, \dots, T\}} \psi_{i^*}$ are

correspondingly plotted in Figs. 3.6(d) and 3.7(d). These figures show that the mean transmittance efficiency $\bar{\eta}$ successfully reached (nearly) unity at convergence for both problems, confirming that the correct DOF, which is 1, is attained. Moreover, $\bar{\psi}_{\max}$, denoting the Euclidean error, falls within the tolerance error, confirming that the target path is correctly traced for both problems. The values of the design variables at convergence should reach either ξ_{\max} or ξ_{\min} in order to identify the synthesized mechanism. Figs. 3.6(e) and 3.7(e) show that most of the design variables reached ξ_{\max} or ξ_{\min} , indicating that the target mechanisms are successfully recovered.

Figures 3.8 and 3.9 show the evolutions of the synthesized mechanisms expressed by the proposed block ground model. In these figures, the lower left block (block 1; see Fig. 3.4(b) for block numbering) represents the input block. The remaining blocks denote rigid blocks belonging to S_L . They are connected to zero-length block-connecting springs, but the springs are not shown explicitly in the plot. Fig. 3.8 shows that rigid blocks 5, 6, 8, and 9 move independently before convergence because the block-connecting springs connected to the blocks do not have the maximum stiffness values. However, they move as a single megablock near or at convergence by forming M-block 5-6-8-9. On the other hand, M-block 6-8-9 excluding block 5 moves as a single megablock in Fig. 3.9. In this case, ${}^{<>B^{(5)}}$ is a floating block that does not affect the motion of the mechanism because it is not connected to any of its adjacent blocks.

In Figs. 3.8 and 3.9, gear blocks belonging to $\langle 1 \rangle S_G$ and $\langle 0.5 \rangle S_G$ are not explicitly plotted. However, $\langle 1 \rangle G^{(l)}$ and $\langle 0.5 \rangle G^{(l)}$ ($l = 2, 3, \dots$) are expressed as gears in different tones which depend on the stiffness values of the corresponding gearing springs. We draw the gear shown in Fig. 3.8 twice as large as that in Fig. 3.9 to indicate that the smaller gear has a gear ratio of 0.5 and the larger gear has a gear ratio of 1. As the iteration proceeds, gears appear more distinctly inside block 3 in the plots, transforming $B^{(3)}$ into $\langle 1 \rangle B^{(3)}$ in Fig. 8 and $\langle 0.5 \rangle B^{(3)}$ in Fig. 3.9. The actual paths of the synthesized mechanisms trace the target paths more accurately as convergence is reached. Although not explicitly listed, $\langle 1 \rangle k_{G_3}$ became k_{\max} for the problem in Fig. 3.8 and $\langle 0.5 \rangle k_{G_3}$ became k_{\max} for the problem in Fig. 3.9 at convergence, while the stiffness values of the other gearing springs become k_{\min} . To identify the synthesized mechanism from the converged block models, the snapshots of the block configurations at different time steps are analyzed. The inter-block connectivity and the spring stiffness values are also examined. (Currently, the identification process is manual but an identification algorithm can be developed, as done in [11] for the nonlinear bar ground model.) The results in Figs. 3.8 and 3.9 demonstrate that gear-linkage mechanisms can be successfully synthesized by the proposed method.

3.4.2 Case Study 2 : Gear-linkage mechanisms with a gear at different locations

Through Case Study 2, we aim to demonstrate that a gear-linkage mechanism with a gear located at various locations can be successfully synthesized by the proposed method. Here, we consider the synthesis of two gear-linkage mechanisms with a gear having a gear ratio of 1, one with a gear at the block 2 location and the other with a gear at the block 3 location. Because the gear-linkage mechanism equipped with an output gear at the block 3 location was synthesized in Case Study 1, we only need to check if the output gear at the block 2 location can be successfully identified in the synthesized mechanism.

The target mechanism to be synthesized is shown in Fig. 3.10(a) while its equivalent representation by the proposed block ground model is shown in Fig. 3.10(b). Fig. 3.10(b) sketches the output motion of the end effector. The ground model used for this problem is identical to the ground model used in Case Study 1; the synthesis is performed with the design space consisting of $S_L \oplus {}^{<1>}S_G \oplus {}^{<0.5>}S_G$. Because the convergence history for this problem is very similar to that shown in Figs. 3.6(d) and 3.7(d), it is not plotted here. The evolution history of the synthesized mechanism configuration is shown in Fig. 3.11. As convergence is reached, the actual path of the synthesized mechanism approaches the target path accurately. It is also confirmed that the stiffness of the gearing spring ${}^{<1>}k_{G_2}$ has reached k_{\max} , forming a gear at the block 2 location. Through Case Study 2, the

proposed method is shown to successfully be able to synthesize a gear-linkage mechanism having a gear at different locations.

3.4.3 Case study 3 : Gear-linkage mechanisms having a different number of gears

Thus far, we have demonstrated the synthesis of gear-linkage mechanisms having a single gear train, i.e., a single output gear in a mechanism. In general, there will be no pre-knowledge of the number of output gears to be used for synthesis problem. Therefore, we consider Case Study 3 to determine if the proposed method can be effective when used to synthesize gear-linkage mechanisms involving either zero, one, or two output gears. Specifically, we consider the synthesis of a linkage-only mechanism (i.e., a mechanism without an output gear), as shown in Fig. 3.12(a), and a geared mechanism with two pairs of gear trains (i.e., a gear-linkage mechanism with two output gears), as shown in Fig. 3.12(b). (A mechanism having only one gear was synthesized in the previous case studies.)

The mechanism shown in Fig. 3.12(a) is a four-bar linkage mechanism without any gear component. Therefore, this mechanism can be synthesized by the existing SBM. However, it is important to check if the mechanism without a gear component can also be successfully synthesized by the developed gear-linkage synthesis method. Additionally, in Fig. 3.12(b), a gear-linkage mechanism having

two output gears is represented by ${}^{<1>}B^{(3)}$ and ${}^{<1>}B^{(7)}$ in the proposed block model.

As noted in the caption of Fig. 3.12, the design domain consisting of $S_L \oplus {}^{<1>}S_G \oplus {}^{<0.5>}S_G$ is used for the problems considered in Case Study 3. The convergence histories for the synthesis problems shown in Figs. 3.12(a) and 3.12(b) are plotted in Figs. 3.13(a) and 3.13(b), respectively. First, stable convergence is observed in both problems; $\bar{\eta}$ reached its maximum value of 1, and the Euclidean error is sufficiently small.

When synthesizing the four-bar linkage mechanism shown in Fig. 3.12(a), Fig. 3.13(a) shows that all of the gearing springs have values close to k_{\min} , implying that all rigid blocks are disconnected from gear blocks. Therefore, the synthesized mechanism shown in Fig. 3.14 has no gear component, representing a linkage-only mechanism. At convergence, the target path is correctly traced by the synthesized mechanism. This example shows that the proposed block ground model can successfully synthesize linkage-only mechanisms.

When synthesizing a geared mechanism involving two output gears, the iteration history is shown in Fig. 3.13(b), which shows stable convergence. The distribution of the spring stiffness values obtained at convergence, also plotted in Fig. 3.13(b), shows that only the gearing springs connecting $B^{(3)}$ to ${}^{<1>}G^{(3)}$ and $B^{(7)}$ to ${}^{<1>}G^{(7)}$ reach their maximum value of k_{\max} , leading to ${}^{<1>}B^{(3)}$ and ${}^{<1>}B^{(7)}$. Consequently, the desired gear-linkage mechanism having two output gears is obtained by our synthesis method and the evolution history of the synthesis

mechanism shown in Fig. 3.15 demonstrates the successful synthesis of the target mechanism.

3.5 Synthesis of various mechanisms with shape optimization.

To design diverse and complicated mechanisms, the design domain should be discretized with high resolution rigid blocks. However, if topology optimization and shape optimization are carried out simultaneously, we can obtain the same results with a lower resolution design domain [12]. Similar to Gear-SBM, a gear-linkage mechanism can be designed to generate more diverse paths than the results of the previous section if shape optimization is carried out simultaneously. We will utilize the shape SBM model from Chapter 3.2 to analyze the shape of the Gear-SBM. The center position and radius of the gear component need to be used to represent the dimensions of the gear component. In other words, design variables corresponding to the center position and radius of the gear component are necessary for shape optimization. However, the complexity and time cost of the optimization process directly depend on the number of design variables. Therefore, it's crucial to represent the mechanism with the least number design variables. To this end, we represent the center of the gear component with a state variable utilizing additional shape design variables by using the shape SBM model from Chapter 3.2, which uses the geometric center of the rigid block as state variables. Additionally, the distance between the geometrical center and the node location can be used to represent the radius of the gear component. The shape SBM model using the geometrical center (Yim et al. [15]) can express the dimensions of the gear component by shape design variables that express the dimensions of the rigid links because the geometrical center as well as the location of each node changes when

the four nodes of the rigid block change relatively. As a result, we suggest a gear-SBM method, as shown in Fig. 3.17, that may simultaneously express the topology and dimensions of gears and rigid parts with a limited number of design variables.

Based on the modeling above, the same optimization equation as in Eq. (3.21) can easily be constructed, and we will proceed with the three case studies of synthesizing three different type of mechanisms. As shown in Fig. 3.18, three different types of gear-linkage mechanism can be synthesized with the single unified method.

3.6 Summary.

Through this study, we presented a new method of topology-optimization-based mechanism synthesis to determine simultaneously the type, number and dimension of mechanisms. The use of two design spaces representing the linkage and gear spaces in an extended framework of the SBM was found effective, where each design space was discretized by rigid or gear blocks. Because every gear block is connected by artificial springs to its counterpart rigid block occupying the same location, the presence of gear components can be controlled by adjusting the stiffness of the springs. If more than one gear ratio is expected to be needed, more than one gear design space can be flexibly used to form additional gear design spaces. Because a gradient-based algorithm was used by employing continuous design variables, the overall optimization-based synthesis method was numerically efficient.

As the verification of the developed approach, several known mechanisms were found to be successfully recovered. Specifically, we were able to synthesize a linkage-only four-bar mechanism, gear-linkage mechanisms having a single output gear at different locations and a gear-linkage mechanism having two output gears. More importantly, the same modeling technique and formulation were used to synthesize dissimilar gear-linkage mechanisms producing different output paths. This implies that the developed method is flexibly effective to synthesize mechanisms of different types.

In spite of the success in determining simultaneously the type, number, and

dimension of a general mechanism by the proposed method, there are several limitations to overcome before the developed method can be practically useful. First, we only tested the developed method to recover known mechanisms. Therefore, we should be able to synthesize unknown unique mechanisms while outperforming existing mechanisms. Second, all synthesis problems under consideration here were planar; the synthesis of spatial gear-linkage mechanisms would be more interesting and challenging. In spite of several issues to overcome, this method is expected to open a new approach towards practically useful automated methods of mechanism synthesis.

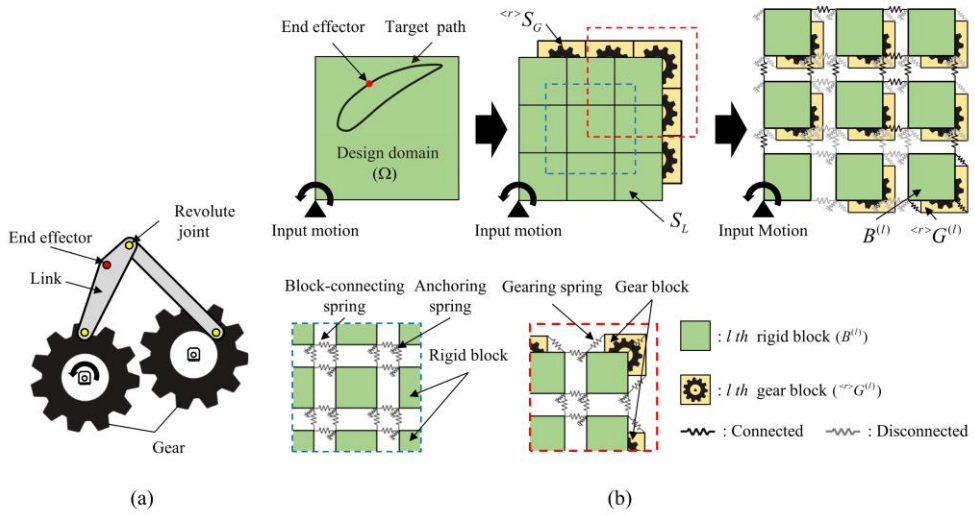


Fig. 3.1 (a) A typical geared mechanism we aim to synthesize by the proposed topology optimization method and (b) the proposed block ground model consisting of two design spaces, the linkage design space S_L , and the gear design space ${}^{<r>S}_G$. (The superscript “ r ” in ${}^{<r>S}_G$ denotes the gear ratio.)

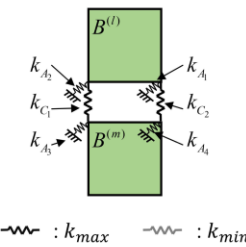


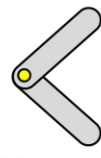
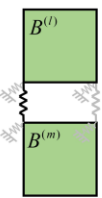
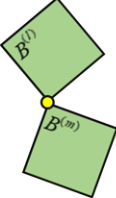
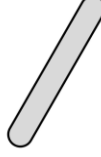
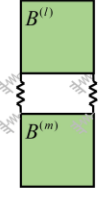


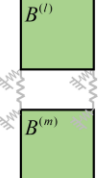
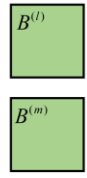
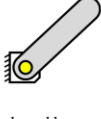
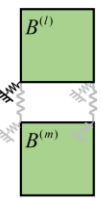
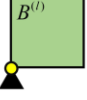
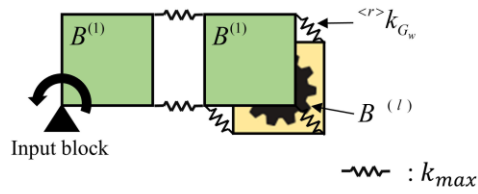
	Mechanism	Block modeling		Stiffness of springs
 <p>  : k_{\max}  : k_{\min} </p>	 2 links are connected with revolute joints			$k_{C_1} = k_{\max}$ <i>otherwise</i> k_{\min}
	 Rigidly connected		 M-block $l-m$	$k_{C_1} = k_{\max}, k_{C_2} = k_{\max}$ <i>otherwise</i> k_{\min}
	 Disconnected			<i>All stiffness of springs are</i> k_{\min}
	 Anchored by revolute joint			$k_{A_1} = k_{\max}$ <i>otherwise</i> k_{\min}

Fig. 3.2 Representation of various joints in the S_L -based SBM. The stiffness of the block-connecting and anchoring springs take on the bound value (k_{\min} and k_{\max}) to simulate various joint states.



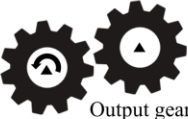
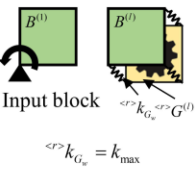
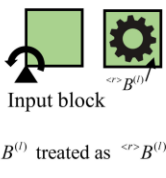
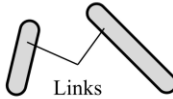
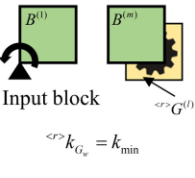
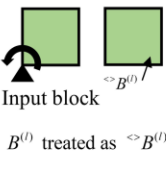
Mechanism	Block modeling	
 Input gear Output gear Geared mechanisms gear connected	 Input block $\langle F \rangle k_{G_w} = k_{max}$	 Input block $B^{(l)}$ treated as $\langle F \rangle B^{(l)}$
 Links Linkage mechanisms no gear connected	 Input block $\langle F \rangle k_{G_w} = k_{min}$	 Input block $B^{(l)}$ treated as $\langle F \rangle B^{(l)}$

Fig. 3.3 Representation of gear and link components in several simple mechanisms using the new notations, $\langle F \rangle B^{(l)}$ and $\langle F \rangle B^{(l)}$.

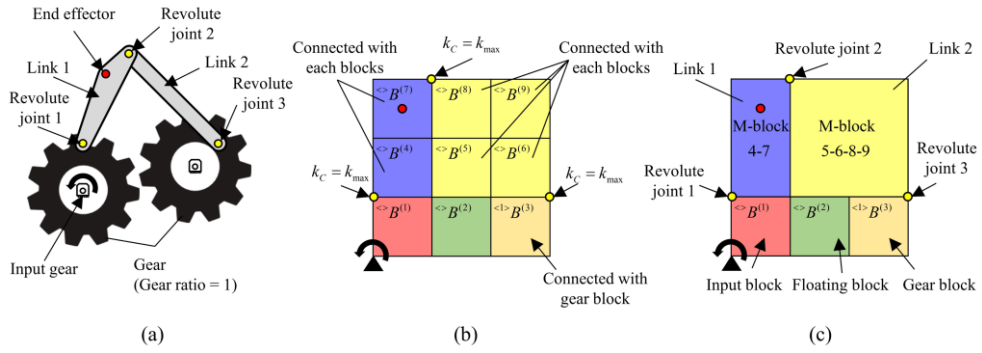


Fig. 3.4 (a) A geared five-bar mechanism (GFBM). (b) The representation of the GFBM by the developed modeling approach. (c) The representation of the GFBM in terms of M-blocks, a floating block, and a gear block.

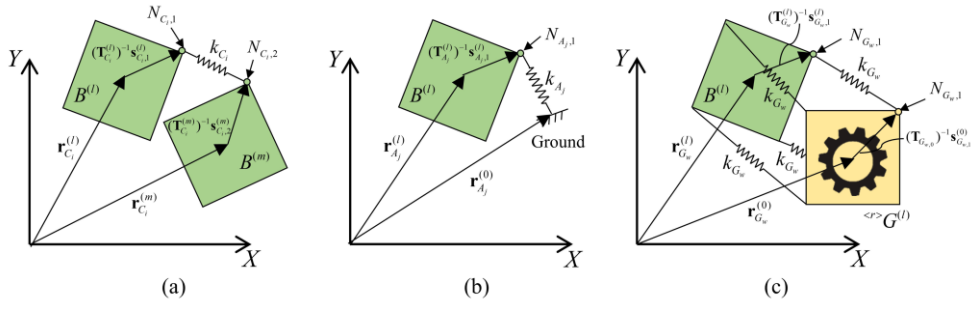


Fig. 3.5 Various configurations inducing the deformation of springs. Each configuration consisting of : (a) $B^{(l)}$, $B^{(m)}$ (an adjacent block of $B^{(l)}$) and the block-connecting spring k_{C_i} ; (b) $B^{(l)}$, the ground, and the anchoring spring k_{A_j} ; and (c) $B^{(l)}$, $\langle r \rangle G^{(l)}$, and a set of gearing springs denoted by $\langle r \rangle k_{G_w}$.

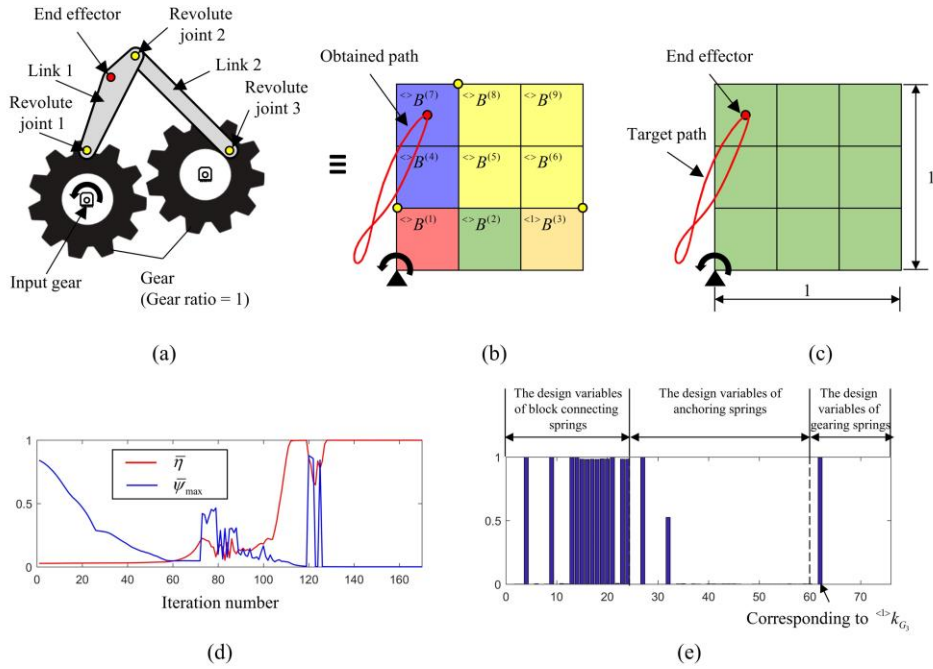


Fig. 3.6 The synthesis of a geared five-bar mechanism having an output gear with a gear ratio of 1 by the proposed formulation: (a) The target mechanism, (b) its representation in terms of rigid and gear blocks, (c) the ground model consisting of $S_L \oplus \langle \cdot \rangle S_G \oplus \langle 0.5 \rangle S_G$ employed for the synthesis, d) the convergence history of $\bar{\eta}$, and $\bar{\psi}_{\max} = \max_{i \in \{1,2,\dots,T\}} \psi_i^*$, (e) the values of the design variables (ξ_i) at convergence.

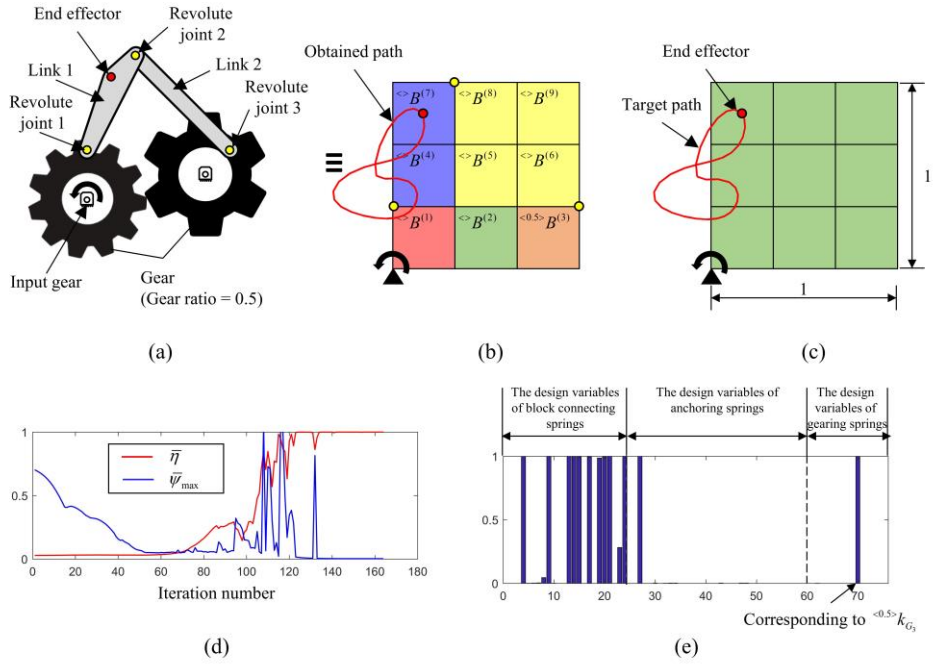


Fig. 3.7 The synthesis of a geared five-bar mechanism having an output gear with a gear ratio of 0.5 by the proposed formulation: (a) The target mechanism, (b) its representation in terms of rigid and gear blocks, (c) the ground model consisting of $S_L \oplus \langle 1 \rangle S_G \oplus \langle 0.5 \rangle S_G$ employed for the synthesis, d) the convergence history of $\bar{\eta}$, and $\bar{\psi}_{\max} = \max_{t^* \in \{1, 2, \dots, T\}} \psi_{t^*}$ (e) the values of the design variables (ξ_i) at convergence.

Iteration Number	Time step $t^* = 9$	Time step $t^* = 18$	Time step $t^* = 27$	Time step $t^* = 36$	Target path — Actual path —
1 (Initial)					
11					
21					
41					
101					
Converged					

Fig. 3.8 The evolution history of the synthesized mechanism expressed by the proposed block ground model for the synthesis problem defined in Fig. 6. The numbers in the figure represent the block number.

Iteration Number	Time step $t^* = 9$	Time step $t^* = 18$	Time step $t^* = 27$	Time step $t^* = 36$	Target path — Actual path —
1 (Initial)					
11					
21					
41					
101					
Converged					

Fig. 3.9 The evolution history of the synthesized mechanism expressed by the proposed block ground model for the synthesis problem defined in Fig. 7. The numbers in the figure represent the block number.

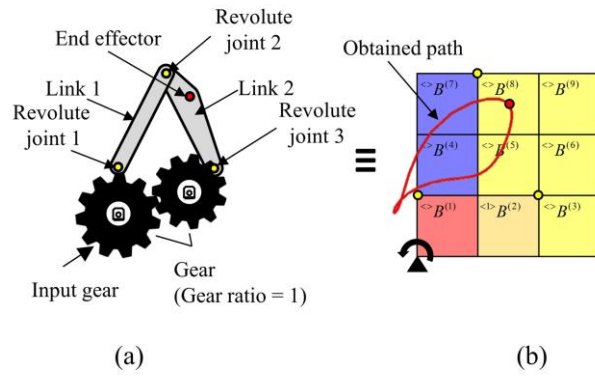


Fig. 3.10 The synthesis of a geared five-bar mechanism having an output gear with the gear ratio of 1 located at the block 2 location. (a) The target mechanism and (b) its representation in terms of rigid and gear blocks.

Iteration Number	Time step $t^* = 9$	Time step $t^* = 18$	Time step $t^* = 27$	Time step $t^* = 36$	Target path — Actual path —*
1 (Initial)					
11					
21					
41					
101					
Converged					

Fig. 3.11 The evolution history of the synthesized mechanism expressed by the proposed block ground model for the synthesis problem defined in Fig. 3.10.

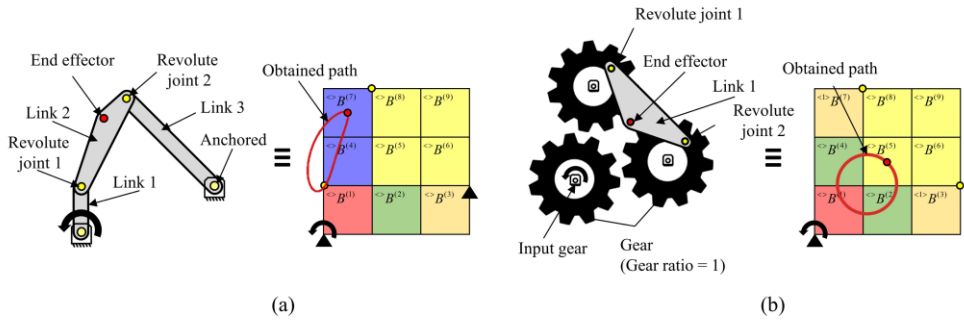


Fig. 3.12 The synthesis of (a) a linkage-only mechanism and (b) a geared mechanism with two gear trains (i.e. two output gears). The ground model consisting of $S_L \oplus {}^{<1>}S_G \oplus {}^{<0.5>}S_G$ is used in applying the proposed topology optimization based synthesis method.

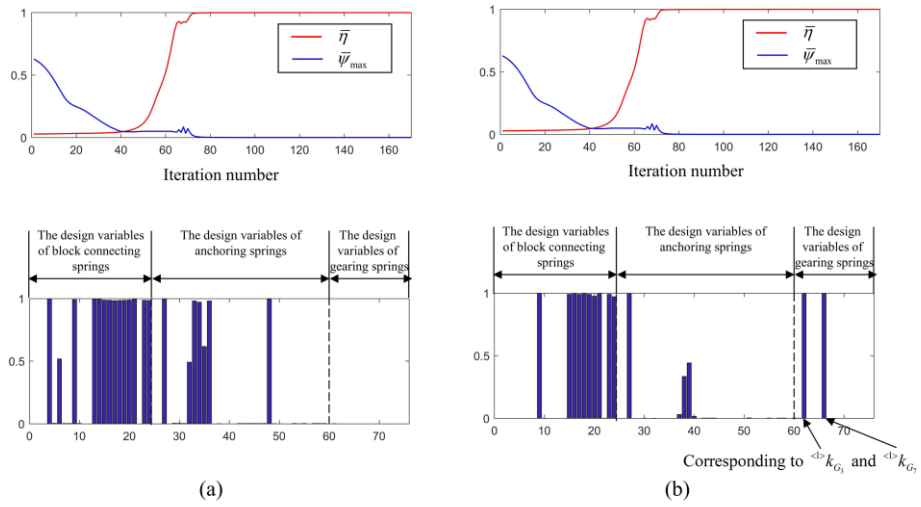


Fig. 3.13 The convergence histories of $\bar{\eta}$ and $\bar{\psi}_{\max} = \max_{i^* \in \{1,2,\dots,T\}} \psi_{i^*}$ and the values of the design variables (ξ_i) at convergence for (a) the problem depicted in Fig. 12(a) and (b) the problem in Fig. 12(b). The design variables having intermediate values are associated with the anchoring springs connected to floating blocks. Therefore, they do not affect the synthesized mechanism configurations.

Iteration Number	Time step $t^* = 9$	Time step $t^* = 18$	Time step $t^* = 27$	Time step $t^* = 36$	Target path — Actual path —*
1 (Initial)					
11					
21					
41					
101					
Converged					

Fig. 3.14 The evolution history of the synthesized mechanism expressed by the proposed block ground model for the synthesis problem defined in Fig. 12(a).

Iteration Number	Time step $t^* = 9$	Time step $t^* = 18$	Time step $t^* = 27$	Time step $t^* = 36$	Target path — Actual path —
1 (Initial)					
11					
21					
41					
101					
Converged					

Fig. 3.15 The evolution history of the synthesized mechanism expressed by the proposed block model for the synthesis problem defined in Fig. 12(b).

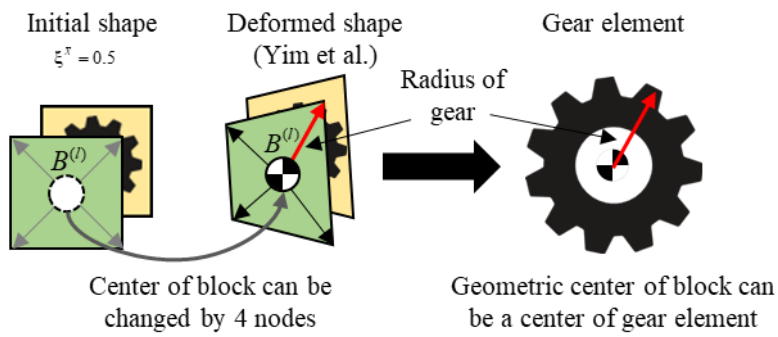


Fig. 3.16 The shape SBM modeling method with geometric center to represent the block shape and gear components

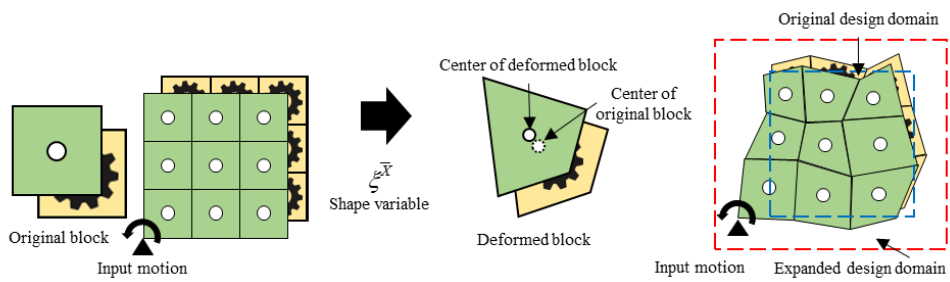


Fig. 3.17 The proposed shape Gear SBM with the shape design variables. With shape design variables we can represent the shape of gear-linkage mechanism

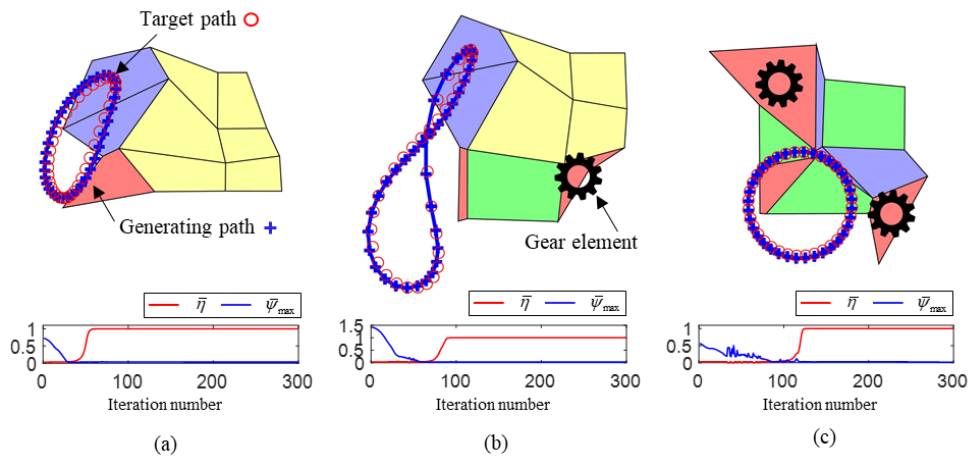


Fig. 3.18 The three synthesis case studies: (a) linkage only mechanism (b) GFBM and (c) two gear linkage mechanism was synthesized

CHAPTER 4.

Topology Optimization of Planar Pulley-Linkage Mechanisms

4.1 Overview

To design a robot mechanism, several mechanical components are required. Among them, the pulley component is a fundamental component used in various robot systems such as robot arms and hands [35-37], since pulley components enable the mechanism to be designed as serial mechanisms, which can synthesize large trajectories. Therefore, the synthesis of pulley-linkage mechanisms has become an essential research subject. However, designing the topology (number and connectivity of pulley components and rigid links) and dimensions of the pulley components simultaneously has been a challenge, as the trajectories of the pulley-linkage mechanism vary significantly based on the topology of pulley components. For this reasons, previous engineers used sequential approaches to determine the topology and dimensions of the pulley-linkage mechanisms [35-40]. For example, they first determine the topology of the pulley-linkage mechanism before using dimensional synthesis to determine the pulley locations and link sizes. However, this approach has limitations, as it may be challenging to find novel

mechanisms beyond the designer's intuition. To overcome this limitation, we propose a topology optimization-based approach for mechanism design that can simultaneously determine the topology and dimensions of the pulley-linkage mechanism.

The topology optimization-based mechanism design approach has taken much attention as it does not require a predetermined topology of the mechanism as a baseline design. To perform topology optimization, the design domain needs to be discretized using a ground structure. It is known that various mechanical components, such as gear components, can be considered in the stacked spring-connected rigid block model (SBM) [41], as shown in Fig. 4.1. The stacked-SBM concept involves stacking the linkage design space with different design spaces, where the stiffness of the artificial zero length springs represents various topology and dimensions of the linkage mechanism. To represent the pulley components, however, we propose the multi stacked SBM to discretize the design domain. To define additional design spaces for other mechanical components, the corresponding block must be defined to discretize the design domain. For instance, a gear block that rotates concerning the input block was used to represent the gear components [41]. Therefore, we propose a new pulley block that rotates concerning each rigid block in the linkage design space to represent the pulley components. If the previous gear-SBM used a single stacking of gear blocks corresponding to input blocks in the linkage design space (Fig. 4.1(a)), the newly proposed pulley-SBM can represent various connectivity of pulley components by multi-stacking all

pulley blocks corresponding to all rigid blocks, as shown in Fig. 4.1(b).

Each pulley block is connected to a rigid block using four pulley springs with the same stiffness design variables, where the stiffness represents the connectivity of the pulley components. Thus, the topology and dimensions of the pulley-linkage mechanism can be represented by the stiffness of two types of springs: the artificial zero-length springs in the linkage design space and the pulley springs. To synthesize the pulley-linkage mechanism, we propose a gradient-based topology optimization formulation to simultaneously determine the stiffness of the two springs. With this modeling method and optimization formulation, we will synthesize the pulley-linkage mechanism and the linkage-only mechanism in the following paper.

4.2 Modeling, analysis and optimization formulation

4.2.1 Modeling method of multi-stacked SBM

The design domain should be discretized into a number of blocks, each of which should be capable of representing mechanical components in order to carry out the mechanism synthesis within the framework of topology optimization. To this end, we propose a modeling technique for simultaneously representing the topology and dimensions of the pulley-linkage mechanism. The proposed multi-stacked SBM ground model, depicted in Fig. 4.1(b), treats the design domain as a superposition of multi design spaces S_L and ${}^{<r>}S_P (m=1,2,\dots,N_b)$. The S_L stands for the linkage design space discretized by rigid blocks $B^{(l)}$, while ${}^{<r>}S_P$ denotes the pulley design space discretized by pulley blocks ${}^{<r>}P^{(l)} (l=1,2,\dots,N_b)$. Here, N_b is the total number of rigid blocks discretizing the design domain. In addition, the size of the pulley blocks ${}^{<r>}P^{(l)} (m=1,\dots,l-1,l+1,\dots,N_b)$ are identical to those of the rigid blocks in $B^{(l)}$. Therefore, as shown in Fig. 4.1(b), the design domain (Ω) can be symbolically defined as

$$\Omega = S_L \oplus {}^{<r>}S_{P(1)} \oplus {}^{<r>}S_{P(2)} \cdots {}^{<r>}S_{P(N_b)} \quad (4.1)$$

To modeling a pulley component, we firstly define the pulley block to represent the pulley component. As shown in Fig. 4.2, ${}^{<r>}P^{(l)}$ is a pulley block stacked on the l -th rigid block ($B^{(l)}$) with an r rotating relationship value with the m -th rigid

block ($B^{(m)}$). For example, in linkage design space (same as previous SBM), the geometric center ($[X_t^{(l)}, Y_t^{(l)}]$) and its pulley angle ($[\theta_t^{(l)}]$) of l -th rigid block are expressed as state variables at time step t [15] :

$$\mathbf{q}_t^{(l)} = [X_t^{(l)}, Y_t^{(l)}, \theta_t^{(l)}]^T \quad (4.2)$$

Because the shape of $B^{(l)}$ and ${}^{<r>}_{(m)}P^{(l)}$ is identical, the geometric center of ${}^{<r>}_{(m)}P^{(l)}$ and $B^{(l)}$ are same. Therefore, the state variables (${}^{<r>}_{(m)}\mathbf{p}_t^{(l)}$) of pulley block (${}^{<r>}_{(m)}P^{(l)}$) can be written as follows

$${}^{<r>}_{(m)}\mathbf{p}_t^{(l)} = [X_t^{(l)}, Y_t^{(l)}, r\theta_t^{(m)}]^T \quad (4.3)$$

Now, we can define the ${}^{<r>}_{(m)}S_P$ with all ${}^{<r>}_{(m)}P^{(l)}$ ($l=1, \dots, m-1, m+1, \dots, N_b$) as shown in Fig. 4.2. In other words, ${}^{<r>}_{(m)}S_P$ is a design space containing all ${}^{<r>}_{(m)}P^{(l)}$ with $B^{(m)}$ and r rotation relationship values, meaning that the corresponding ${}^{<r>}_{(m)}P^{(l)}$ is connected to $B^{(m)}$ as a pulley component. And it can be said that the previous gear design space [41] in Fig. 4.1(a) can be represented as ${}^{<r>}_{(1)}S_P$ when the input block is 1-st block (${}^{<r>}S_G = {}^{<r>}_{(1)}S_P$). Therefore, we can represent the various configuration (connectivity) between pulley components by multi stacking the ${}^{<r>}_{(m)}S_P$ ($m=1, 2, \dots, N_b$) over the S_L .

To represent different topologies and dimensions of pulley-linkage mechanisms, the design domain is discretized into several blocks, each of which is connected by artificial zero length springs with their stiffness values. Therefore, there are two different types of artificial zero length springs in this proposed modeling method,

one that connects block and block (block connecting spring) or block and ground (anchoring spring) to represent rigid links and revolute joints, and another type of artificial zero-length spring is pulley springs that connect four corners of pulley block and rigid block. Fig. 4.3 shows how design domain discretized by three adjacent rigid blocks ($B^{(1)}, B^{(2)}, \text{ and } B^{(3)}$) and three pulley blocks (${}^{<r>}_{(1)}R^{(2)}, {}^{<r>}_{(1)}R^{(3)}, \text{ and } {}^{<r>}_{(2)}R^{(3)}$) can represent the pulley connection mechanism. To simplify the design domain, we only consider ${}^{<r>}_{(m)}R^{(l)}$ ($l > m$) pulley blocks in this Fig. 4.3. First, let's talk about how linkage design space can represent the rigid links and revolute joints with its corresponding stiffness values. As illustrated in Fig. 4.3, it is assumed that adjacent rigid blocks (or a rigid block and the ground) are connected by block-connecting springs (the anchoring springs) that have stiffness values. When the block-connecting spring's (anchoring spring's) stiffness is expressed \mathbf{k}_C (\mathbf{k}_A), this can vary between the lower limit state $\mathbf{k}_C = 0$ ($\mathbf{k}_A = 0$) and the upper limit state $\mathbf{k}_C = k_{\max}$ ($\mathbf{k}_A = k_{\max}$) (k_{\max} : a pre-selected value). The lower limit state means that the rigid blocks are disconnected, and upper limit state means the rigid blocks are connected at that corner. As a result, various mechanism states can be represented as shown in Fig. 4.3(b) by using different connectivity states with block-connecting springs and anchoring springs that adopt their lower or upper stiffness values. To learn more, go to Yu et al. [12].

Here, we describe the function of the pulley design space ${}^{<r>}_{(m)}S_R$, a newly introduced for representing pulley components. As depicted in Fig. 4.3(a), all

pulley blocks (${}^{<r>}R_{(1)}^{(2)}$, ${}^{<r>}R_{(1)}^{(3)}$, and ${}^{<r>}R_{(2)}^{(3)}$) share a geometric center of rigid blocks $B^{(l)}$, and they are all connected to the rigid blocks at the four corners by four zero-length pulley springs. Additionally, the four pulley springs are controlled by the same stiffness value of ${}^{<r>}k_{(m)R}^{(l)}$ to reduce the design variables same as previous method [41]. Under the condition of ${}^{<r>}k_{(m)R}^{(l)} = k_{\max}$, $B^{(l)}$ rotates in a manner that is identical to that of ${}^{<r>}R_{(m)}^{(l)}$ which rotates with respect to the r rotation relationship with $B^{(m)}$. Other then, when ${}^{<r>}k_{(m)R}^{(l)} = k_{\min}$, the rotation of $B^{(l)}$ are not affected by ${}^{<r>}R_{(m)}^{(l)}$ as shown in Fig. 4.3(c). Additionally, as shown in Fig. 4.3(c), ${}^{<r>}k_{(1)R}^{(2)} = k_{\max}$ means $B^{(1)}$ and $B^{(2)}$ are connected by pulley component and also ${}^{<r>}k_{(2)R}^{(3)} = k_{\max}$ means $B^{(2)}$ and $B^{(3)}$ are connected. With the combination of pulley spring's stiffness as shown in left side of Fig. 4.3(c), serially connected pulley-linkage as shown in the right side of Fig. 4.3(a) can be represented.

4.2.2 Analysis method to multi-stacked SBM

In the previous section, we used a multi-stacked SBM to represent a pulley-linkage mechanism with the stiffness of artificial zero-length springs. Quasi-static nonlinear analysis can be used to conduct kinematic analysis of SBM-based mechanisms. If the position of the input block is given for each time step, analysis should be used to determine the positions of the other rigid blocks. Let's say, for instance, that $B^{(1)}$ identifies rotation as the input motion. The total state variable

vector (\mathbf{v}_t) in this case represents the states of all rigid blocks in the time step (t), with the exception of $B^{(1)}$. This can be expressed as follows:

$$\mathbf{v}_t = \left[\left(\mathbf{q}_t^{(2)} \right)^T, \left(\mathbf{q}_t^{(3)} \right)^T, \dots, \left(\mathbf{q}_t^{(N_b)} \right)^T \right]^T \quad (4.4)$$

In terms of total state variable vector (\mathbf{v}_t), the quasi-static force equilibrium for SBM method can be written as [11-13, 41]:

$$\mathbf{F}_{\text{int},t}(\mathbf{v}_t) - \mathbf{F}_{\text{ext},t} = 0 \quad (t=1, \dots, T; \text{ where } T \text{ is total time step}) \quad (4.5)$$

$\mathbf{F}_{\text{int},t}$ is the internal force in design domain caused by artificial zero length springs (block connecting springs, anchoring springs, and pulley springs) and calculated as $\mathbf{F}_{\text{int},t}(\mathbf{v}_t) = dU_{SBM,t} / d\mathbf{v}_t$. And this $U_{SBM,t}(\mathbf{v}_t)$ can be obtained from the stretched lengths (δ_{C_i} for i -th block connecting spring, δ_{A_j} for j -th anchoring spring and ${}^{<r>}_{(l)}\delta_R^{(m)}$ for corresponding pulley spring) of all artificial zero length springs in design domain as follows:

$$U_{SBM,t} = \sum_{i=1}^{N_c} \frac{1}{2} k_{C_i} \left(\delta_{C_i} \right)^2 + \sum_{j=1}^{N_a} \frac{1}{2} k_{A_j} \left(\delta_{A_j} \right)^2 + \sum_{m=1}^{N_b} \sum_{l=1}^{N_b} 4 \cdot \left(\frac{1}{2} {}^{<r>}_{(l)} k_R^{(m)} \left({}^{<r>}_{(l)} \delta_R^{(m)} \right)^2 \right) \quad (4.6)$$

where, N_c and N_a is the total number of block connecting and anchoring springs. And $\mathbf{F}_{\text{ext},t}$ is the external force in the opposite direction of the desired path ($\hat{\mathbf{r}}_t^{\text{end}}$) with the magnitude of F_0 as follows:

$$\mathbf{F}_{\text{ext},t} = F_0 \cdot \frac{\hat{\mathbf{r}}_{t-1}^{\text{end}} - \hat{\mathbf{r}}_t^{\text{end}}}{\left\| \hat{\mathbf{r}}_{t-1}^{\text{end}} - \hat{\mathbf{r}}_t^{\text{end}} \right\|} \quad (\text{where, } F_0 = 1) \quad (4.7)$$

\mathbf{F}_{ext} was intentionally introduced to control the rotatability of the mechanism in the

previous SBM-based synthesis method. Now, we can obtain the generating motion of pulley-linkage mechanism from quasi static force equilibrium from Eq. (4.5). Details of the process and calculation of the equation can be found in Refs [12, 15].

4.2.3 Optimization formulation for stacked SBM

In previous section, we discussed how to analyze the motion of pulley-linkage mechanism using a multi-stacked SBM method that represents the various topologies and dimensions of the mechanism. Here, considering the desired paths, we offer an optimization formula for designing the 1-DOF pulley linkage mechanism. With the proposed multi-stacked SBM, designing a pulley-linkage mechanism means determining the stiffness values of the block connecting springs, anchoring springs and pulley springs. The following design variables are used to conveniently interpolate the stiffness of each spring [41]:

$$k_{C_i} = k_{\max} \left(\xi_{C_i} \right)^3, k_{A_i} = k_{\max} \left(\xi_{A_i} \right)^3, \text{ and } {}^{<r>}_{(l)} k_R^{(m)} = k_{\max} \left({}^{<r>}_{(l)} \xi_R^{(m)} \right)^3 \quad (4.8)$$

Therefore, the design variables (ξ) to be determined through the optimization process are as follows:

$$\xi = \{ \xi_{C_1}, \xi_{C_2}, \dots, \xi_{C_{N_c}}, \xi_{A_1}, \xi_{A_2}, \dots, \xi_{A_{N_a}}, {}^{<r>}_{(1)} \xi_R^{(2)}, {}^{<r>}_{(1)} \xi_R^{(3)}, \dots, {}^{<r>}_{(N_b)} \xi_R^{(N_b-1)} \}^T \quad (4.9)$$

Now, we can construct a gradient-based optimization method that is numerically effective to synthesize the desired mechanism because all design variables are real values between 0 and 1. As a result, the optimization formulation for the synthesis of pulley-linkage mechanisms is established as follows:

$$\begin{aligned}
& \underset{\xi \in R^{N_c + N_a + N_R}}{\text{Minimize}} && 1 - \bar{\eta} \\
& \text{Subject to} && \Psi_t(\xi) \leq \varepsilon \quad (t = 1, 2, \dots, T) \\
& && (\varepsilon: \text{a small value of tolerance})
\end{aligned} \tag{4.10}$$

where N_R is the total number of pulley springs. In earlier SBM-based topology optimization, the mean value of work transmission efficiency ($\bar{\eta}$) was utilized as the objective function to manage the degree of freedom of the synthesized mechanism as 1-DOF [11]. The explicit expression of work transmittance efficiency η_t at time step t is given as [11]

$$\eta_t = \frac{W_{out,t}}{W_{inp,t}} = \frac{W_{out,t}}{W_{out,t} + U_{SBM,t}} \quad (t = 1, 2, \dots, T) \tag{4.11}$$

In Eq. (4.11), the work transmittance efficiency η_t represents the ratio of the output work $W_{out,t}$ to the input work $W_{inp,t}$. The last expression in Eq. (4.11) is obtained by means of $W_{inp,t} = W_{out,t} + U_{SBM,t}$. $W_{out,t}$ is caused by $\mathbf{F}_{ext,t}$ at the end effector and can be calculated as follows:

$$\Psi_t(\xi) = \|\mathbf{r}_{Q,t}(\xi) - \hat{\mathbf{r}}_{Q,t}\| \quad (t = 1, 2, \dots, T) \tag{4.12}$$

Using the optimization formulation (4.10), the moving asymptotes method [34] was used to update the design variable. When employing a gradient-based optimization optimizer to update design variables, analytical sensitivities of objective function and constraint equations are necessary. Since they can be calculated rather easily, they are not provided clearly here.

4.3 Synthesis of various mechanisms by the proposed method

Some synthesis problems will be conducted to check the validity and effectiveness of the suggested method for synthesizing various mechanisms, such as rigid links and pulley components. To demonstrate whether the suggested method can consider diverse pulley-linkage mechanisms, we conducted mechanisms synthesis problems with different target paths while employing the same modeling and formulation. The 3×3 discretized design domain is used to solve the following synthesis problems, and -1 is considered as a rotation relationship value ($r = -1$). In this chapter, we only consider ${}^{<-1>}_{(m)}P^{(l)}$ ($l > m$) because ${}^{<-1>}_{(m)}P^{(l)}$ and ${}^{<-1>}_{(l)}P^{(m)}$ have the same effect when $r = -1$. Thus, the design domain (Ω) can be defined as:

$$\Omega = S_L \oplus {}^{<-1>}_{(1)}S_P \oplus {}^{<-1>}_{(2)}S_P \cdots {}^{<-1>}_{(8)}S_P \quad (4.13)$$

Different rotation relationship value design spaces ${}^{<r>}_{(1)}S_P \oplus {}^{<r>}_{(2)}S_P \cdots {}^{<r>}_{(8)}S_P$ can be stacked and employed if more complex rotation ratios are needed same as previous gear-stacked SBM technique to consider the gear ratio [41]. To avoid providing a biased initial circumstance for gradient-based optimization approach, the design variable's initial value is set to $0.5 \approx (\xi_{\min} + \xi_{\max})/2$ and the following values for other parameters utilized during the entire optimization process are:

$$\varepsilon = 0.05, \quad \xi_{\min} = 10^{-4}, \quad \xi_{\max} = 1, \quad k_{\max} = 10^3, \quad T = 36 \quad (4.14)$$

In earlier gradient-based mechanism topology optimization synthesis [12, 15, 41], the values (4.14) are shown to be effective.

The first synthesis problem can be represented as Fig. 4.4(a). To verify the effectiveness of the proposed method, the target path can be obtained from the mechanism within the design domain. With the synthesis problem definition in Fig. 4.4(a), we can define the optimization formulation (4.10) to determine 96 design variables (24 block connecting design variables ξ_{C_i} , 36 anchoring design variables ξ_{A_j} and 36 pulley design variables $\begin{smallmatrix} <-1> \\ (l) \end{smallmatrix} \xi_R^{(m)}$). Fig. 4.4(b) illustrates the synthesized stacked SBM as a result of the optimization procedure. The synthesized M-blocks 1-4 and M-blocks 7-8-9 mean the megablock which is rigidly connected between blocks and dummy blocks mean the rigid blocks that cannot affect the motion of synthesized results. Additionally, the evolutionary history in Fig. 4.5(b) and the iteration history of the objective function and constraint equations in Fig. 4.5(a) ensure that the synthesized results satisfy the design conditions. And following the postprocess, it is possible to state that the synthesized mechanism is the 1-DOF pulley-linkage mechanism depicted in Fig. 4.5(c).

And other synthesis problems are conducted with different target motions as shown in Fig. 4.6. Various mechanism can be synthesized with same modeling and optimization formulation except for the different target paths. As a result of synthesized with different target paths, different types of mechanism pulley-linkage mechanism (Fig. 4.6(a)), linkage only mechanism (Fig. 4.6(b)) and gear-linkage mechanism (Fig. 4.6(c)) can be synthesized at the same time. Therefore, various topologies and dimensions of pulley-linkage mechanism even linkage only

mechanism can be synthesized with a single method.

Another synthesis problem with 4×2 discretized design domain is conducted, where multi serial 1-DOF pulley-linkage mechanism can be synthesized. As shown in Fig. 4.8 two serial connected pulley mechanism (${}^{<-1>}_{(1)}R^{(7)}$ and ${}^{<-1>}_{(7)}R^{(8)}$) are synthesized. Because we used multi-stacked SBM, we can also obtained multi serial connected pulley-linkage mechanism.

To design diverse and complicated mechanisms, the design domain should be discretized with high resolution rigid blocks. However, if topology optimization and shape optimization are carried out simultaneously, we can obtain the same results with a lower resolution design domain [12]. We will utilize the shape SBM model from Chapter 2 to analyze the shape of the pulley-SBM. As shown in Fig. 4.9, we can simultaneously synthesize the topology and dimensions of pulley-linkage mechanism with low resolution.

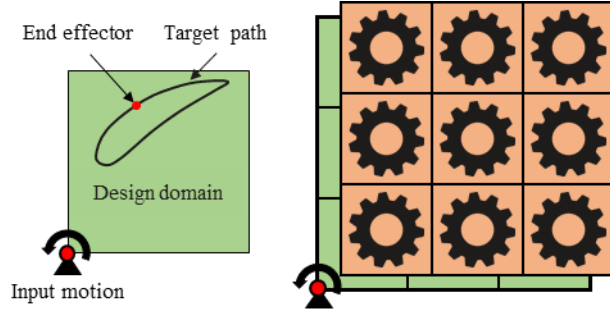
4.4 Summary.

In this study, we present a novel method for topology optimization-based mechanism synthesis that can consider both parallel and serial mechanisms, which extends the mechanism topology optimization framework to include pulley and link components simultaneously. To achieve this, we propose pulley blocks that can represent all rotational relations with other rigid blocks, which represent the rigid links, and use a multi-stacked SBM to represent the linkage and pulley components. By connecting every pulley block to its counterpart rigid block occupying the same location with artificial springs, the presence of pulley components can be controlled by adjusting the stiffness of the springs. This multi-stacked method effectively considers the relationship between multiple components.

Our proposed method includes all previous synthesis methods that use linkage-only SBM and gear SBM, as pulley components can be represented as gear components with anchoring conditions. Moreover, our optimization-based synthesis method, which uses a gradient-based algorithm with continuous design variables, is numerically efficient.

We successfully verified our approach by synthesizing several known mechanisms, such as a linkage-only four-bar mechanism, gear-linkage mechanisms, and multi-pulley serial mechanism. Importantly, our method demonstrates the flexibility to synthesize dissimilar mechanical components mechanisms that produce different output paths using the same modeling technique and formulation. Therefore, our developed method can be effectively used to synthesize mechanisms

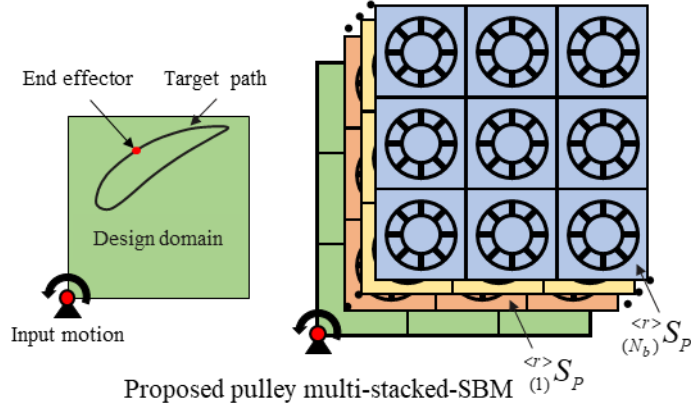
of different types.



Previous gear stacked-SBM

$$\Omega = S_L \oplus \langle r \rangle S_G$$

(a)



Proposed pulley multi-stacked-SBM

$$\Omega = S_L \oplus \langle r \rangle S_P \oplus \langle r \rangle S_P \cdots \langle r \rangle S_P$$

(b)

Fig. 4.1 The main concept of proposed pulley multi-stacked SBM. (a) the previous gear stacked-SBM only stacked one layer. However, the proposed pulley multi-stacked SBM stacked multi design space for rotational relationship with each rigid blocks.

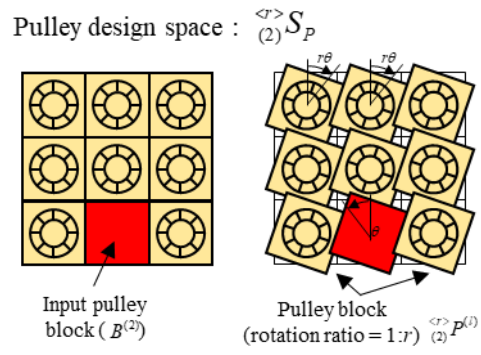


Fig. 4.2 The representation of pulley blocks and pulley design space.

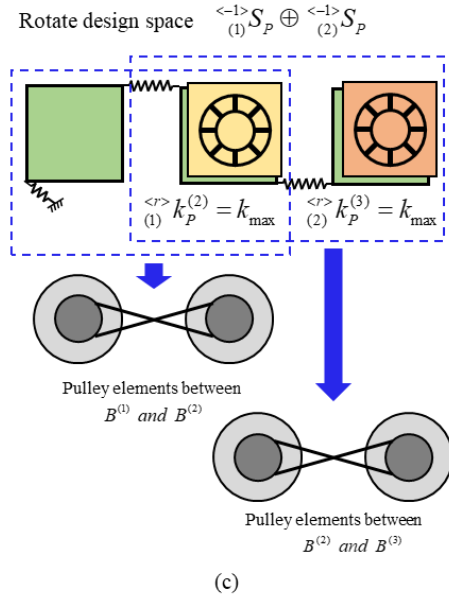
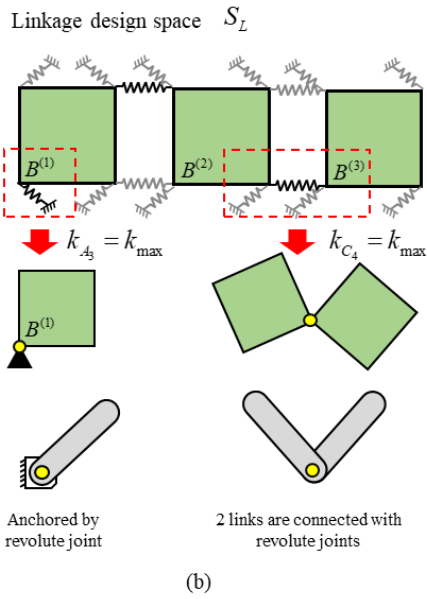
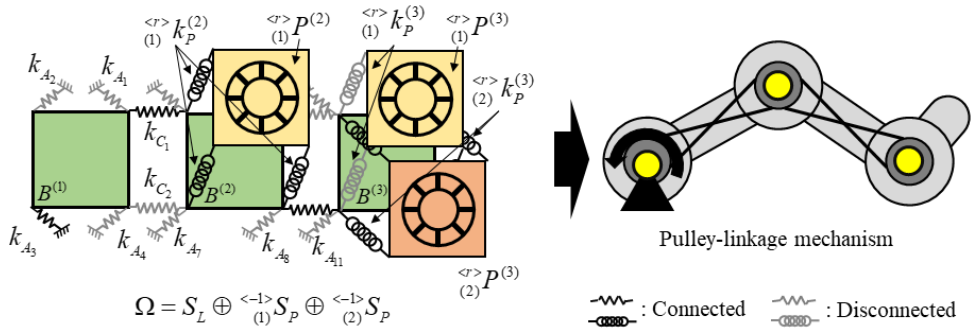


Fig. 4.3 The representation of pulley-linkage mechanism with proposed modeling method. (a) the corresponding modeling method can represent the pully linkage mechanism. (b) the details of linakge design space and (c) pulley design space.

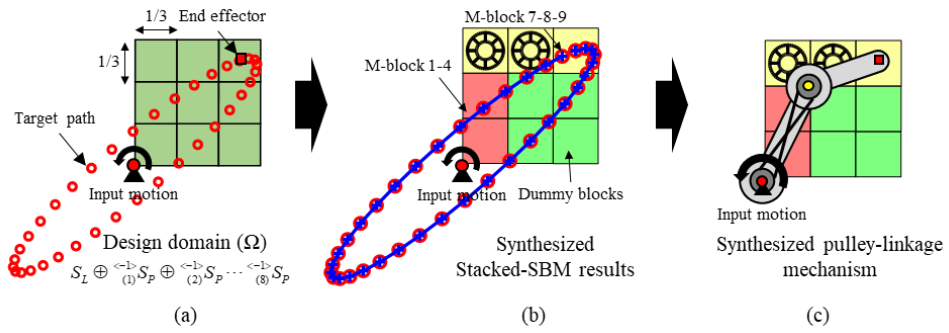


Fig. 4.4 (a) the definition of synthesis problems with 3X3 descritized design space. (b) the results after the optimiziation process and (c) its coresponding results of pulley-linkage mechanism.

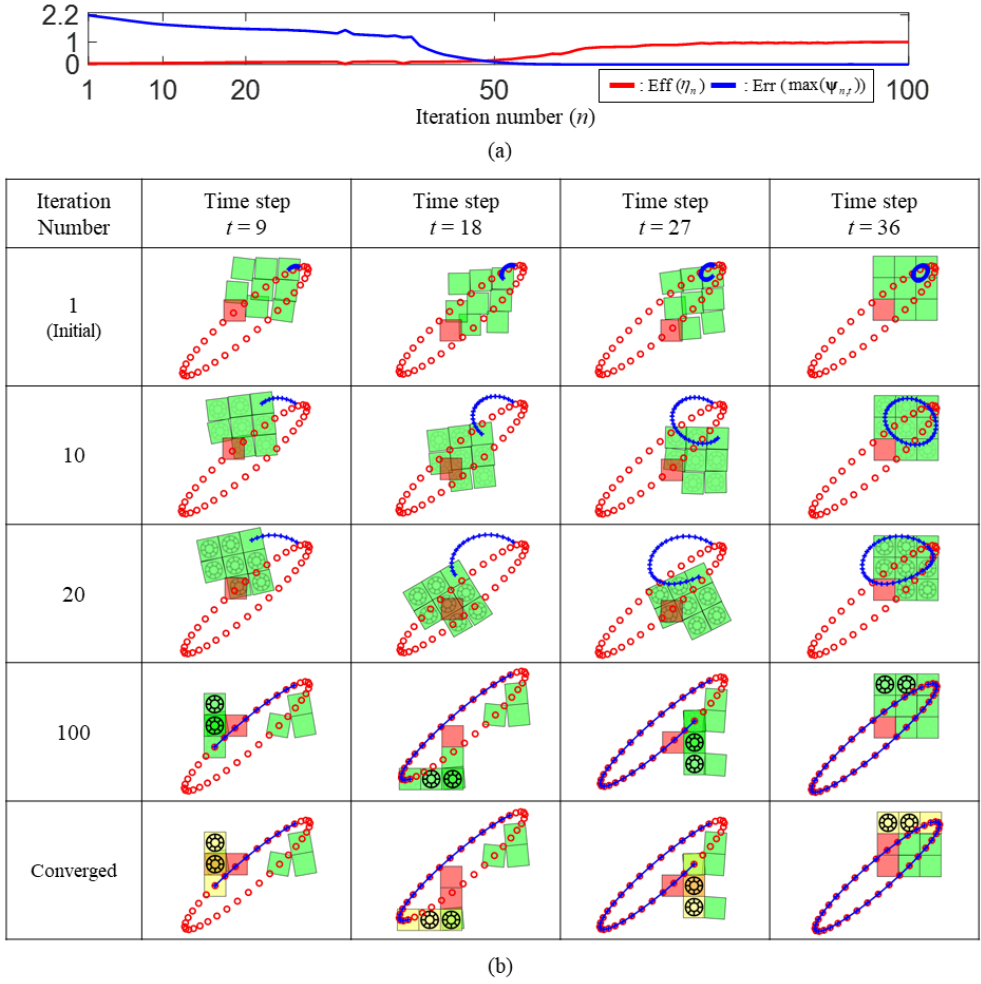


Fig. 4.5 The iteration history (a) and the evolutionary history of the synthesis problem.

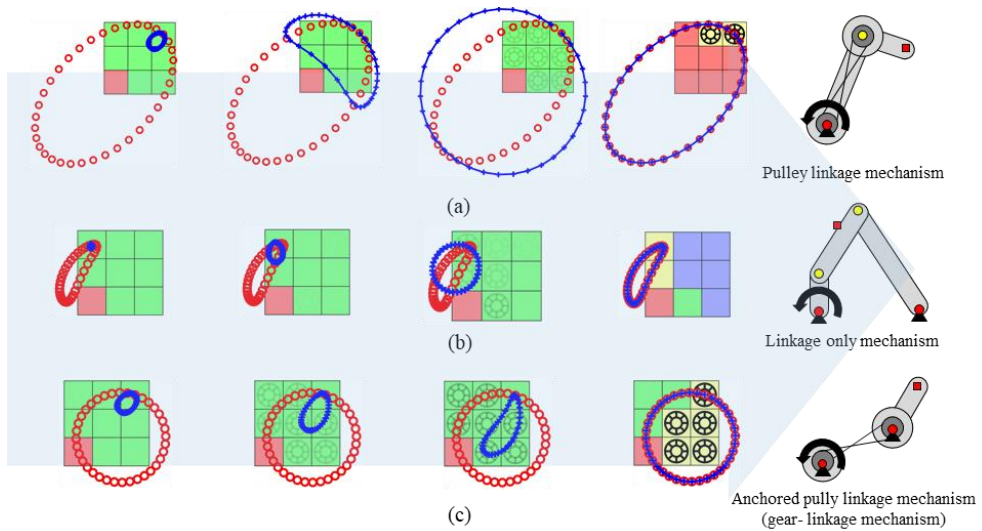


Fig. 4.6 The synthesis results of different types of mechanism (a) pulley-linkage mechanism, (b) linkage only mechanism, and (c) gear-linkage mechanism (anchored pulley-linkage mechanism).

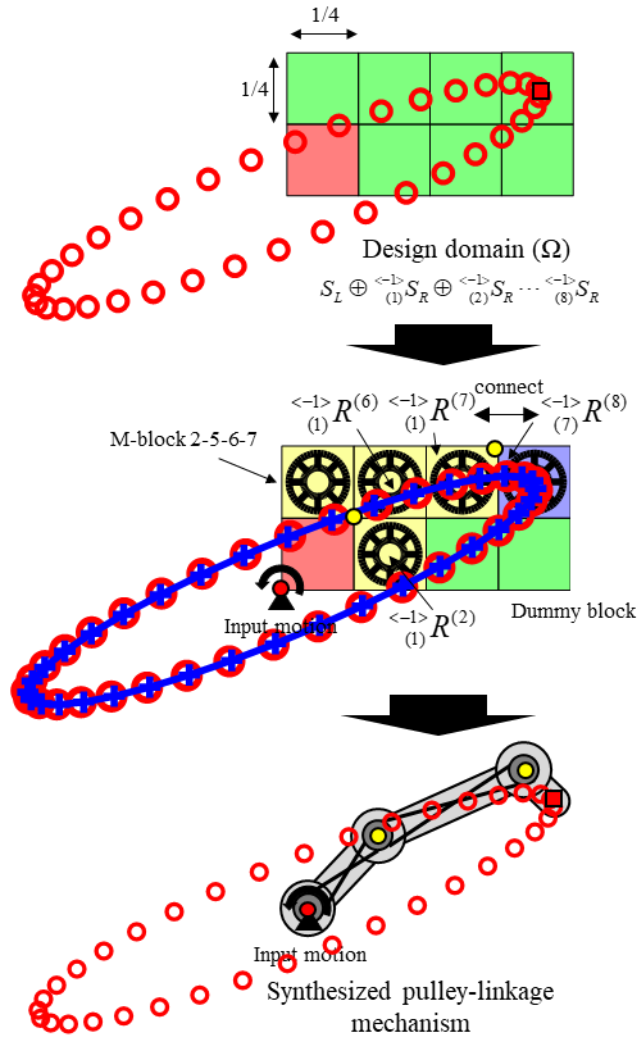


Fig. 4.7 The synthesis results of multi pulley components mechanism.

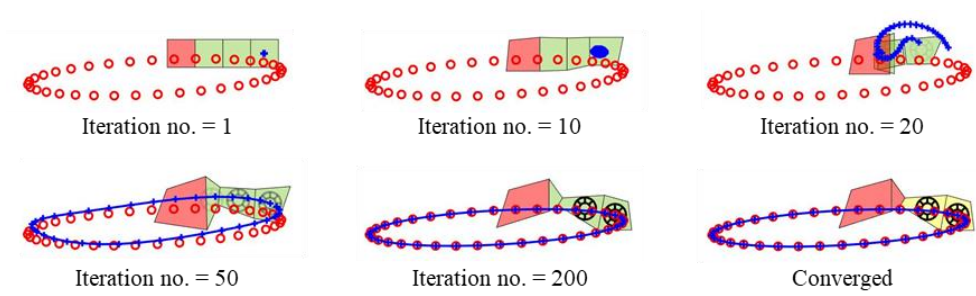


Fig. 4.8 The synthesis results with simultaneously consider the shape of pulley components with its evolutionary history.

CHAPTER 5.

Topology Optimization of Planar Spring-Linkage Mechanisms

5.1 Overview

The primary function of a mechanism is to convert a simple input motion into the desired motion at the end effector. When synthesizing mechanisms, it is not appropriate to consider only the desired motion if obstacles and environmental changes need to be considered, such as maintaining grasping motion for various objects, as in the case of adaptive grippers [42-49]. Motion can be limited when obstacles are present, and thus, it is crucial to incorporate obstacle conditions when synthesizing mechanisms. This has led to the investigation of mechanism synthesis methods that consider obstacles and environmental changes as important research subjects [45-56]. To this end, multi-degree-of-freedom (DOF) mechanisms were usually used in earlier studies, employing additional driving actuators to accommodate obstacles and environmental changes [57-60]. In contrast, the spring-linkage mechanism with single driving actuator has several advantages, such as

requiring fewer actuators, a simpler control method, and lower sensing precision due to the use of passive spring components [46, 52]. Because, the spring-linkage mechanism can exert an underactuated DOF from passive springs when faced with obstacles and environmental changes. However, a systematic method to synthesize or design a 1-DOF spring-linkage mechanism has not been developed. This limitation motivated the development of an autonomous synthesis method to synthesize 1-DOF planar spring-linkage mechanisms. The goal is to develop an automated optimization-based method that considers both the desired motion and the shape of obstacles when synthesizing 1-DOF planar spring-linkage mechanisms. When considering motions and obstacles simultaneously, the required mechanisms differ depending on the presence or absence of obstacles (the absence state may be said to be the case where the obstacle size is zero). For example, a 1-DOF fully actuated linkage mechanism is required to generate the desired motion in the absence of obstacles, as shown in Fig. 5.1(a), whereas a 1-DOF underactuated spring-linkage mechanism is required to overcome obstacles, as shown in Fig. 5.1(b). Since the topology of the underactuated spring-linkage mechanism is based on multi-DOF and the topology of the fully actuated linkage mechanism is based on 1-DOF, determining the topology and dimensions of the baseline rigid link mechanism requires different design methods depending on the presence or absence of obstacles (not to mention the determination of topology and dimensions of the spring components). As a result, there was no method to consider both a fully actuated and an underactuated mechanism simultaneously with a single

driving actuator in the mechanism motion generation synthesis problem.

To synthesize the fully actuated linkage mechanism, for example, the sequential synthesis process determining the topology of the baseline mechanism using the designer's experience and intuition and then determining the dimensions of the mechanism was traditionally studied [61-63]. Further, recently, there has been much interest in topology optimization-based methods that simultaneously synthesize the topology and dimensions of fully actuated linkage mechanisms [8, 11, 13, 64]. Unlike traditional methods, topology optimization-based methods do not require a baseline design, which is why they have received significant attention. And, these methods have been successfully applied to real-world synthesis problems. To this end, ground structure modeling, such as the nonlinear-bar model [2, 11, 64] and spring-connected rigid block model (SBM) has been used for mechanism topology optimization. These models represent various mechanism topologies in a single unified modeling method. In addition, an energy-based formulation to control the rotatability of a single driving actuator [8, 9, 11-15, 30, 41, 64] was used with the unified modeling method. However, the existing topology optimization methods are only applicable to fully actuated mechanisms with linkage only mechanism. And this linkage only 1-DOF fully actuated mechanism cannot overcome the unexpected obstacles.

On the other hand, a 1-DOF underactuated spring-linkage mechanism can overcome unexpected obstacles with maintaining desired motion. Because underactuated DOF can consider the obstacles and environmental changes, some

adaptive spring-linkage mechanisms were discussed [45, 47, 56] In this study, we focus on overcoming possibility of obstacle shape and desired motion. To design a 1-DOF underactuated spring-linkage mechanism, researchers have studied a method for optimizing the dimensions and configuration of the spring components for a fixed multi-degree-of-freedom (multi-DOF) linkage mechanism [56, 65-67]. However, determining the topology of the baseline rigid link mechanism still relies on the designer's experience and intuition, which can be limiting as trial-and-error methods were used. That is, there was no way to consider the topology of the baseline rigid link mechanism in the previous underactuated spring-linkage mechanism synthesis method. Eventually, to consider two different topologies (1-DOF for fully actuated and multi-DOF for underactuated) simultaneously, a new method is needed to consider topology and dimensions of rigid links and spring components. To this end, we extend the previous rigid link ground model (spring-connected rigid block model) [7, 15] to a spring-linkage mechanism and extend the previous method [11] of controlling the degree of freedom of the rigid link mechanism to both fully actuated mechanism and underactuated spring-linkage mechanism. Therefore, simultaneously handling different mechanism types and controlling different mechanism DOFs with the desired motion and shape of the obstacle in the context of topology optimization will be addressed anew.

Before presenting our method to synthesize mechanism with the desired motion and shape of obstacles, it is important to pinpoint several major issues that need to be addressed in developing a topology optimization-based synthesis method of

spring-linkage mechanisms (in this paper, the meaning of spring-linkage mechanism include the linkage only mechanism). First, it is necessary to develop a ground model that can represent the topology and dimensions of both the rigid links and spring components. Second, the synthesis method must consider the shape of obstacles and their desired motion. And third, it is important to represent the rotatability of the spring-linkage mechanisms using continuous design variables, allowing for the incorporation of numerically efficient gradient-based optimizers. To address these issues, we propose a new stacked spring-linkage SBM, which is capable of representing both rigid links and spring components. The SBM may be suitable for determining the connectivity between the spring component and the rigid link in the synthesis of the spring-linkage mechanism because the SBM can control the connectivity between different mechanical components, such as gear components, with a stacked method [41]. However, elastic components such as spring components can be underactuated and affect rotatability, which is a different problem from previous topology optimization methods that only consider rigid components. To overcome this challenge, we share state variables of real springs with SBM rigid blocks. Additionally, we will apply the energy-based method for representing rotatability [11] used in the linkage mechanism will be applied to the spring-linkage mechanism. Below, we briefly explain how the above ideas solve several major issues. A more detailed account of it will be presented in Sec. 5.2.

To handle rigid links and spring components simultaneously in an optimization-based synthesis approach, as shown in Fig. 5.2, we stacked two design spaces

occupying the same physical area: one design space (S_L : linkage design space) for rigid link synthesis ground models and another design (S_s : spring design space) for spring synthesis ground models. The linkage design space S_L is the same as the design space used in the previous SBM [15]. By the SBM, the linkage design domain (S_L) is discretized by rigid blocks connected by artificial zero-length springs of varying stiffness values. When the stiffnesses of the artificial springs have upper limit values and lower limit values (more precisely, the stiffness will be interpolated as a function of the topology design variable), the linkage mechanism can be represented. On the other hand, the spring design space S_s contains all possible spring configurations in the physical domain, representing individual real spring components. The topology (configuration) of the spring components in the spring design space S_s can also be indicated by its corresponding stiffness value having upper (presence) and lower (absence) bound values (the stiffness of real spring is also interpolated as a function of the spring design variable). The intermediate value of spring design space does not mean that the stiffness value of the spring is the intermediate value but is only used for the gradient-based optimization synthesis process. Therefore, after the mechanism is synthesized, the stiffness values of the spring components should only take the upper and lower value. Thus, the topology of spring-linkage mechanisms will be determined by the stiffness values of two sets of springs. One is a set for an artificial zero-length spring that connects the rigid blocks of S_L to each other, and the other is a set that

represents an actual spring in S_s . And, each side of the spring component in the spring design space shares the geometric center of each rigid block in the linkage design space to represent the dimensions of spring lengths. Therefore, the dimensions of rigid link and spring components can be determined through design variables representing the block shape S_L . Details of the proposed approach are also described in Sec. 5.2.

Next, we briefly explain our method of considering the shape of the obstacle in the topology optimization approach. When obstacles are given, motion perturbation from the desired motion is required, as depicted in Fig. 1(b). To express the rotatability of spring-linkage for motion perturbations, we use the total elastic energy from artificial zero-length springs in the linkage design space. This elastic energy-based method was previously utilized in the SBM-based topology synthesis approach to control the degree of freedom of the synthesized mechanism. The concept of controlling 1-DOF in the previous SBM is extended to rotationality from a single driving actuator. For instance, to overcome obstacles, the configuration of the baseline rigid link mechanism needs to be altered, and the artificial zero-length spring should not be stretched by perturbed motion. In that case, the total elastic energy from artificial springs in the configuration of a rotatability-capable mechanism can be expressed as zero [11]. Consequently, we introduce a new definition of the sum of the artificial zero-length springs with the desired motion and all cases of perturbation motions to represent the rotatability of the spring-linkage mechanism. Furthermore, since this energy-based value is

continuous, gradient-based optimization can be employed for better optimization. We also formulate other constraint equations, such as the Euclidean error between the desired motion and the mean square error of the spring design variable. Details of the proposed optimization formulations are described in Sec. 5.3.

This paper is organized as follows. Since previous topology optimization-based methods did not consider rigid links and spring components simultaneously, Sec. 5.2 is fully committed to modeling techniques and kinematic analysis procedures. Sec. 5.3 presents a gradient-based mechanism synthesis for topology optimization with optimization formulation. Numerical case studies are presented in Sec. 5.4, where the synthesis results with different obstacle shape conditions. Furthermore, we apply the proposed method to the real gripper design problem.

5.2 Modeling and Analysis

5.2.1 Spring-linkage stacked spring connected block model

To perform a topology optimization-based mechanism synthesis method, the design domain (feasible region) must be discretized into several components, and a combination of these components could be able to represent the desired mechanism. Unlike previous topology optimization-based methods applicable to synthesizing linkage-only mechanisms, both spring components and rigid links must be synthesized simultaneously under the synthesis conditions. To this end, we propose a new stacked SBM modeling method for the spring-linkage mechanism. Fig. 5.2 shows a proposed ground model in which the design domain is treated as an overlap of two design spaces (S_L and S_s). The symbol S_L represents the linkage design space which is discretized by a rigid block $B^{(l)}$ ($l = 1, \dots, N_b$), and the symbol S_s represents the spring design space which is all possible spring components connected between the center of each rigid block (for complexity, we consider the adjacent blocks to connect the springs in this paper). Here N_b is the total number of rigid blocks in the linkage design space. The notion of S_L consisting of $B^{(l)}$ (l -th block) has been used in earlier studies [15]. However, the notion of S_s and stacking method between S_L and S_s representing the spring-linkage mechanism are newly proposed here.

We will briefly demonstrate how the previous SBM (linkage design space) can

represent the various topologies and dimensions of the linkage mechanism. Two adjacent rigid blocks (or a rigid block and the ground) are assumed to be connected with block-connecting springs (the anchoring springs) with stiffness values, as shown in Fig. 5.2(b). Both block-connecting and anchoring springs are artificial zero-length springs introduced to represent the topologies of linkage mechanism (not to be confused with artificial springs with actual spring components in the spring design space). When the block-connecting spring's stiffness is expressed \mathbf{k}_C , this can vary between the lower limit $\mathbf{k}_C = 0$ (numerically, $\mathbf{k}_C = \varepsilon \approx 0$) and the upper limit $\mathbf{k}_C = k_{\max}$ (k_{\max} : a pre-selected value). The anchoring spring stiffness \mathbf{k}_A also varies between $\mathbf{k}_A = 0$ and $\mathbf{k}_A = k_{\max}$. And the lower limit state means that the rigid blocks are disconnected, and the upper limit means that the rigid blocks are connected at that corner. Therefore, with different connectivity states with block-connecting springs and anchoring springs which take on their lower or upper stiffness values, various mechanism states (rigidly connected, connected by a revolute joint, and anchored by a revolute joint) can be represented as shown in the right side of Fig. 5.2(b). And, it is more convenient to use the normalized design variables $0 < \xi_C \leq 1$ and $0 < \xi_A \leq 1$ to make $\mathbf{k}_C = k_{\max} \cdot (\xi_C)^3$ and $\mathbf{k}_A = k_{\max} \cdot (\xi_A)^3$, instead of using \mathbf{k}_C and \mathbf{k}_A directly as design variables, as in earlier studies [8, 12, 13, 15, 41]. These two design variables (ξ_C and ξ_A) for representing the linkage mechanism topology are combined to represent them as ξ^K and will be called topology design variables. The coordinates of the grid points that discretize a

given design domain into a rigid block can be represented by vector symbols ξ^x ($0 < \xi^x < 1$). This shape-controlling design variable ξ^x is called the dimension design variable and does not affect the topology of the linkage mechanism. Thus, the various topology and dimensions of the linkage mechanism in the linkage design space can be represented by real-valued design variables ξ^K and ξ^x that vary between 0 and 1; see Yu et al. [12] for more information.

We will now describe the spring design space and how the proposed stacking method with linkage and spring design space can represent various spring-linkage mechanisms. As shown in Fig. 2(c), the spring design space consists of all possible spring components connected between adjacent rigid blocks. The spring components used in the spring design space are supposed to connect any of the two rigid blocks. To represent the connectivity, we introduce the following symbol, $n = n(i, j)$: the n -th spring component are connected between the i -th block $B^{(i)}$ and j -th links $B^{(j)}$. Each spring component's corresponding stiffness value (\mathbf{k}^S : $0 \approx \varepsilon \leq \mathbf{k}^S \leq k_{\max}$) can be expressed as a spring design variable (ξ^S) and has a $\mathbf{k}^S = k_{\max}^S \cdot \xi^S$ ($0 < \xi^S \leq 1$) relationship. Upper subscription S was used to avoid confusing the stiffness value of the artificial springs (\mathbf{k}_C and \mathbf{k}_A). If ξ^S reaches its maximum value $\xi^S = 1$ at the end of the spring-linkage mechanism synthesis, the corresponding spring is declared to exist, and if ξ^S reaches its minimum value $\xi^S = \varepsilon \approx 0$, it is declared to be non-exist. In other words, we represent the presence

of spring components with their stiffness value. This approach was same as the above topology design variables. Therefore, we can represent spring components' topology (configuration) with real-valued continuous design variables ξ^s . However, after the mechanism is synthesized, ξ^s represents only the lower bound (0) or upper bound (1) value corresponding to the disconnection or connection state of the spring component because we first consider the topology of the spring component. Suppose springs with different stiffness values need to be used. In that case, one of the multi-candidate spring design spaces can be stacked with various $k_{\max}^{s'}$ values, just like the previous gear-stacked SBM method considering gear ratios [41].

Those two design spaces are stacked in the design domain, as shown in Fig. 3. When they are stacked with each other, each side of spring components in the spring design space is overlapped at the geometric center of the rigid block in the linkage design space. If the state variables of l -th rigid block $B^{(l)}$ at time step t is $\mathbf{q}_t^{(l)}$, $\mathbf{q}_t^{(l)}$ can be represented by the geometric center of l -th rigid block $[X_t^{(l)}, Y_t^{(l)}]$ and rotation angle $\phi_t^{(l)}$ with respect to the global coordinate:

$$\mathbf{q}_t^{(l)} = [X_t^{(l)}, Y_t^{(l)}, \phi_t^{(l)}]^T \quad (5.1)$$

Then, one side of the spring component, which is connected in $B^{(l)}$ is located at $[X_t^{(l)}, Y_t^{(l)}]$ in time step t . Because dimension design variables (ξ^x) that determine the shape of a block not only represent the locations of four nodes in the rigid block (this node can determine the positions of the revolute joint) but also change the

geometric center of the block, the dimensions (initial length) of spring components can be represented by the dimension design variables (ξ^x). And this stacking method with sharing state variables decreases the use of extra shape design variables for the spring components. Therefore, the motion (state) of the spring-linkage mechanism can be expressed as state variables of the entire rigid blocks. The analysis method for determining these state variables of all blocks will be mentioned in the next subsection. Now, we can represent the various topologies and dimensions of spring-linkage mechanisms as shown in Fig. 5.2(a) with the continuous real-valued design variables ξ^K , ξ^S , and ξ^x . And we can represent the motions of spring-linkage mechanism with $\mathbf{q}_l^{(l)}$ ($l=1, \dots, N_b$). The optimization process for synthesizing these design variables (ξ^K , ξ^S , and ξ^x) will be mentioned in Sec. 5.3.

5.2.2 Kinematic analysis of stacked spring-linkage SBM

The configuration of the spring-linkage mechanism should satisfy the mechanical constraints at the revolute joint and minimize the stored elastic energy from the spring components. The above two conditions apply to both the 1-DOF fully actuated linkage mechanism and the underactuated spring-linkage mechanism in Fig. 5.1 since the total elastic energy of the fully actuated linkage mechanism is zero or does not affect the linkage motion (this will be mentioned again in the following case study problem). To obtain the motion of the spring-linkage

mechanism, we have to perform a kinematic analysis based on the proposed stacked SBM with the above conditions. The kinematic analysis of the SBM-based mechanism can be conducted through a quasi-static nonlinear analysis. That is, the movements of all blocks from a prescribed input driving actuator are obtained through the quasi-static equilibrium with the state variables of all rigid blocks. For example, suppose the input driving actuator motion is designated as the rotation at block 1 ($B^{(1)}$). In that case, the states of all rigid blocks except input block 1 are represented by the total state variable vector (\mathbf{v}_t) at the time step (t). This can be expressed as follows.

$$\mathbf{v}_t = \left[\left(\mathbf{q}_t^{(2)} \right)^T, \left(\mathbf{q}_t^{(3)} \right)^T, \dots, \left(\mathbf{q}_t^{(N_b)} \right)^T \right]^T \quad (5.2)$$

And the total state variable vector \mathbf{v}_t should satisfy the below equilibrium equations (3) of mechanical constraints from revolute joints and minimum potential energy from actual spring:

$$\begin{aligned} & \text{Minimize } E_{spring,t} \\ & \text{subject to } \mathbf{F}_{int}(\mathbf{v}_t) - \mathbf{F}_{ext} = 0 \end{aligned} \quad (5.3)$$

$E_{spring,t}$ is the potential energy from actual springs and $\mathbf{F}_{int}(\mathbf{v}_t) - \mathbf{F}_{ext} = 0$ is the substitution of the mechanical constraints in a physics-based force equilibriums in SBM [12]. The total strain energy stored in the spring-linkage mechanism from N_s number of actual springs (do not confuse the artificial springs \mathbf{k}_C and \mathbf{k}_A) can be written as

$$E_{spring,t} = \sum_{w=1}^{N_s} \frac{1}{2} k_w^S \left(\left\| \mathbf{q}_t^{(l)} - \mathbf{q}_t^{(m)} \right\| - \left\| \mathbf{q}_0^{(l)} - \mathbf{q}_0^{(m)} \right\| \right)^2 \quad (5.4)$$

where, k_w^S is the stiffness value of the w -th spring component, which is connected between the geometric center of l -th rigid block and m -th rigid block ($w = \mathbf{w}(l,m)$), and 0 means the initial time step (initial lengths) as shown in Fig. 5.4.

In Eq. (5.3), we represent the mechanical constraints from revolute joints by the force equilibrium in SBM as constraints equation. The number and location of revolute joints cannot be predetermined during the optimization process during mechanism topology optimization. For this reason, previous SBM-based topology optimization has successfully represented the mechanical constraints during optimization process by the total elastic energy of artificial zero-length springs in the SBM design domain [12, 13, 41]. Since the mechanical constraint of the revolute joint means the constraint in the X and Y directions, in the case of revolute joints, the artificial zero-length spring does not stretch. This means that elastic energy is not generated in the linkage design space (see Fig. 5.2(b)) to satisfy the mechanical constraints during the optimization process. Again, do not confuse the artificial zero-length spring in the linkage design space and the actual spring in the spring design space. Therefore, the equilibrium equation for the mechanical constraint of the revolute joint in the spring-linkage mechanism can be written as follows

$$U_{SBM,t} = \sum_{n=1}^{N_c} \frac{1}{2} k_C^{(n)} \cdot \left(\delta_t^{(n)} \right)^2 + \sum_{n=1}^{N_A} \frac{1}{2} k_A^{(n)} \cdot \left(\delta_t^{(n)} \right)^2 = 0 \quad (5.5)$$

This elastic energy can be obtained from stretched lengths ($\delta_t^{(n)}$) at the time step t of the corresponding n -th artificial zero-length spring ($k_C^{(n)}$ or $k_A^{(n)}$) where, N_C (N_A) is the total number of block-connecting springs (anchoring springs). And then, Eq. (5.5) can also be replaced by a force equilibrium equation as follows:

$$\mathbf{F}_{\text{int}}(\mathbf{v}_t) - \mathbf{F}_{\text{ext}} = 0 \quad (5.6)$$

where $\mathbf{F}_{\text{int}}(\mathbf{v}_t)$ is the internal forces from artificial spring, such as $\mathbf{F}_{\text{int}}(\mathbf{v}_t) = dU_{SBM,t} / d\mathbf{v}_t$. And \mathbf{F}_{ext} is the external force in the direction opposite to the desired motion ($\hat{\mathbf{r}}_t^{\text{end}}$) with the magnitude of F_0 as follows:

$$\mathbf{F}_{\text{ext}} = F_0 \cdot \frac{\hat{\mathbf{r}}_{t-1}^{\text{end}} - \hat{\mathbf{r}}_t^{\text{end}}}{\|\hat{\mathbf{r}}_{t-1}^{\text{end}} - \hat{\mathbf{r}}_t^{\text{end}}\|} \quad (\text{where, } F_0 = 1) \quad (5.7)$$

\mathbf{F}_{ext} was intentionally introduced to control the rotatability of the mechanism in the previous SBM-based synthesis method. Details of the process and calculation of the equation can be found in Refs. [12, 13]. Now, based on Eq. (5.3), we can determine the generating motion of the spring-linkage mechanism through a quasi-static analysis with the given input motion of block 1 at the time step (t).

5.3 Optimization formulation for synthesizing spring-linkage mechanism

Section 5.2 described a stacked SBM method that can represent various topologies and dimensions of the spring-linkage mechanism and how to analyze its motion. This section presents an optimization formulation for synthesizing the 1-DOF spring-linkage mechanism, considering the desired motion and the shape of the obstacle. Since all design variables are real-valued, we can build numerically efficient gradient-based optimization formulation to synthesize the desired mechanisms. Therefore, the objective function and constraint equations will be defined in continuous design variables to construct the optimization formulation to update the design variables.

Designing a spring-linkage mechanism with the proposed stacked SBM means that the topology design variables (ξ^K), dimension design variables (ξ^X), and spring design variables (ξ^S) are determined under the optimization process. That is, the design variables (ξ) to be determined through the optimization process are as follows

$$\xi = \{\xi_1^K, \xi_2^K, \dots, \xi_{N_k}^K, \xi_1^X, \xi_2^X, \dots, \xi_{2N_n}^X, \xi_1^S, \xi_2^S, \dots, \xi_{N_s}^S\}^T \quad (5.8)$$

where N_k and N_n is the total number of artificial zero-length springs and number of nodes in linkage design space and N_s is the total number of actual spring components in spring design space. The synthesized 1-DOF spring-linkage mechanism should follow the desired motion and be able to overcome obstacles.

Therefore, the following optimization formulation (5.9-5.11) is established to reflect the above design conditions (A situation in which an obstacle is not required is considered to be zero in size of obstacle):

$$\underset{\xi \in \mathbf{R}^{N_k+2N_n+N_s}}{\text{Minimize}} \quad U_{SBM}(\xi) + U_{SBM}^{obs}(\xi) \quad (5.9)$$

$$\text{subject to} \quad \Psi_t(\xi) \leq \varepsilon \quad (t = 1, 2, \dots, T) \quad (5.10)$$

$$\eta_{spring} \leq 0 \quad (5.11)$$

$U_{SBM}(\xi) + U_{SBM}^{obs}(\xi)$ is the objective function to ensure that the synthesized mechanism is rotatable with a single driving actuator even the obstacle is given. $U_{SBM}(\xi)$ is the elastic energy from artificial zero-length springs in linkage design space (Eq. (5)) when there is no obstacle as follows:

$$U_{SBM} = \sum_{t=1}^T U_{SBM,t} \quad (5.12)$$

where, T is the total time step. Same as Eq. (5.12), $U_{SBM}^{obs}(\xi)$ is the elastic energy from artificial zero-length springs in linkage design space when considering the shape of obstacles as $U_{SBM}^{obs} = \sum_{t=1}^T U_{SBM,t}^{obs}$. $\Psi_t(\xi)$ is a constraint equation to ensure that the synthesized mechanism generates the desired motion and η_{spring} is a constraint equation to control the topology of spring components in spring design space. To simultaneously consider the two mechanical components with stacked design spaces, the optimization formula was constructed through one equation $\Psi_t(\xi)$ from the correlated results between two design spaces (generating motion

can be obtained from the correlated equation in Eq. (5.3)). And two more equations such as $U_{SBM}(\xi) + U_{SBM}^{obs}(\xi)$ and η_{spring} functions which are obtained from linkage and spring design space respectively. Because stacked SBM modeling methods consist of two design spaces, we have to consider correlation functions between two design spaces and component-related functions in each design space. Their explicit formula will be given below and the symbol ε denotes a tolerance error.

The objective function $(U_{SBM}(\xi) + U_{SBM}^{obs}(\xi))$ was newly introduced to simultaneously consider the baseline topology of rigid links and the shape of the obstacle. And this objective function can be obtained from the linkage design space. $U_{SBM}(\xi)$ is the total elastic energy in linkage design space from the input motion of every time step and can be easily calculated. And the $U_{SBM,t}(\xi) = 0$ (minimized) means that the configuration of corresponding design variables can rotatable from a single input motion [11]. Therefore, minimizing $(U_{SBM,t}(\xi) = 0)$ means that the mechanism can completely transmit the input motion to the end effector. This energy-based method can be extended when the obstacle is given. When the shape of obstacle $(\hat{\mathbf{r}}_t^{obs})$ is given, the position of the end effector (\mathbf{r}_t^{end}) at time step (t) has to be moved to $\hat{\mathbf{r}}_t^{obs}$ for overcoming the obstacle. In that case, we can formulate the following optimization to obtain the position of the rigid block to overcome the obstacle:

$$\begin{aligned} & \text{Minimize } U_{SBM,t}^{obs}(\mathbf{v}_t^{obs}) \\ & \text{subject to } \mathbf{r}_t^{end}(\mathbf{v}_t^{obs}) = \hat{\mathbf{r}}_t^{obs} \end{aligned} \quad (5.13)$$

where \mathbf{v}_t^{obs} states of all rigid blocks except input block 1 when overcoming the obstacles. As a result of Eq. (5.13), if the mechanism can overcome the obstacle (the corresponding mechanism can change its configuration of baseline linkage mechanism), the minimized value of $U_{SBM,t}^{obs}$ should be zero (actual springs, in this case, were assumed to be stretched somehow). Thus, the mechanism can overcome the given shape of an obstacle ($\hat{\mathbf{r}}_t^{obs}$) when $U_{SBM}^{obs} = 0$ (minimized) ($U_{SBM}^{obs} = \sum_{t=1}^T U_{SBM,t}^{obs}(\mathbf{v}_t^{obs})$). Therefore, $U_{SBM} + U_{SBM}^{obs}$ must be zero (numerically ε)

when the spring-linkage mechanism can generate the desired motion and overcome the obstacle. That is why we use $U_{SBM} + U_{SBM}^{obs}$ as an objective function to minimize in Eq. (5.9) to simultaneously handle the desired motion and shape of an obstacle. In addition, energy conversion values for different types of obstacles ($U_{SBM}^{obs'}$) can be added to Eq (5.9) to consider more diverse types of obstacles.

The constraint equation Ψ_t is defined as the Euclidean distance between desired motion ($\hat{\mathbf{r}}_t^{end}$) and the generating motion at the end effector (\mathbf{r}_t^{end}) at the time step:

$$\Psi_t(\xi) = \|\mathbf{r}_t^{end} - \hat{\mathbf{r}}_t^{end}\| \quad (t = 1, 2, \dots, T) \quad (5.14)$$

\mathbf{r}_t^{end} can be determined by carrying out a quasi-static nonlinear analysis in Sec. 5.2.2. Constraint equation η_{spring} is introduced to ensure that all spring states reach either existence or nonexistence state ($\xi_n^S = 0$ or 1) at the end of the optimization

convergence, which is the mean square error from 0.5 ($0.5 \approx 0.5 \cdot (\xi_{\min} + \xi_{\max})$) as follow :

$$\eta_{spring} = \frac{1}{0.25N_s} \sum_{n=1}^{N_s} (\xi_n^S - 0.5)^2 \quad (0 = \eta_{\min} \leq \eta_{spring} \leq \eta_{\max} = 1) \quad (5.15)$$

With the optimization formulation (5.9-5.11), the design variable was updated using the method of moving asymptotes [34]. Analytical sensitivities of objective function and constraint equations related to design variables are required to update design variables using a gradient-based optimization optimizer. However, they are not given explicitly here because they are relatively easy to calculate.

5.4 Synthesis of various mechanisms by the proposed method

The proposed synthesis method to synthesize the 1-DOF spring-linkage mechanism is used to conduct the following two synthesis case problems. First case studies are the problems to ensure whether the proposed method achieves the intended purpose with same desired path and different obstacles shape synthesis conditions. And second case study deals with synthesizing a new adaptive gripper. With two case studies, we check the validity and effectiveness of the proposed synthesis approach.

Case study 1: synthesis of spring-linkage mechanism with the same desired motion with different obstacle conditions.

Case study 2: synthesis of the new 1-DOF underactuated spring-linkage adaptive gripper.

To solve the mechanism synthesis problems in case studies 1 and 2, the initial values of the design variables were set as $0.5 \approx (\xi_{\min} + \xi_{\max})/2$ not to give biased initial conditions on the gradient-based optimization method. In addition, the values of other parameters used for the entire optimization process were set as follows:

$$\varepsilon = 0.05, \xi_{\min}^K = 10^{-4}, \xi_{\min}^S = 10^{-4}, \xi_{\min}^X = 10^{-2}, \xi_{\max} = 1, k_{\max} = 10^3, k_{\max}^S = 10 \quad (5.16)$$

The values (5.16) were effective in the earlier gradient-based mechanism synthesis methods [12, 13, 15, 41].

5.4.1 Case Study 1: synthesis of various shapes of obstacles

This section investigates if the proposed formulation (5.9-5.11) can successfully synthesize the spring-linkage mechanism in considering the same desired motion with different shape of obstacles. We used the desired motion obtained from a mechanism to demonstrate the validity and effectiveness of the proposed method. Specifically, we will perform three synthesis problems with different shapes of obstacles to check that the different topologies and dimensions of the spring-linkage mechanism can be synthesized. For the spring-linkage mechanism synthesis conditions, the target motion (Fig. 5.5(a)) and the 3×3 discretized stacked SBM (Fig. 5.3) were equally used with three different shapes of obstacles (Fig. 5.5(b)). The first synthesis condition is when there is no obstacle (the obstacle size is 0, as shown in the first row in Fig. 5.5(b)). Additionally, the second and third synthesis conditions are problems for the obstacles of different sizes. The second obstacle is a perturbation of magnitude 0.2 in the Y -direction on the desired motion in the time step $t = 5 \sim 8$, as seen in the second row of Fig. 5.5(b). And the third obstacle is an obstacle with the same conditions as the second obstacle, except that the size is 0.01, as depicted in the third row in Fig. 5.5(b). As a result of the synthesis processes, three different spring-linkage mechanisms (the first case of Fig. 6 and the second and third cases of Fig. 8) with different topologies and dimensions were synthesized. With the desired motion (Fig. 5.5(a)) and non-obstacles condition (first row of Fig. 5.5(b)) same as Fig. 5.1(a) synthesis case, 1-DOF fully actuated linkage mechanism is synthesized as shown in Fig. 5.6(a). As the iteration

progresses, the objective function and the constraint equations in Eq. (5.9-5.11) were converged within the convergence criterion in Fig. 5.6(b), and its evolutionary history is presented in Fig. 5.7. Because there is no obstacle in this first synthesis problem, the objective function $U_{SBM}(\xi) + U_{SBM}^{obs}(\xi)$ should be $2 \cdot U_{SBM}(\xi)$ because $U_{SBM}^{obs}(\xi) = U_{SBM}(\xi)$. The unnecessary spring components (blue spring-like lines) disappear, and the connectivity of the rigid blocks changes to generate the desired motion during the optimization process. Although the generating motion does not perfectly match the target motion in Fig. 5.6(c), it is possible to generate a similar motion within a specified acceptance range (ε). Previous studies have made similar observations [12, 15].

Let's see more details about the synthesized results from stacked SBM. The first column in Fig. 5.6(a) contains the synthesized results from the stacked SBM. The connectivity relationship of synthesized topology design variables corresponding to the baseline mechanism is Stephenson III 6-bar linkage mechanism. In the synthesized results in Fig. 5.6(a), we called for rigidly connected rigid blocks as mega-block like M-block 4-7 ($B^{(4)}$ and $B^{(7)}$ are rigidly connected to each other). And we also called the dummy block (M-block 2-3-6), which is not the synthesized part of the mechanism. The topology design variables between dummy blocks do not converge to the values of the lower and upper limits but do not affect the results and generating motion of the synthesized mechanism [9, 15]. The synthesized spring components (spring design variables) in this first synthesis problem are all dummy springs unaffected by the spring-linkage mechanism's kinematic motions.

Even if synthesized dummy springs are removed from the spring-linkage mechanism, the generating motion from the synthesized mechanism is unaffected. So, we can remove the dummy springs from the synthesized results during the post process. After the post-processing with the dummy springs and dummy blocks, we can get the 1-DOF fully actuated Stephenson III 6-bar linkage mechanism. Because the first synthesis problem does not require the adaptive situation for obstacle, the 1-DOF fully actuated linkage mechanism is synthesized. This result can demonstrate that the proposed methodology can cover the results of the previous topology optimization synthesis method of 1-DOF fully actuated linkage mechanism.

The shapes of obstacles in the second and third mechanism synthesis problems are different in size for the same time step ($t = 5 \sim 8$), as shown in Fig. 5.5(b). By performing mechanism synthesis on different shapes of obstacles with the same desired motion, we want to prove that the desired mechanism synthesis method can reflect the shape of the obstacle. We can synthesize two spring-linkage mechanisms, as shown in Fig. 5.8, with the optimization formulation (5.9-5.11). 5-bar spring-linkage mechanism with 4 spring components is synthesized (the other four springs on the M-block-2-3-5-6-8-9 are dummy springs that are not stretched during mechanism operation) with obstacle 2 (high obstacle). As depicted in Fig. 5.9(a), a spring-linkage mechanism with a 5-bar underactuated spring-linkage mechanism can produce a perturbation motion that can overcome obstacle 2. These perturbation motions are mainly affected by the topology and dimensions of the

baseline rigid link mechanism. The baseline rigid link mechanism of the synthesized spring-linkage mechanism is a 5-bar linkage mechanism, and the corresponding perturbation domain of baseline mechanism is shown in Fig. 5.9(b). The perturbation domain means that the mechanism is configurable with its configuration and that the shape of the obstacle is included within the perturbation domain. Therefore, the spring-linkage mechanism can overcome the obstacle by changing its configuration. Therefore, as you can see, obstacle 2 can be overcome with a synthesized mechanism.

With the synthesis problem with obstacle 3, which is smaller than obstacle 2, we can synthesize 7-bar underactuated spring-linkage mechanism with 6 spring components. As you can see in the perturbed domain in Fig. 5.10(a), the synthesized 7-bar mechanism can overcome obstacle 3 because the shape of the obstacle is included under the perturbed domain. However, the synthesized mechanism based on obstacle 3 cannot overcome obstacle 2 because this perturbed domain in Fig. 5.10(b) cannot cover obstacle 2, which is much larger than obstacle 3. Therefore, the synthesized mechanism through the optimization formulation can reflect the shape of obstacles. Therefore, through the synthesis problem of Case 1, it was proven that the proposed design method can synthesize a mechanism while simultaneously considering both the presence or absence of obstacles and the shape of obstacles. In previous mechanisms synthesis methods, spring components were typically added for introducing adaptability after segmenting one of the links of the baseline mechanism [47]. However, because the underlying mechanism (no

obstacle case) is a 6-bar linkage mechanism, we could not get results from the obstacle 2 (5-bar linkage mechanism) situation with previous methods. That is to say, the proposed method of simultaneously synthesizing the rigid link's topology and dimensions with the spring component is a very effective and valuable design approach to synthesizing adaptive mechanisms.

The proposed design methodology is based on gradient-based optimization, which means that multiple local optima can exist depending on the initial design values. For example, let's consider the synthesized 5-bar underactuated spring-linkage mechanism depicted in Fig. 5.8(a), which represents one possible result under the small obstacle condition. To validate this, optimization was performed using specifically tailored initial values for the small obstacle design condition. Fig. 5.11(a) (middle side illustrates the synthesized mechanism and the right side illustrates the perturbed domain) corresponds to the optimization results obtained when random design variables (left side of Fig. 5.11(a)) near the conditions of a large obstacle (Fig. 5.8(a)) were used as initial values. Since the small obstacle falls within the perturbed domain of the synthesized mechanism, we can confidently assert that this spring-linkage mechanism is well-synthesized under the small obstacle shape. It closely resembles the 5-bar underactuated spring-linkage mechanism depicted in Fig. 5.8(a) under the large obstacle shape condition. Furthermore, as shown in Fig. 5.11(b), optimization was performed using random design variables (shown on the left side of Fig. 5.11(b)), resulting in a 5-bar underactuated spring-linkage mechanism with a different spring configuration. By

examining the perturbed domain of this synthesized mechanism on the right side of Fig. 5.11(b), it was confirmed that it can effectively overcome obstacles. Hence, the proposed gradient-based optimization synthesis method can yield various local optimal values depending on different initial conditions, all of which satisfy the desired design requirements. However, to minimize biased synthesized results caused by these initial conditions, appropriate initial conditions are set as $0.5 \approx (\xi_{\min} + \xi_{\max}) / 2$.

5.4.2 Case study 2: Synthesis of the 1-DOF adaptive gripper mechanism

This section attempts to synthesize an adaptive gripper by applying the proposed synthesis method to the actual design problem. With a single driving actuator, the 1-DOF fully actuated linkage gripper can generate underlying grasping motions. Effective grasping motions, however, are sometimes unachievable when interacting between gripper and objects of varying sizes. On the other hand, by further deformations from spring components, the 1-DOF underactuated spring-linkage adaptive gripper may generate the grasping motion with objects of various sizes. Therefore, the 1-DOF adaptive gripper must be able to generate both the underlying grasping motions and additional adaptive motions that can grasp objects of various sizes. To synthesize the spring-linkage mechanism from the path

generation synthesis problem as a topology optimization method, we must define the synthesis problem as the target motions. The existing 1-DOF fully actuated gripper's generating motions at the center of phalanx 2 and the end tip of phalanx 3 were chosen as the underlying target grasping motions [68]. The paths generated by phalanx 2 and 3 (the center of phalanx 2 and the end of phalanx 3) were considered target motions to represent the kinematic functionality of grasping motion since contacts in both phalanx 2 and 3 may occur to grasp an object effectively. And when the object is grasped at phalanx 2, the adaptive motion is designed to let phalanx 3 go forward by 10 degrees to better grasp it. For some real-world design synthesis problems, such as Case Study 2, there is no information on the baseline mechanism that generates the target motions. Furthermore, designing a mechanism that simultaneously considers adaptive motions and multi-end-effectors is particularly challenging. In this case study, the conventional 1-DOF fully actuated linkage gripper was used to define the target motions for this design problem. The following synthesis processes were carried out without using the reference information of the conventional gripper.

To synthesize the adaptive gripper, we first discretize the design domain (feasible design area) with 6×3 stacked SBM, as shown in Fig. 5.12. The design domain size and resolution were set to account for the size of the target motions in Fig. 5.12. And then, with the mechanism synthesis definitions in Fig. 5.12, we can define the optimization formulation (5.9-5.11) for finding the 229 design variables (126 topology design variables, 56 dimension design variables, and 47 spring

design variables). From the iteration history (Fig. 5.13(c)) and evolutionary history (Fig. 13(d)), the 1-DOF underactuated spring-linkage mechanism is successfully synthesized (Fig. 5.13(a)). The synthesized underactuated mechanism is a 10-bar spring-linkage mechanism with 13 spring components, as shown in Fig. 5.13(a). The corresponding design variables are shown in Fig. 5.13(b). Furthermore, the synthesized mechanism can generate the target motions, as shown in Fig. 5.13(e). Based on the synthesis results, the proposed design methodology can synthesize complex mechanisms that are difficult for designers to think about and design on their own.

The synthesized results, however, are too complicated to be fabricated. Therefore, the following constraint equation is added to the optimization formulation to limit the number of springs synthesized to reduce this complexity:

$$\begin{aligned}
& \underset{\xi \in \mathbf{R}^{N_k + 2N_n + N_s}}{\text{Minimize}} && U_{SBM}(\xi) + U_{SBM}^{obs}(\xi) \\
& \text{subject to} && \Psi_t(\xi) \leq \varepsilon \quad (t = 1, 2, \dots, T) \\
& && \eta_{spring} \leq 0 \\
& && 1 \leq \sum_{n=1}^{47} \xi_n^S \leq 7
\end{aligned} \tag{5.17}$$

And all other synthesis definitions are the same as Fig. 5.12. As a result of optimization formulation in Eq. 5.17, we can obtain an adaptive gripper as shown in Fig. 5.14. The synthesized adaptive gripper is a 7-bar spring-linkage mechanism with one spring component as shown in Fig. 5.14(a). The corresponding design variables in Fig. 5.14(b) and iteration history in Fig. 5.14(c) assure that the adaptive gripper is well synthesized. And also, Fig. 5.14(d) shows the synthesized

gripper can generate the desired motions well. Still, it is hard to directly control the number of rigid links in SBM-based topology optimization. But by using an additional constraint equation to limit the number of spring components in Eq. 5.17, we can obtain the feasible 1-DOF spring-linkage adaptive gripper that can possibly be used.

Additional simulations have been conducted to verify that the synthesized gripper can effectively grasp objects of various sizes with additional deformations of spring components. The gripper should be in contact with the objects at phalanx 2 and phalanx 3 to effectively identify the object. And it can be confirmed that the synthesized adaptive gripper can grasp various objects through a simulation from ADAMS (the multibody dynamics simulation solution from MSC Software Corporation), as shown in Fig. 5.15(a). Since the grippers are symmetrical with two identical mechanisms, the simulation was performed with a one-sided mechanism and a fixed location without gravity. As the simulation from different object sizes, the synthesized adaptive gripper with the proposed mechanism can grasp various objects for further deformations from spring components, as shown in Fig. 5.15(b).

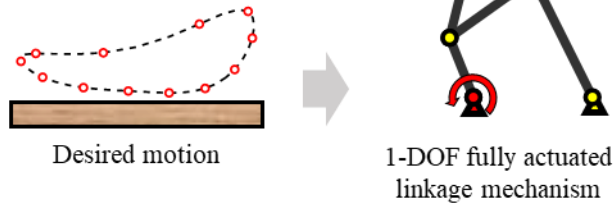
5.5 Summary

In this study, we presented a novel method for synthesizing mechanisms that can account for desired motion while also considering the presence and shapes of obstacles. To achieve this, we proposed a topology-optimization-based approach that can synthesize the dimensions and topology of both spring components and rigid links. Our approach uses a ground structure model that stacks two design spaces, allowing us to define the topologies and dimensions of spring components and rigid links. By sharing state variables between these design spaces, we can reduce the number of dimension design variables that affect the optimization's difficulty and time cost. Using continuous design variables to represent the topology and dimensions of different spring-linkage mechanisms also makes the gradient-based optimization synthesis process more numerically efficient overall.

We successfully validated our approach by recovering several synthesis problems under diverse obstacle circumstances. Our approach enabled us to synthesize 1-DOF underactuated spring-linkage mechanisms and 1-DOF fully actuated linkage mechanisms, both with and without obstacles. We also demonstrated the ability to synthesize an adaptive gripper that can grasp obstacles of different shapes using our proposed methods. Despite the success of our approach, there are limitations to how the complexity of synthesized mechanisms can be controlled. To better use the synthesis approach, we need to use complicated spring component configurations in the spring design space, which increases the computational cost and difficulty of optimization. Therefore, controlling the

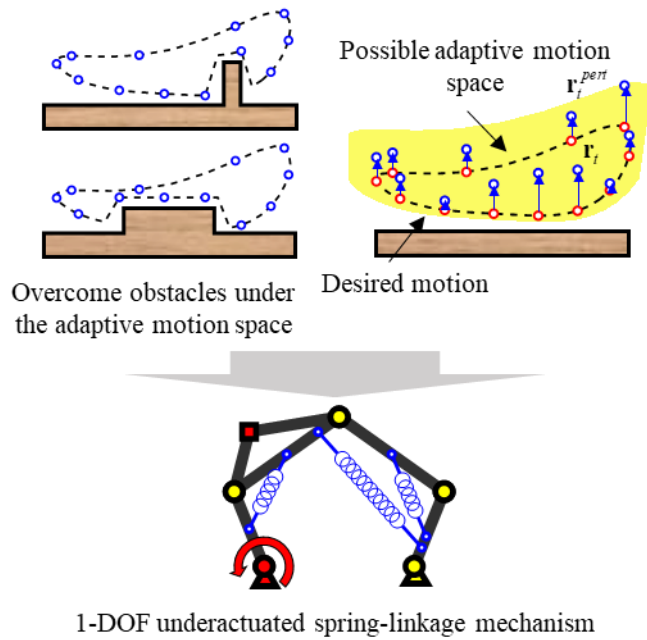
complexity of the spring-linkage mechanism will be an interesting and challenging research topic for future studies. Overall, our methodology is expected to pave the way for more useful automated methods for adaptive mechanism synthesis.

Adaptive motions cannot be considered



(a)

Adaptive motions can be considered



(b)

Fig. 5.1 Depending on the situation, different mechanisms are needed for a single-driving actuator. (a) If the desired motion is the only consideration, a 1-DOF fully actuated linkage mechanism is required. (b) However, if adaptive motion is necessary, such as overcoming obstacles, a 1-DOF underactuated spring-linkage mechanism is needed.

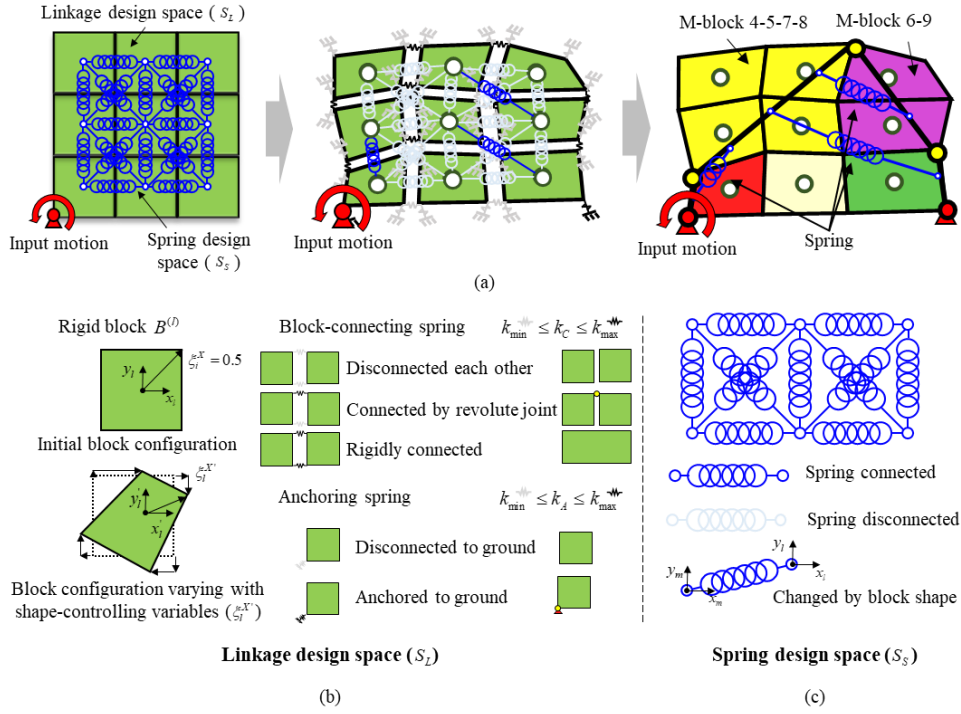


Fig. 5.2 The proposed method for synthesizing the spring-linkage mechanism involves (a) outlining the topology and dimensions within a stacked block ground model. This model includes two design spaces: (b) a link design space (S_L) and (c) a spring design space (S_S).

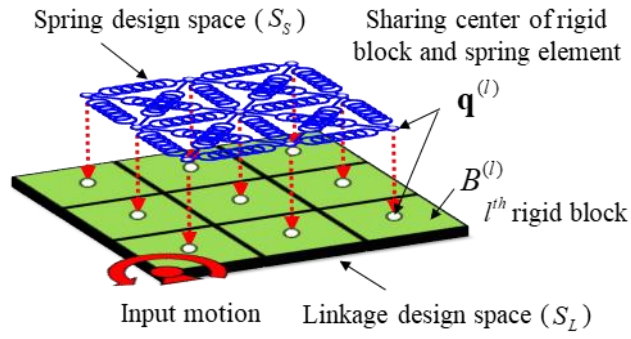


Fig. 5.3 In the proposed stacking method, state variables are shared between the linkage and spring design spaces.

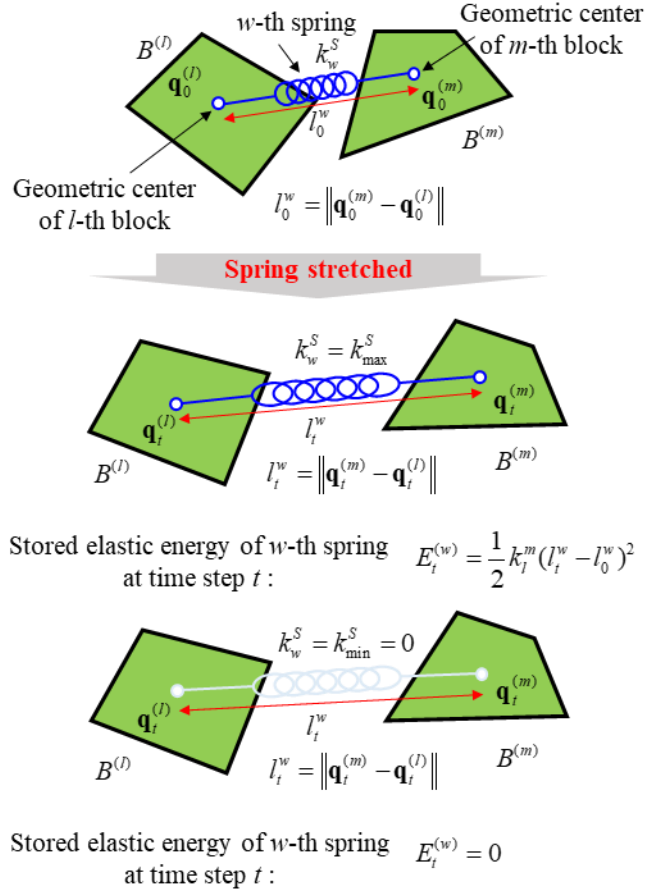


Fig. 5.4 The stored elastic energy of actual spring components in stacked SBM.

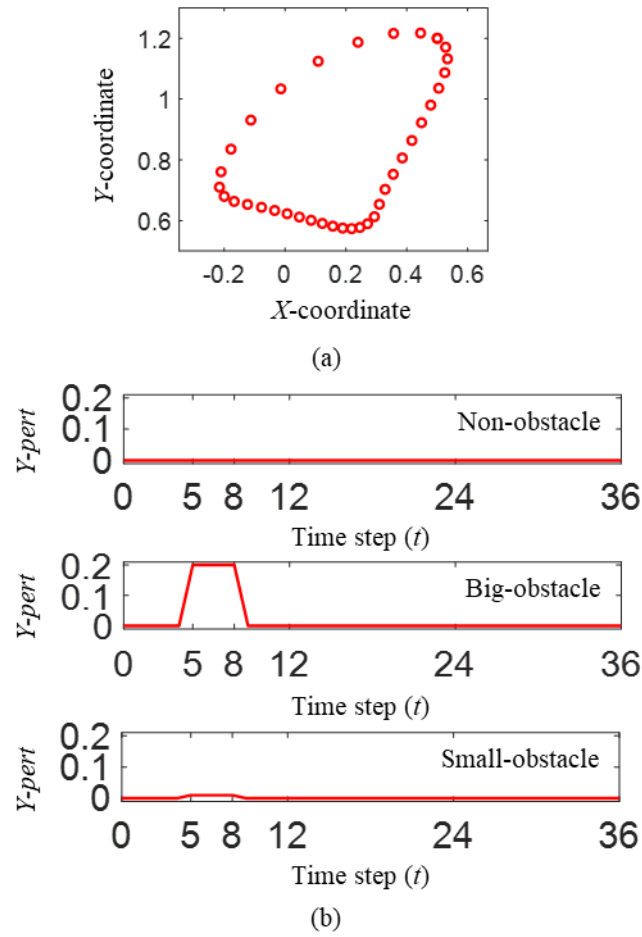


Fig. 5.5 (a) Target motion of case study 1 and (b) three different obstacle shape conditions.

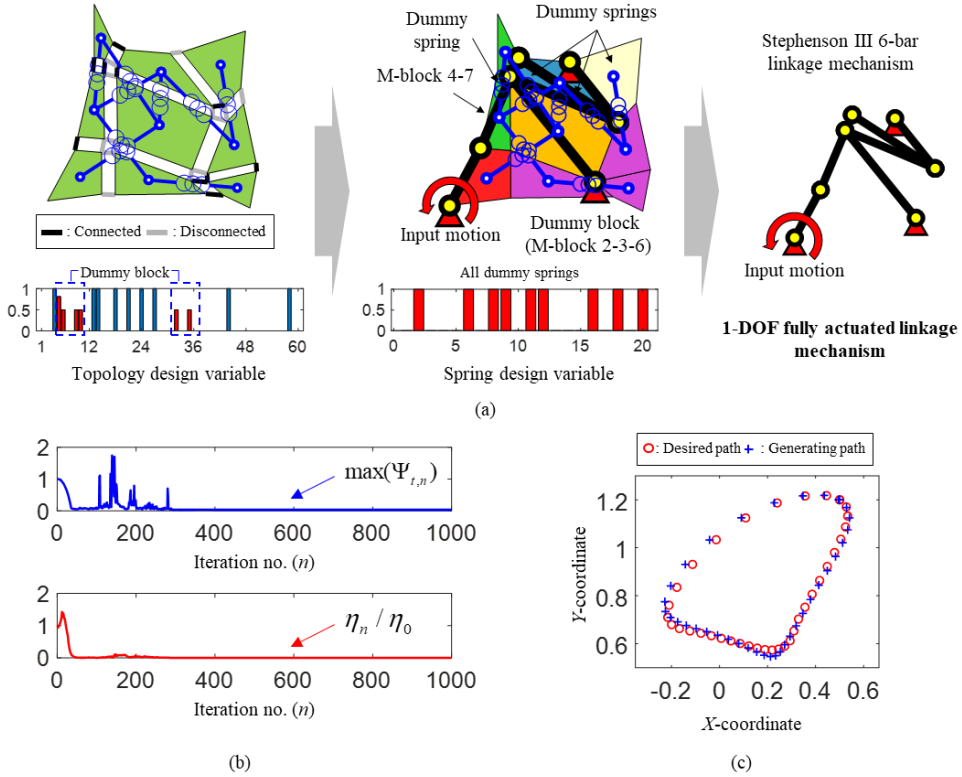


Fig. 5.6 The results of the first condition of case study 1 include: (a) the synthesized results and their corresponding topology and spring design variables (note that the red ticks in the bar graph represent the dummy block and dummy springs), (b) the convergence history of the constraint equations and objective function, and (c) a comparison between the desired motion and the synthesized motion.



Fig. 5.7 The evolutionary history of the synthesized mechanism, as expressed by the proposed block ground model, pertains to the synthesis problem defined in Fig. 6.

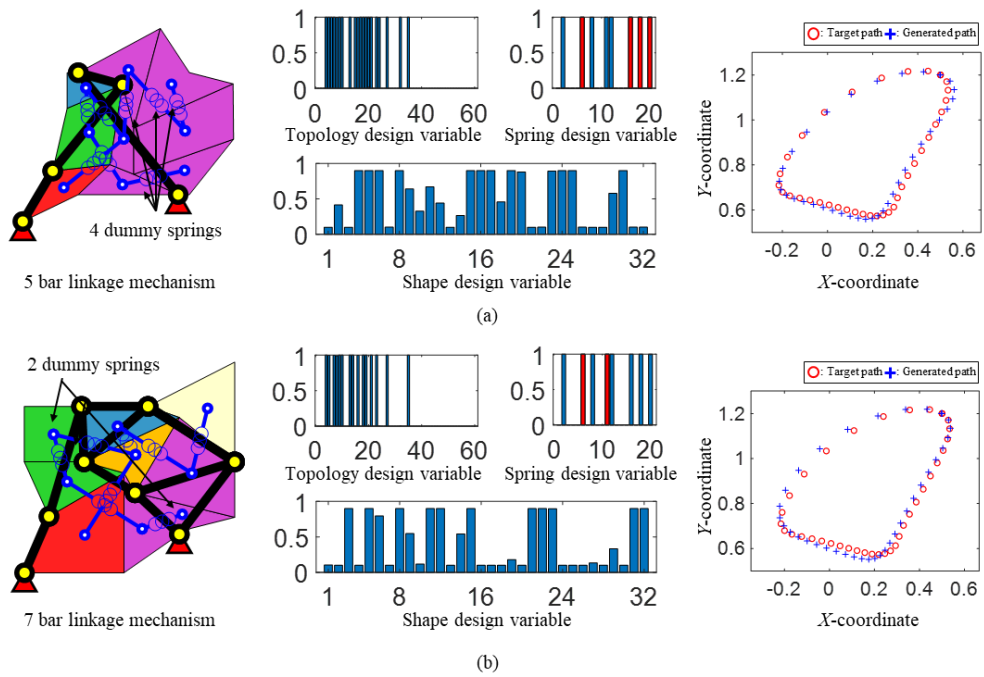


Fig. 5.8 The synthesized results for the second and third obstacle conditions in Case Study 1 are presented as (a) and (b), respectively. (Note that the red ticks in the bar graph indicate the presence of dummy springs.)

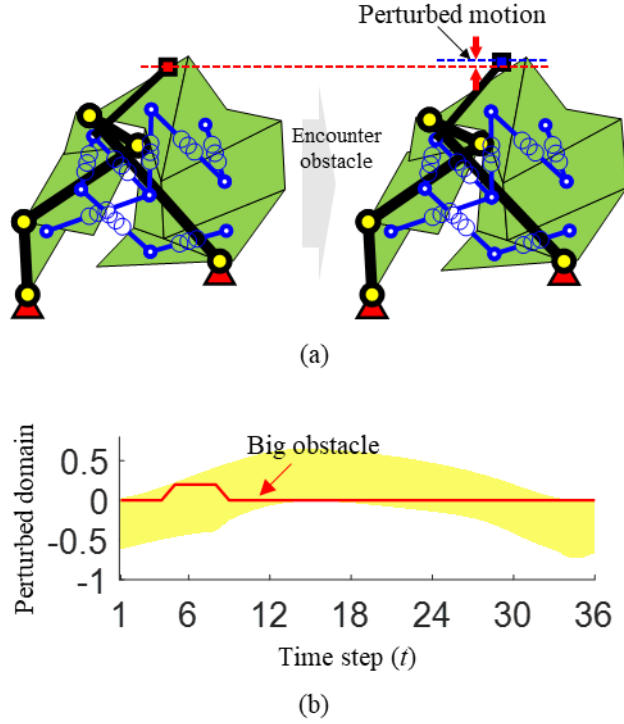
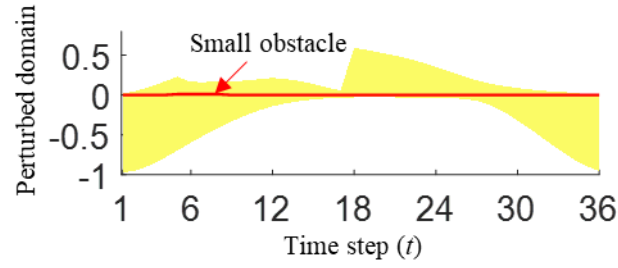
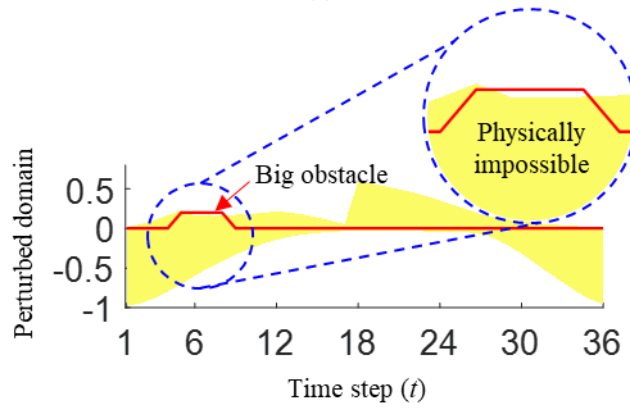


Fig. 5.9 (a) The 5-bar underactuated spring-linkage mechanism synthesized for the big obstacle conditions is capable of moving into a perturbed motion. (b) As the corresponding perturbed region is situated over the shape of the big obstacle, the synthesized mechanism is able to successfully overcome it.



(a)



(b)

Fig. 5.10 Regarding the synthesized spring-linkage mechanism from the small obstacle condition, (a) the perturbed region is situated over the small obstacle, allowing it to successfully overcome such obstacles. (b) However, it is not capable of overcoming the big obstacle from the second obstacle condition.

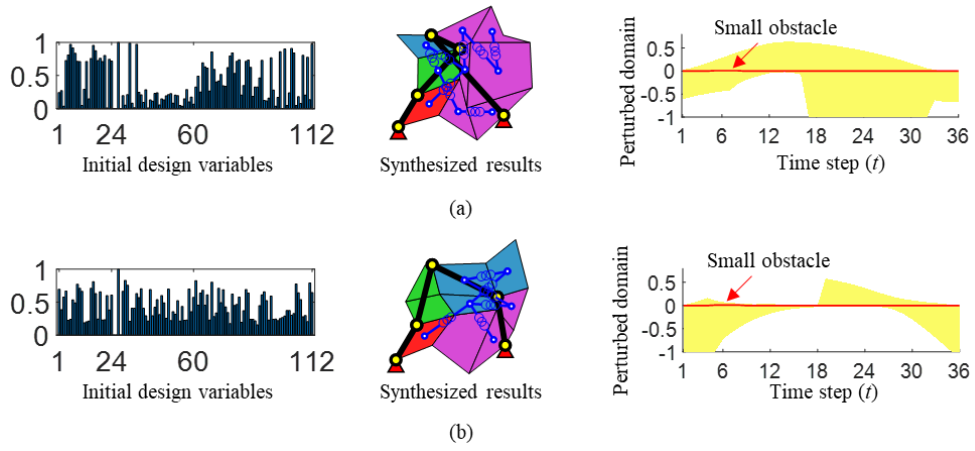


Fig. 5.11 The synthesized mechanism and its perturbed domain obtained from different initial design variables. In (a), the initial design variables close to the synthesized results shown in Fig. 5.8(a), while in (b), randomly generated initial design variables are used.

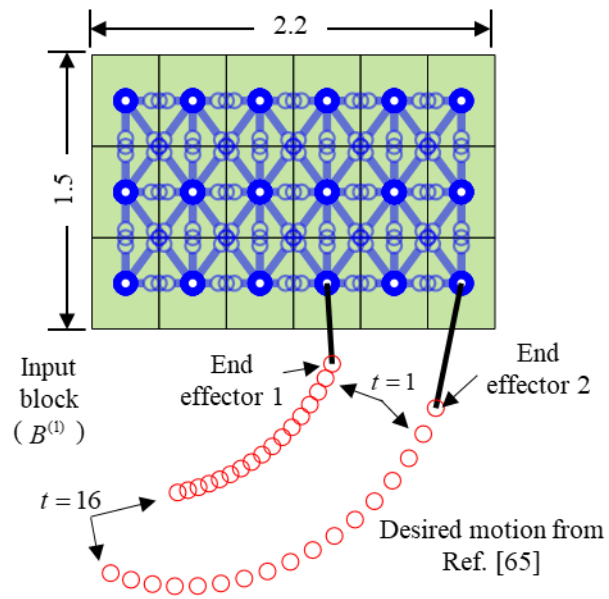


Fig. 5.12 The problem definitions of synthesizing 1-DOF adaptive gripper.

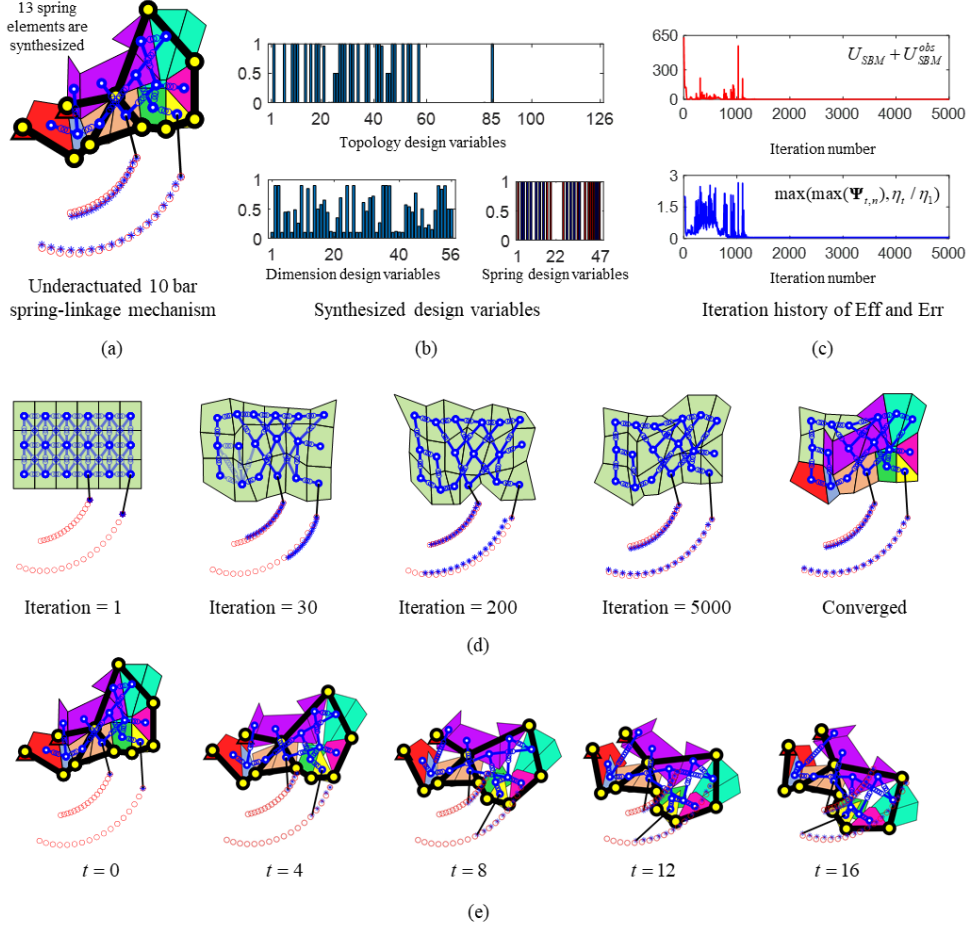


Fig. 5.13 The overall results of synthesizing the adaptive gripper include: (a) the successful synthesis of a 1-DOF underactuated 10-bar spring-linkage mechanism, as well as (b) its corresponding design variables (note that the red ticks in the bar graph represent the presence of dummy springs). The success of the overall synthesis can be confirmed by (c) the iteration history of objective functions and constraint equations, as well as (d) its evolutionary history. Furthermore, (e) the synthesized 1-DOF adaptive gripper is capable of generating the desired motions effectively.

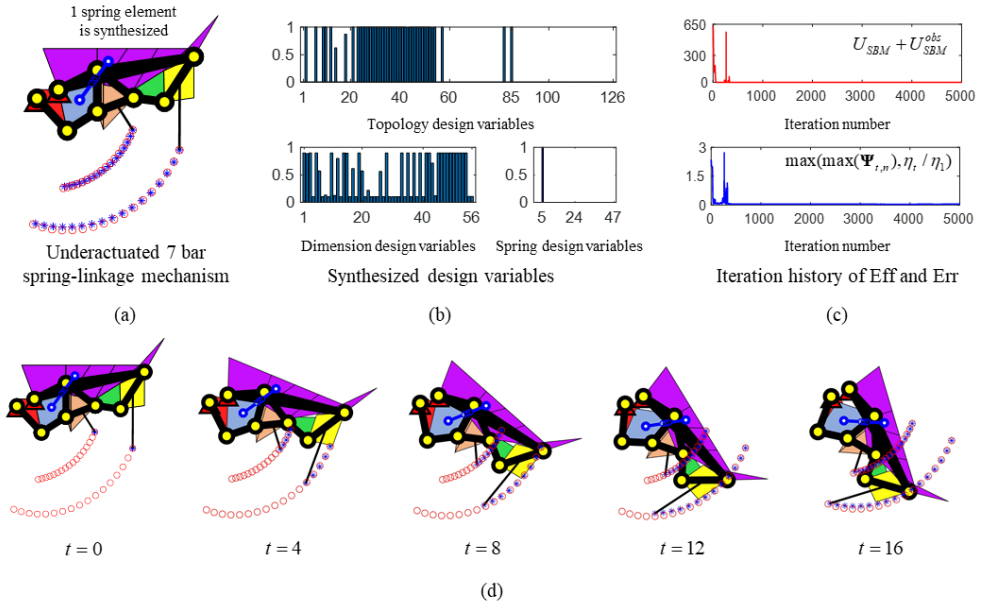
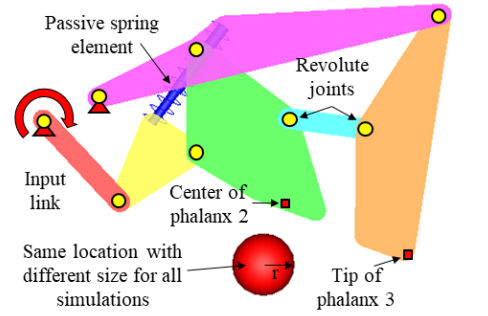
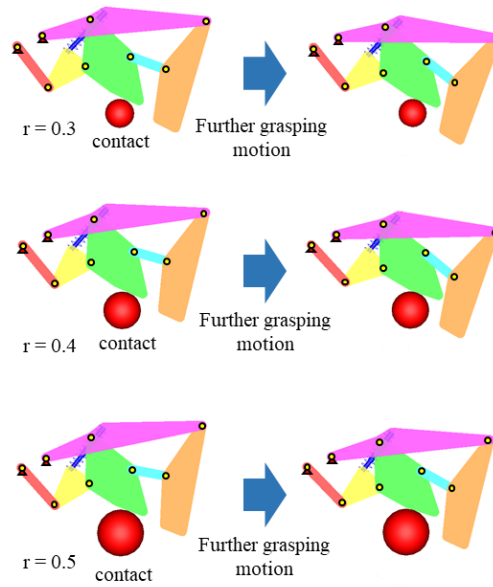


Fig. 5.14 The overall results of synthesizing the adaptive gripper using the optimization formulations presented in Eq. 17 include: (a) the successful synthesis of a 1-DOF underactuated 7-bar spring-linkage mechanism, along with (b) its corresponding design variables. The success of the overall synthesis can be confirmed by (c) the iteration history and (d) the generated motions.



1-DOF underactuated 7 bar spring-linkage mechanism

(a)



(b)

Fig. 5.15 (a) the simulation grasping situation for the synthesized adaptive gripper.
(b) the simulation results between different sizes.

CHAPTER 6.

Conclusions

In this dissertation, we propose a new modeling and formulations for different mechanical components, considering the topology and dimensions applied to link, gear, pulley, and spring components. This proposed methodology can be expanded to the various mechanical components-based mechanism topology optimization and can be applied to real-world synthesis problems. A key idea for considering different mechanical components is to stack each mechanical component design space on top of the linkage design space, which was a previous linkage-only modeling method. Additionally, we have developed a new optimization formulation that addresses the underactuated DOF issues that arise from considering spring components. In each chapter of this study, we successfully addressed various mechanism design problems. For example, in chapter 3, we explored gear-linkage mechanisms, in chapter 4, we investigated pulley-linkage mechanisms, and in chapter 5, we examined spring-linkage mechanisms.

Chapter 2 introduces a new shape SBM that minimizes the number of design variables required for mechanism dimensions. As the number of design variables directly affects our optimization-based mechanism synthesis problems, it is crucial

to keep this number as low as possible. Unfortunately, considering dissimilar mechanical components requires adding design variables for topology and dimension-related design variables. Nevertheless, the proposed shape SBM's design variables can affect not just the four nodes of the block but also its rigid block's mass center. This aspect can minimize the dimensions related design variables for additional mechanical components.

Chapter 3 proposes a novel topology optimization method for gear-linkage mechanism. The study demonstrates that this method can simultaneously determine the type, number, and dimensions of mechanisms. This approach was the first successful synthesis of a mechanism involving both linkages and gears using gradient-based topology optimization. To model this gear-linkage mechanism, two design spaces are introduced, including linkage and gear design spaces. Each space is discretized using rigid or gear blocks connected by artificial springs, with the stiffness of these springs controlling the presence of gear components. Additional gear design spaces can be added flexibly if multiple gear ratios are expected. In addition, the use of continuous design variables and a gradient-based algorithm allows for an efficient optimization-based synthesis method. This study was a significant milestone in enabling the design of various dissimilar mechanical components in the following chapter's mechanism topology optimization.

Chapter 4 proposes a mechanism topology optimization considering pulley mechanism. This study expands the gear-linkage mechanism topology optimization study in Chapter 3 and enables the mechanism topology optimization of not only

for gears but also for pulley components. To consider the pulley component, a pulley block was defined, and instead of stacking one gear design space, multiple pulley spaces were stacked over the linkage design space to succeed in expressing the pulley component that was complicatedly engaged. As the pulley component is applied in mechanism topology optimization, this study is of great significance in that it succeeded in considering both serial mechanism and parallel mechanism for the first time. And this success has made it possible for mechanism topology optimization to be applied to design problems that simultaneously consider various dissimilar mechanical components, such as robot design.

Chapter 5 addressed a novel mechanism synthesis problem, which differed significantly from those handled in the previous chapters. While the previous chapters exclusively focused on synthesizing 1-DOF fully actuated mechanisms using rigid components such as links, gears, and pulleys, Chapter 5 introduced a mechanism topology optimization approach that incorporated spring components with rigid links to synthesize 1-DOF underactuated spring-linkage mechanisms. To represent the topology and dimensions of the spring-linkage mechanism, we proposed a design space that stacked the spring and linkage design spaces. We also shared the state variables of spring components and rigid blocks, allowing us to represent the dimensions of spring components using the dimensional design variables for rigid blocks. Moreover, we designed a mechanism capable of overcoming obstacles by utilizing the underactuated DOF of the spring component. To achieve this, we developed a new optimization formulation that considered the

shape of obstacles. With this proposed modeling method and optimization formulation, we successfully synthesized a spring-linkage mechanism that can surmount various obstacle shapes. In addition, we succeeded in designing a novel 1-DOF adaptive gripper based on the proposed design methodology.

To sum up, we proposed new method to consider the dissimilar mechanical components in mechanism topology optimization. Although this is not designed in consideration of spring components, gear components, pulley components, and rigid links at the same time, it is possible to expand to one unified design method through an example in which 1-DOF fully actuated linkage mechanism is designed if there are no obstacles in chapter 5. Through this proposed methodology, I think that the mechanism topology optimization method will be applied to various robot mechanism designs.

APPENDIX A.

Using mechanism big data to reduce the design variables in mechanism topology optimization

A.1 Overview

In this appendix A, we will discuss about how to control the number of design variables in mechanism topology optimization. Since all the mechanism topology optimization processes in this dissertation are based on gradient-based optimization, reducing the number of design variables is crucial. This is why we have suggested the new shape SBM, which considers the dimensions of rigid links and other mechanical components along with the mass center of the rigid block. However, it is inevitable to increase the number of design variables to deal with various mechanical components simultaneously, and nonlinear mechanism synthesis problems become more challenging with an increase in design variables. Therefore, this appendix A focuses on developing a new synthesis method that combines a neural network. As we aim to overcome this limitation of current mechanism topology optimization method, this study is devoted to the development of a new synthesis method that combines a neural network-based big data approach and a

gradient-based shape optimization approach.

It is worth emphasizing that the core part of our approach is a neural network-based big data approach to determine the topology of a mechanism and the end-effector location simultaneously. The neural network-based approach, which is known to be advantageous when mapping nonlinear relationships [69], is suitable for this problem considering that no other approach appears to be capable of realizing the simultaneous determination of a mechanism topology and the corresponding end-effector location for a given target path. For the synthesis step, the design domain (limiting the maximum dimensions of a synthesis mechanism) is assumed to be given and the big data approach is utilized within this domain. Once the topology and the end-effector location are determined, the dimensions of the mechanism determined by the big data approach can be finely tuned by a gradient-based optimization method.

Before explaining the key aspects of our approach below, we review earlier investigations using big data approaches for mechanism synthesis. Vasiliu and Yanou [70] and Khan et al. [71] determined the link lengths of a 4-bar mechanism using a Fourier-transformed path dataset. Galán-Marín et al. [72] used a big data approach in which wavelet-converted target path information was used to determine the dimensions of a 4-bar mechanism. Other related studies can be also found in the literature [73-78]. The aforementioned studies, however, were mainly concerned with dimensional synthesis in which a mechanism with a fixed topology, such as a 4-bar or 6-bar mechanism, is pre-selected. It should be noted that without

using a unified model to represent a mechanism of different topology, it would be difficult to generate big data in a systematic and unified manner. The literature review indicates the absence of an earlier approach to determine M_T and \mathbf{r}_Q simultaneously either using a big data approach or by mechanism topology optimization. In this respect, our study appears to be the first attempt to determine M_T and \mathbf{r}_Q simultaneously.

At this point, we present an overview of the proposed approach, which is depicted in Fig. A.1. First, we are mainly concerned with the synthesis of a mechanism which generates a complete closed path, which will be described in terms of its Fourier descriptors, as sketched in Fig. A.1(a). If the generated path is complete, the corresponding mechanism should be fully rotatable, implying that the motion of its input link (such as rotational motion) can be fully transferred to the desired motion of its end-effector. As illustrated in Fig. A.1(a), the first step (Step 1) is focused on the development of a neural network-based big data approach that can simultaneously determine the topology and its end-effector location for a given target path. Here, it should be noted that a linkage mechanism consisting of links and revolute joints is represented by what is known as the spring-connected rigid block model (SBM) [7-9, 12-15, 41], referring to a ground model capable of representing linkage mechanisms with different topologies and shapes. In this modeling approach, an allowable domain for a mechanism is discretized by a set of rigid blocks connected by zero-length elastic springs of variable stiffnesses. When the springs reach their upper or lower bound stiffness levels, mechanisms of

various topologies can be represented. Here, the key motivation to employ the SBM for the big data approach stems from the fact that the SBM can generate diverse mechanisms of different configurations only with a single model via prescribed discretization. (More details are given in the next paragraph.) In Step 2, the specific dimensions of the linkages are determined by a shape optimization algorithm once \mathbf{r}_Q and M_T are determined. The remaining figures, Fig. A.1(b) and Fig. A.1(c) respectively present a schematic of the mechanism data generation process using the SBM and present the overall procedure of the neural network-based approach. The data generation scheme will also be explained in the next paragraph because it is unique to the SBM.

Next, we briefly explain our method of generating mechanism data using the SBM for a big data approach. For the generation of mechanism data, the stiffness values of the zero-length springs are randomly generated to ensure the diversity of the mechanism configuration data used to train the neural network. However, the SBM with a certain set of stiffness values may represent either a physically unrealizable mechanism or a mechanism that does not allow full rotatability. These mechanisms should be screened out when constructing the dataset. As an indicator useful for checking whether a generated mechanism expressed by the SBM is a physically realizable mechanism with full rotatability, we propose the calculation of the mean value of the work transmittance efficiency ($\bar{\eta}$) of a generated mechanism. The work transmittance efficiency is the ratio of the output work done by some force applied at the end-effector of a mechanism to the input work by the

input link. It has been shown [11] that if $\bar{\eta}$ reaches unity, which is its maximum value, the corresponding mechanism is a fully rotatable, physically realizable one-degree-of-freedom (1-DOF) mechanism. Thereby, we can keep only mechanisms for which $\bar{\eta} = 1$ (more practically, $\bar{\eta} \approx 1$) in the data and filter out the others.

This paper proceeds as follows. Because the spring-connected rigid block model (SBM) is used to model mechanisms with various topologies, Section A.2 presents a brief description of the SBM and discusses how to create a dataset to build a neural network using the SBM. In Section A.3, we discuss the proposed mechanism synthesis method using the dataset generated in Section A.2. Dimensional synthesis using a gradient-based optimization method is also explained in Section A.3, where the detailed dimensions of the synthesized mechanism created with the neural network are determined by dimensional synthesis. The validity and usefulness of the proposed mechanism synthesis method are demonstrated in Section A.4 using various case studies. Conclusions are given in Section A.5.

A.2 Generation of big data using the SBM for neural network training

The proposed mechanism synthesis method involves two synthesis steps, a topology synthesis step and a dimensional synthesis step, as shown in Fig. A.1. During the topology synthesis step, both the mechanism topology (M_T) and its end-effector location (\mathbf{r}_Q) are simultaneously determined using a neural network constructed with big data pertaining to the mechanism (henceforth ‘mechanism big data’) once a target path is prescribed.

During the construction of mechanism big data for neural network training, three key issues must be addressed. First, big data composed of mechanisms with different topologies must be generated, such as 4-bar, 6-bar and multi-links mechanisms, while the end-effector location can be fairly arbitrarily located. To facilitate the generation of mechanisms with different configurations (topologies and dimensions), we will use the spring-connected rigid block model (SBM) [7] as proposed in the introduction, which is a unified model capable of representing mechanisms of various topologies and dimensions. For instance, the SBM can be discretized into nine (3×3) blocks, each of which is inter-connected by zero-length springs with variable stiffnesses, as sketched in Fig. A.1. In that the SBM for a specified domain size and discretization level is capable of representing quite a few different topologies and dimensions of mechanisms, the SBM makes it very convenient for the generation of mechanism data for a neural network. This is why

the SBM is adopted in this study. In addition, when employing the SBM for mechanism data generation, we locate the end-effector of a synthesized mechanism at any rigid block i.e., at any link forming the synthesized mechanism. If the block shape is changed, therefore, the specific end-effector location also changes.

Second, we are interested in the synthesis of fully rotatable mechanisms, implying that the input link motion can be fully transferred to the desired motions of their end-effectors. Because the mechanism big data are initially generated with randomly assigned values of the spring stiffness and randomly located grid points of the SBM, not all of the generated mechanisms will necessarily possess full rotatability. Thus, the generated mechanism data should be screened efficiently. Here, we propose the use of the work transmittance efficiency [11] as an fully rotatability indicator such that if it reaches its maximum value (which is unity), the corresponding mechanism is declared as a mechanism of full rotatability and thus becomes an component of the mechanism big data. More details will be discussed in Section A.2.2.

Third, the input and output vectors for the neural network to be constructed should be carefully selected for the best neural network performance. Because we use the SBM as a unified model to generate various mechanisms, the vector ξ^K consisting of the stiffness values of the zero-length springs of the SBM will be used as the output vector to represent the mechanism topology (M_T). During the construction of the output vector \mathbf{P}^E , which is referred to as the end-effector

locator, all components of \mathbf{P}^E are zero except for its i th component when \mathbf{r}_Q is located in the i th rigid block. To facilitate the subsequent discussions, the symbol M_T will be expanded to refer to mechanisms with a specific stiffness variable (ξ^K) and end-effector locator (\mathbf{P}^E). To represent the prescribed path of a mechanism end-effector, the Fourier descriptors of its centroid distance function are used. More details about this subject will be presented in Section A.2.3.

A.2.1 SBM for unified mechanism modeling

The design domain of linkage mechanism synthesis is discretized into N_b rigid blocks that are inter-connected by zero-length block-connecting springs of variable stiffnesses. Each of the rigid blocks is also connected to the ground by zero-length anchoring springs of variable stiffnesses. The SBM in the paper is discretized into 3×3 rigid blocks. Clearly, the use of a more refined block discretization can represent more complicated mechanisms, though it also incurs a higher computational cost. A recent study [12] showed that if a low-resolution mesh yields a mechanism within an allowable error bound, the use of a high-resolution mesh can yield the same mechanism. It has also been demonstrated [8, 12, 13] that a large class of 4-bar, 6-bar and other multi-links mechanisms can be represented by an SBM using 3×3 rigid blocks. While this work considers revolute joints only, an extended SBM version [8, 9, 41] capable of representing prismatic and general joints and gears in addition to revolute joints has been developed. Although the use

of an SBM with more than 3×3 blocks allows the synthesis of more complicated mechanisms than those mentioned above, a 3×3 SBM will be used here to avoid excessive computational time for the generation of the mechanism configuration data. Also, a more advanced spring-connected rigid block model as given in Refs [8, 9] for the proposed big data approach were used, more general mechanisms having prismatic joints and gears in addition to links and revolute joints could be synthesized. Because, this would result in significant increase in the computation time to generate mechanism big data, we will work with a standard 3×3 SBM through this work. If the SBM developed for spatial mechanisms is further incorporated into the proposed method, it may be extended to deal with spatial mechanisms.

A.2.2 Screening for selecting fully rotatable 1-DOF mechanisms

Using the method described in Section A.2.1, we can generate a large number of mechanisms with different configurations yielding various paths of their end-effectors. However, not all of the randomly generated mechanisms can be fully rotatable 1-DOF mechanisms; some of them could be physically unrealizable or not fully rotatable despite the fact that they may be 1-DOF mechanisms. As a means by which to screen the generated mechanism data and to select fully rotatable 1-DOF mechanisms, we propose the use of the concept of the work

transmittance efficiency used in Kim and Kim [11]. The mean value of the work transmittance efficiency $\bar{\eta}$ is defined as

$$\bar{\eta} = \frac{1}{T} \sum_{t^*=1}^T \eta_{t^*} \quad (T: \text{total time step}) \quad (\text{A.1})$$

where the work transmittance efficiency (η_{t^*}) at a certain time t^* is defined as the ratio between the input work (W_{inp,t^*}) and the output work (W_{out,t^*}):

$$\eta_{t^*} = \frac{W_{out,t^*}}{W_{inp,t^*}} = \frac{W_{out,t^*}}{W_{out,t^*} + U_{t^*}} \quad (\text{A.2})$$

Recall that because external force \mathbf{F}_{ext,t^*} is applied to the end-effector, W_{inp,t^*} and W_{out,t^*} needed in Eq. (A.2) can be calculated. If $\eta_{t^*}=1$, the internal energy (U_{t^*}) stored in the block-connecting and anchoring springs both become zero because $W_{inp,t^*} = W_{out,t^*} + U_{t^*}$. If this condition is satisfied throughout all time steps during the input motion, all of the input energy is transferred to generate the motion of the end-effector without inducing any deformation in the springs of the SBM. In this case, the resulting mechanism becomes a fully rotatable mechanism. Earlier work [11] also demonstrated that if $\bar{\eta}=1$ (maximum value), i.e., if $1-\bar{\eta}=0$ (minimum value), the resulting mechanism is an 1-DOF mechanism. Therefore, a randomly generated mechanism generated by the method described Section A.2.1 is identified as a fully rotatable 1-DOF mechanism if the following criterion is satisfied:

$$1-\bar{\eta} \ll \varepsilon = 0.01 \quad (\text{A.3})$$

In theory, ε should be zero, but we set $\varepsilon = 0.01$ to allow some numerical tolerance in the kinematic analysis. Fig. A.2 shows a few examples of the generated mechanisms. As indicated in Fig. A.2, only the generated mechanisms in Fig. A.2(a) and Fig. A.2(c) are included in the dataset because they satisfy criterion (A.2) and are therefore declared as fully rotatable 1-DOF mechanisms. It should be noted that earlier methods used to check the full rotatability of mechanisms use different strategies depending on the mechanism topology [79, 80], whereas the proposed criterion can be applied to mechanisms having any topology. Indeed, the proposed criterion equally applies to the 4-bar mechanism in Fig. A.2(a) and to the 6-bar mechanism in Fig. A.2(c). As in earlier studies using the SBM [8, 12], one can identify mechanism configurations (topology and shape) without much difficulty once the values of ξ^K and ξ^x are known.

A.2.3 Representation of the mechanism dataset for the neural network

The neural network to be constructed is assumed to yield M_T and \mathbf{r}_Q for a given target path at the end-effector of a mechanism to be synthesized. The performance of a big data approach can be affected by the choice of the input and output vectors of the neural network. The mechanism topology M_T is represented in terms of the topology variables ξ^K , which will be used as the output vector of the neural network. The end-effector location \mathbf{r}_Q is represented in terms of the

end-effector locator vector \mathbf{P}^E below, which will be used as another output vector of the neural network. The vector \mathbf{P}^E is defined as

$$\mathbf{P}^E = \{p^1, p^2, \dots, p^{N_b} \mid p^i = 1 \text{ when } \mathbf{r}_Q = \mathbf{r}^{(i)}, \text{ else } p^i = 0\} \quad (\text{A.4})$$

where $\mathbf{r}^{(i)}$ denotes the position vector of the center of the i th block. Thus, we use $[\xi^K, \mathbf{P}^E]$ as the output vector in the neural network, which is defined as shown below (see Fig. A.1(c)):

$$[\xi^K, \mathbf{P}^E] = [\xi_1^K, \xi_2^K, \dots, \xi_{N_K}^K, p^1, p^2, \dots, p^{N_b}] \quad (\text{A.5})$$

In Eq. (A.5), N_K represents the number of topology variables controlling the spring stiffnesses in the SBM. Because we use a 3×3 SBM ($N_b = 9$) in this study, $N_K = 60$.

As an input vector to the neural network to be constructed, information regarding the given target path should be provided. Here, we use Fourier-transformed descriptors, which can be obtained from the centroid distance function of the desired path [24]. Referring to Fig. A.3(a), where the target path is sketched, we define the arc length (s_t) as the length between the initial point ($P(x_0, y_0)$) and point $P(x_t, y_t)$ at time t . If the centroid position of the target path is denoted by $C(x_c, y_c)$, the distance between $C(x_c, y_c)$ and $P(x_t, y_t)$ is defined as the centroid distance function with $\mathbf{r}_t = \|P(x_t, y_t) - C(x_c, y_c)\|$. If the centroid distance function is expressed in terms of the normalized arc length $\tilde{s}_t = s_t / L$ (L : total length of the

target path), it is denoted by $f(\tilde{s}_t)$, which is plotted in Fig. A.3(b). The advantage of using this description is that it does not require prescribed timing information and is independent of a reference coordinate system [81]. The Fourier descriptors were used as a preferred method to describe a path in earlier studies [24, 81-84] and were also used in gradient-based mechanism synthesis approaches using the SBM [12, 13]. The function $f(\tilde{s}_t)$ can be efficiently represented by the Fourier coefficients (a_i and b_i) as

$$f(\tilde{s}_t) = \sqrt{(x(\tilde{s}_t) - x_c)^2 + (y(\tilde{s}_t) - y_c)^2} \approx a_0 + \sum_{n=1}^p [a_n \cos(2n\pi\tilde{s}_t) + b_n \sin(2n\pi\tilde{s}_t)] \quad (\text{A.6})$$

where p indicates the highest term in the Fourier series. The Fourier coefficients of a typical curve are illustrated in Fig. A.3(c). The Fourier descriptor vector \mathbf{C} to be used as the input vector in our neural network is defined as

$$\mathbf{C} = [a_0, a_1, a_2, \dots, a_p, b_1, b_2, \dots, b_p]^T \quad (\text{A.7})$$

In this study, $p = 15$ is used, as this value was found to be reasonably capable of describing all paths considered in the case studies sufficiently accurately.

During the preparation of the dataset for the neural network to be constructed, we generated mechanisms using the variables ξ^K, ξ^X , and \mathbf{P}^E having randomly assigned values and obtained various mechanisms along with the paths of their end-effectors. After screening the generated mechanism big data using the work transmittance efficiency function, 600,000 fully rotatable 1-DOF mechanisms along with their end-effector paths were collected. (When identifying 1-DOF

mechanisms, there may appear some floating blocks not connected to the input link and the end-effector. These blocks are disregarded when forming mechanisms using the method described in the literature [9]. Among them, 500,000 dataset were used to train the neural network. Because $p=15$ is utilized in the Fourier descriptions of the central distance functions of the end-effector paths, the dimension of the input vector \mathbf{C} is 31×1 . As the output vector, we use $[\xi^K, \mathbf{P}^E]$ to determine the topology and end-effector location of a synthesized mechanism. Note that ξ^x should not be included in the output vector because ξ^x , while completely unrelated to the mechanism topology, contributes to the generation of mechanisms of different (or diverse) dimensions even for an identical vector $[\xi^K, \mathbf{P}^E]$.

To check if a set of the chosen input and output vectors (\mathbf{C} and $[\xi^K, \mathbf{P}^E]$) is a proper choice to relate the paths and topologies of the mechanisms for mechanism synthesis, we visualize the mechanism dataset between the output vector ($[\xi^K, \mathbf{P}^E]$) and the input vector (\mathbf{C}). Owing to the high dimensionality of the output vector and input vector, a dimension reduction process is needed for the mechanism dataset. The output vector $[\xi^K, \mathbf{P}^E]$, which is a $(60+9) \times 1$ column vector, is compacted into one integer (sorted from the column $[\xi^K, \mathbf{P}^E]$ in an ascending order). Therefore, each integer value corresponds to a specific combination of the topology and end-effector location. We also reduce the 31 components of the column vectors corresponding to \mathbf{C} to the first three principal components (Fig.

A.4(a)) and two components (Fig. A.4(b)) by a principal component analysis (PCA). In the figures, dots of the same color correspond to the same combination of the topology and end-effector location. To plot the mechanism dataset, we use 6,000 mechanisms composed of 1% of the generated data. Fig. A.4 shows that dots of the same color representing the same output vector are clustered, indicating that $[\xi^K, \mathbf{P}^E]$ is a reasonable output related to the input vector \mathbf{C} .

A.3 Mechanism synthesis process

In Section A.2, the generation of the big data for mechanism synthesis was described. This big data will be used to determine the topology (M_T) and the end-effector location (\mathbf{r}_Q) using a trained neural network, as suggested in Fig. A.1. In the topology synthesis step, which will be discussed in Section A.3.1 in detail, we use a simple neural network which maps the Fourier descriptor (\mathbf{C}) of the desired path to the topology and end-effector location ($[\xi^K, \mathbf{P}^E]$) of the linkage mechanism. Once M_T and \mathbf{r}_Q are determined, the next step involves the execution of dimensional synthesis (explained in Section A.3.2) to determine the dimensions (M_D) of the synthesized mechanism by gradient-based optimization. To streamline the synthesis process, the dimensional synthesis step also employs the SBM and work transmittance efficiency used in the topology synthesis step.

A.3.1 Topology synthesis step

In the topology synthesis step, we use a neural network to determine the output $[\xi^K, \mathbf{P}^E]$ of the mechanism for a given input \mathbf{C} . Here, we construct a neural network with five hidden layers with 31 input nodes (corresponding to the 31×1 input vector \mathbf{C}) and 69 output nodes (corresponding to the $(60+9) \times 1$ output vector $[\xi^K, \mathbf{P}^E]$). Each hidden layer has 500 nodes, a number deemed reasonable to deal with the present problem. ReLU [85] is used as the activation function of each

node.

Among the 600,000 generated dataset, a dataset consisting of 500,000 of these was used to train the neural network, while the remaining 100,000 were used for test. It took approximately six hours to train the neural network, requiring 10,000 iterations. It was found that the trained neural network correctly predicted $[\xi^K, \mathbf{P}^E]$ with an accuracy rate of 97.4% for \mathbf{C} belonging to the test dataset, implying that 97.4% of the target (M_T, \mathbf{r}_Q) output vectors was correctly generated for given \mathbf{C} belonging to the test dataset. Also, because $[\xi^K, \mathbf{P}^E]$ of $[\xi^K, \xi^X, \mathbf{P}^E]$ generating a given \mathbf{C} is correctly predicted through the trained neural network, ξ^X is determined easily by gradient-based optimization with the determined mechanism topology. In terms of each path generator mechanism with its cognate mechanism, 97.4% accuracy appears to be an unexplainable result. Because the proposed method is based on the design domain (which limits the maximum dimensions of mechanism), not all cognate mechanisms can be expressed in the design domain. Nevertheless, this high level of accuracy in spite of the use of a simple neural network largely stems from the properly chosen input vector \mathbf{C} that describes the target path and the output vector $[\xi^K, \mathbf{P}^E]$ that describes (M_T, \mathbf{r}_Q) . Some discussions pertaining to the remaining incorrectly predicted 2.6% of the data from the test dataset is presented in Section A.4.3 in relation to the performance of the proposed method.

A.3.2 Dimensional synthesis step

Once a mechanism is determined in terms of $[\xi^K, \mathbf{P}^E]$ for a given \mathbf{C} using the topology synthesis step described in Section A.3.1, the next step is to determine the dimensions of the links forming the mechanism of the determined topology. Because the topology synthesis step determines only the topological configuration, the target path can be more precisely traced by adjusting the dimensions of the link components and the position of the end-effector. Because the same SBM employed in the topology synthesis step is used in this step, the dimensional synthesis serves to determine ξ^X , which affects the locations of the grid points of the SBM, which in turn affects the sizes of the links forming the mechanism synthesized in the topology synthesis step. It should be noted that the $[\xi^K, \mathbf{P}^E]$ values remain unchanged in the dimensional synthesis step. Therefore, the dimensional synthesis can be efficiently completed. Because the SBM used here is discretized into 3×3 rigid blocks, there are 16 grid points, each of which having two coordinates (X, Y) . Therefore, ξ^X has 32 design variables and thus $N_s = 32$.

To determine ξ^X , the following optimization problem, which can be efficiently solved by a gradient-based optimizer, is established:

$$\begin{aligned} & \underset{\xi^X \in \mathbf{R}^{N_s}}{\text{Minimize}} && 1 - \bar{\eta} \\ & \text{subject to} && |a_n - a_{n,des}| \leq \varepsilon \quad (n = 0, 1, \dots, p) \\ & && |b_n - b_{n,des}| \leq \varepsilon \quad (n = 1, 2, \dots, p) \end{aligned} \tag{A.8}$$

Here, $\bar{\eta}$ is the mean value of the work transmittance efficiency η , as defined in

Eq. (A.2), and $a_{n,des}$ and $b_{n,des}$ are the Fourier descriptors of the target path of the end-effector of the mechanism being synthesized in the course of solving the optimization problem expressed by Eq. (A.8). More detailed accounts of solving Eq. (A.8) using the method of moving asymptotes [34] can be found in the literature [12, 13]. As used in Section A.2.2, the minimization of $1-\bar{\eta}$ (equivalently, the maximization of $\bar{\eta}$) ensures that the synthesized mechanism remains a fully rotatable 1-DOF mechanism during the dimensional synthesis process. It also means that the Grashof condition continues to be met during the optimization [11]. The constraints $|a_n - a_{n,des}| \leq \varepsilon$ impose the condition by which the generated path at the end-effector follows the target path within tolerance error ε . For a sufficiently small tolerance error value ($\varepsilon \leq 0.05$), the use of a Fourier descriptor as a constraint function during the optimization process can guarantee geometric properties for which no timing information is prescribed [13]. Furthermore, if the timing information of the target path is given (i.e., the precision point problem), we can also replace the Euclidean error as a constraint function in the dimensional synthesis step, as was done in a previous study [12]. A few remarks should be made at this point. There were earlier studies determining (ξ^K, ξ^X) simultaneously using a gradient-based approach (e.g., [12]), but it appears to be impossible to set up a gradient-based synthesis problem capable of finding all variables $(\xi^K, \xi^X, \mathbf{P}^E)$ simultaneously. On the other hand, to determine $(\xi^K, \xi^X, \mathbf{P}^E)$ simultaneously using a big data approach alone is practically impossible because

the size and number of the mechanism big data become too large to handle, especially when attempting to determine the mechanism dimensions accurately. In this respect, the proposed two-step approach can be a highly efficient, practically implementable synthesis approach for determining $(\xi^K, \xi^X, \mathbf{P}^E)$ when only the target path is given.

A.4 Mechanism synthesis process

In this section, we consider several synthesis problems using the developed method. For all problems solved in this section, we consider paths (or the corresponding mechanisms) that do not belong to the dataset consisting of the aforementioned 600,000 dataset used to construct the neural network described in Section A.3. In this way, the usefulness of the proposed mechanism synthesis approach can be better demonstrated.

For all problems considered here, we use the same trained neural network constructed during the topology synthesis step. The values of the parameters used for the entire process (topology and dimensional syntheses) are set as follows,

$$k_{\max} = 10^4 \quad \varepsilon = 0.05 \quad \xi_{\min}^K = 10^{-3} \quad \xi_{\min}^X = 10^{-2} \quad T = 36 \quad (\text{A.9})$$

while $\xi^X = 0.5$ is used as the initial value of the design variable in each case ξ^X for the dimensional synthesis. The values in (A.7) were shown to be effective in earlier gradient-based mechanism topology syntheses [8, 12, 13, 41]. This section consists of three parts:

Section A.4.1: Test problems. We start with two known mechanisms (randomly generated 4-bar and 6-bar mechanisms in the design domain) with pre-determined end-effector locations. Using them, we generate the paths of their end-effectors. Then, we check if the developed method can recover the two known mechanisms and their end-effector locations successfully.

Section A.4.2: General mechanism synthesis for given paths for which the path-

generating mechanisms are unknown. For example, we will consider synthesizing a mechanism to generate the trajectory of a finger in the reference frame of a swimmer over his/her full stroke cycle.

Section A.4.3: Performance test of the proposed method: a) examination of the failed 2.6% of the test dataset in the neural network, b) computational cost for actual synthesis, and c) other issues.

A.4.1 Test problems

In this section, we consider the synthesis of two mechanisms (4-bar and 6-bar mechanisms) not belonging to the considered dataset consisting of 600,000 dataset to check if our method can recover these mechanisms and their end-effector locations successfully if the paths of their end-effectors are given as the target paths. As reference mechanisms for the validity test of the developed method, we considered the two mechanisms, 4-bar and 6-bar mechanisms, as shown in Fig. A.5. The second column in Fig. A.5 shows the synthesis results after applying the topology synthesis step (step 1); one can clearly see 4-bar and 6-bar mechanisms and their end-effector locations for Case Studies 1 and 2, respectively. The corresponding topology variables and end-effector locators are plotted in the same column. One can see that both topology variables and end-effector locators presented in the first and second columns are identical, which implies that a topology and an end-effector location (M_T, \mathbf{r}_Q) identical to those of the reference

mechanisms were obtained from the topology synthesis step. The third column shows the synthesized results after the dimensional synthesis step (step 2) and the fourth column compares the target paths and the synthesized paths generated by the mechanisms synthesized by the proposed two-step synthesis method. Clearly, the target paths are successfully traced by the synthesized mechanisms having topologies (4-bar and 6-bar) identical to those of the mechanisms used to generate the target paths. A more detailed discussion is presented below with reference to Figs. A.5, 6 and 7.

While the synthesis results after steps 1 and 2 are summarized in Fig. A.5, the detailed procedures of the proposed synthesis method are described in Fig. A.6 for Case Study 1. Fig. A.6(a) shows the procedure used to compute the Fourier descriptor vector \mathbf{C} (with $p=15$) of the target path, which is used as the input vector to the trained neural network. Fig. A.6(b) illustrates the determined mechanism topology (4-bar mechanism) and end-effector location expressed in terms of $[\xi^K, \mathbf{P}^E]$. The SBM representation of the synthesized mechanism is illustrated as the output of the neural network; short black solid lines between adjacent blocks represent the connected states ($\xi_i^K=1$) and the small filled red square in Block 3 represents the end-effector location. Going back to Fig. A.5(a), one can see that the topology variables given below the reference mechanism used to generate the target path are identical to those given below the synthesized mechanism after the topology synthesis step. This indicates that the proposed

neural network successfully determines the mechanism of the given topology. Fig. A.6(c) shows the result of the dimensional synthesis step, which changes the shapes of the rigid blocks while the mechanism topology and end-effector location remain unchanged in this step. Fig. A.6(d) confirms that the path generated by the synthesized mechanism is virtually identical to the target path. Fig. A.7 shows the evolution history of the rigid blocks of the SBM by gradient-based dimensional synthesis at different time steps t^* . It also shows that the generated path by the synthesized mechanism converges to the given path as the optimization iteration proceeds. Because $\bar{\eta}$ was kept at nearly unity, only the history of the constraint function is plotted in Fig. A.7.

For Case Study 2, the observations made in Case Study 1 are mostly valid; accordingly, detailed accounts are skipped here. Referring to Fig. A.5(b), it is clear that the synthesized mechanism is a 6-bar mechanism which is topologically identical to the mechanism used to generate the target path; this is readily apparent if comparing the values of the topology variables plotted in the first and second plots in Fig. A.5(b). Dimensional synthesis was then performed to determine the detailed dimensions of the synthesized 6-bar mechanism. However, the detailed dimensions are not a perfect match to those of the given mechanism, although the path generated by the synthesized mechanism is virtually identical to the target path. The main reason for this difference is that within the acceptable range of tolerance error, there is more than one mechanism capable of generating the same path (within a given tolerance range). Similar observations were also made in

earlier studies [8, 12, 13, 41]. As is apparent, the proposed synthesis method successfully found a mechanism by which to generate the target path.

A.4.2 General mechanism synthesis

In this section, we attempt to synthesize general mechanisms for given end-effector paths for which mechanisms generating the paths can be assumed to be unknown. Specifically we consider three paths: 1) **Target path 1**: a path describing the two-dimensional trajectory of a finger in the reference frame of a swimmer over his/her full stroke cycle [86], shown in Fig. A.8(a), 2) **Target path 2**: another path generated due to the anteroposterior and dorsoventral motion relative to a turtle's body throughout its limb cycle [87], shown in Fig. A.8(b), and 3) **Target path 3**: a path considered in Refs [88, 89] which has timing information, shown in Fig. A.8(c). To apply this Target path 3 in our design domain, I reduced the overall size to 1/2 and used it symmetrically for $y = x$. The problems are to find linkage mechanisms that generate these three paths, if such realizations are possible. To solve these problems with conventional approaches, mechanisms with different candidate topologies and corresponding end-effector locations may be repeatedly considered until a desired path is synthesized. On the other hand, the proposed approach can be advantageous in that it does not require a specific baseline mechanism topology or end-effector location, allowing a streamlined mechanism synthesis process. In this respect, these problems are very feasible for testing the effectiveness of the proposed method.

The mechanism synthesis process for Target path 1 is summarized in the form of graphical illustrations in Fig. A.9(a). As was done for the problems considered in Section 4.1, the $[\xi^K, \mathbf{P}^E]$ values are determined from the topology synthesis step; the synthesized mechanism is a 4-bar mechanism with its end-effector located at Block 4 ($p^4 = 1$). The dimensional synthesis problem expressed by Eq. A.10 is then solved to determine the link dimensions of the 4-bar mechanism. Fig. A.9(b) shows the synthesized mechanism (4-bar mechanism) and Fig. A.9(c) compares the target path and the path generated by the synthesized mechanism. As indicated by Fig. A.9(c), the path generated by the end-effector of the synthesized mechanism is nearly identical to the target path, indicating the effectiveness of the proposed method. The results for Target path 2 are given in Fig. A.10. An 8-bar mechanism is synthesized, as shown in Fig. A.10(c). The path generated by the synthesized mechanism compares favorably with the target path. The results for Target path 3 are given in Fig. A.11. A 4-bar mechanism is synthesized, as shown in Fig. 13(c). Because this problem considers timing, the Euclidean error was used as a constraint function in Eq. A.10. These three examples clearly demonstrate that the proposed synthesis method effectively synthesizes a mechanism that generates a given path for which information on the corresponding baseline mechanism is lacking.

A.4.3 Examination of the performance of the neural

network-based approach

In this section, we examine the performance of the proposed method. After we examine the failed 2.6% of the test dataset in the neural network, we discuss the computational cost of the proposed method for actual synthesis.

a) Examination of the failed 2.6% of the test dataset

It was observed in Section A.3.1 that the trained neural network correctly predicts the topology variables and the end-effector locators ($[\xi^K, \mathbf{P}^E]$) for approximately 97.4% of the test dataset. However, we will demonstrate that not all of the failed 2.6% results are obsolete because a given path could be generated by a mechanism different from that used to generate target path \mathbf{C} . This is possible because mechanisms of different topologies and end-effector locations (i.e., different (ξ^K, \mathbf{P}^E) combinations) can in fact generate nearly the same path if their link dimensions are appropriately adjusted. To show this, we consider the problem given in Fig. A.12. To avoid the adverse effects on the performance of the neural network, the number of nodes in the neural network needs to be sufficiently large in each layer. In the present, each layer has 500 nodes.

The illustration on the upper left side of Fig. A.12 shows a reference 4-bar mechanism represented in the SBM, along with the corresponding generated path, which will be considered as the target path here. The values of the topology variables $\xi_i^K \in \{0,1\}$ used to represent the mechanism by the SBM are indicated by the corresponding mega-block description. The topology variables and the end-

effector locators of the reference mechanism are denoted by $({}^R\xi^K, {}^R\mathbf{P}^E)$. (As noted before, a mega-block of the same color functions as a single rigid block or link.) To find a mechanism to generate the target path obtained by the reference mechanism, we applied the developed neural network-based topology synthesis method. The synthesis results are shown under the subtitle “Step 1” in Fig. A.12. The synthesized mechanism configuration and its end-effector location, represented by $({}^S\xi^K, {}^S\mathbf{P}^E)$, are not identical to those of the reference mechanism $({}^R\xi^K, {}^R\mathbf{P}^E)$, although the synthesized mechanism is also a 4-bar mechanism.

To observe the differences in detail, one can compare the mega-block representations of the reference and synthesized mechanisms, which are expressed, respectively, by (Input block 1, Mega-blocks 2-3 and 4-5-6-7-8-9) and (Input block 1, Mega-blocks 2-3-4-5-6 and 7-8-9). In addition, the end-effector locations (indicated by the small red squares located at the centers of the corresponding blocks) are not the same. At this point, we consider the subsequent dimensional synthesis for the synthesized mechanism in the proposed topology synthesis step, as illustrated under the title “Step 2” in Fig. A.12. Here, it is clear that the path of the synthesized mechanism traces the target path of the referenced mechanism well, as shown in the illustration on the lower right side of Fig. A.12.

To support the findings demonstrated above, Fig. A.13 is prepared. From the results shown in Fig. A.4, we compiled a dataset corresponding to a set of mechanisms with $({}^R\xi^K, {}^R\mathbf{P}^E)$ and another dataset with $({}^S\xi^K, {}^S\mathbf{P}^E)$ and plotted them

in the space of the three principal PCA axes. Blue open dots denote the $({}^R\xi^K, {}^R\mathbf{P}^E)$ dataset while orange open dots denote the $({}^S\xi^K, {}^S\mathbf{P}^E)$ dataset. Note that dots of the same color correspond to the same (ξ^K, \mathbf{P}^E) value with different \mathbf{C} values (equivalently, different ξ^x values). The figure shows that the mechanisms generating the target path and synthesized paths lie in the overlapped region of the two datasets of $({}^R\xi^K, {}^R\mathbf{P}^E)$ and $({}^S\xi^K, {}^S\mathbf{P}^E)$. This suggests that (nearly) the same path can be generated with different (ξ^K, \mathbf{P}^E) values if their dimensions are properly adjusted by a dimensional synthesis step, as proposed here.

b) Computational cost for actual synthesis

It is clear that considerable computation time is required when constructing a neural network, but the actual synthesis can be quite efficient once a neural network is constructed. Once a network is constructed, it can be used equally for other path generating problems. Aiming to compare the computational cost of the proposed neural network-based approach against that of a gradient-based simultaneous topology and shape optimization method developed in the literature [12], we consider the synthesis problem depicted in Fig. A.14(a), which is taken from the referenced study [12]. Previous work provided the input link location and target path to the location of the output end-effector, but this study solved the same problem without end-effector information. This problem appears to be useful for comparing the computation load during the actual synthesis of both approaches

using the same 3×3 SBM, although more complex design conditions are provided when using the proposed method.

When the proposed approach was applied, the same 4-bar linkage mechanism shown in Fig. A.14(a) was successfully obtained; thus, the synthesis details from the proposed method are skipped here. Instead, we focus on the total iteration number and CPU time, as indicated in Fig. A.14(b). As the figure shows, the computational cost required during the actual mechanism synthesis step is quite low once a desired neural network is constructed. This mainly stems from the fact that the gradient-based optimization method in the literature [12] uses a total of 92 design variables, representing the sum of 60 topology and 32 shape design variables simultaneously. Again, if the computation time used for neural network construction (most of the computation time during the data generation process) is also included, the present method is far less efficient than the gradient-based method. However, the present method can be advantageous because once the mechanism big data is constructed, it can determine the mechanism topology and end-effector location simultaneously, an achievement otherwise difficult to achieve.

c) Other issues

In addition to the issues considered in parts a) and b) above, one may consider developing a “universal” neural network for mechanism synthesis with which virtually general paths, either closed or open, can be synthesized. At the current development stage as described in this work, the developed neural network only

applies to the synthesis of 1-DOF fully rotatable mechanisms generating complete paths. Therefore, if mechanisms generating open paths or both open and closed paths are to be synthesized, more advanced neural networks would be needed.

Another issue is the uniqueness of the synthesized mechanism. Apparently, there can be more than one mechanism to generate the target path within the range of tolerance error. While finding all candidate mechanisms is practically important and useful, the present approach yields only one candidate mechanism because the neural network used is trained so as to generate only one candidate, with subsequent shape optimization applied to the single candidate mechanism. In spite of this limitation, the proposed method, which simultaneously determines a mechanism topology and its effector location, may be useful to those attempting to reach this goal. The use of more advanced neural networks (including the use of a generative model [77]) to find multiple optimal mechanism configurations with the idea of the simultaneous determination maintained will be an important future research subject.

A.5 Conclusion

This paper is concerned with the determination of the topology, the dimensions of a mechanism, and the corresponding end-effector location only when a target path is given. In that there are no earlier studies that simultaneously determine especially a mechanism topology and its end-effector location (relative to the input drive link), the problem itself is highly challenging. Through this study, we demonstrated that our new two-step synthesis approach can be a practically useful method. The first step is a neural-network-based synthesis step that simultaneously determines a mechanism topology and its end-effector location and the second step is a gradient-based dimensional synthesis step during which the specific dimensions of the links of the mechanism synthesized in the first step are determined. In the course of the synthesis, the use of the SBM was found to be very effective for generating mechanisms with diverse topologies and dimensions in a unified manner while also facilitating the subsequent dimensional synthesis. The neural network was trained using 500,000 mechanism dataset and tested using 100,000 mechanism dataset, and the accuracy of the network was found to be 97.4%. This high accuracy in spite of the use of a relatively simple neural network is mainly attributed to the proper choice of the Fourier descriptor input vector representing the target path as well as the length-zero spring stiffness and end-effector locating output vector based on the SBM. Using several numerical examples, we showed that mechanisms not belonging to the dataset consisting of 600,000 dataset were successfully synthesized to generate quite general target paths.

Further, the present method was limited to the automated synthesis of planar linkage mechanisms generating closed paths, it is expected to be extended to the synthesis of planar linkage mechanisms generating both closed and open paths and also spatial linkage mechanisms.

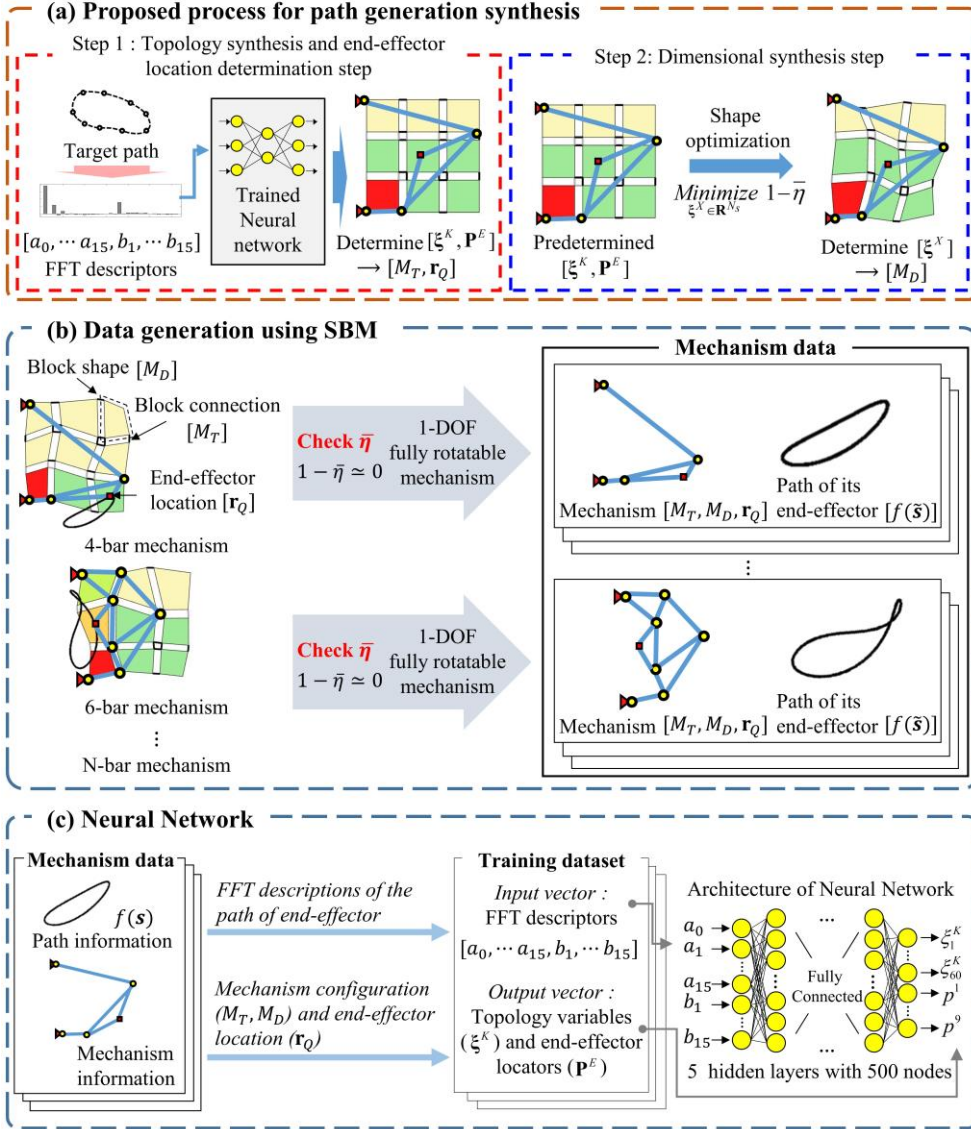


Fig. A.1 (a) The overall process of the proposed method for mechanism synthesis, (b) data generation using the SBM and a method to confirm full rotatability using the work transmittance efficiency ($\bar{\eta}$), and (c) a constructed neural network.

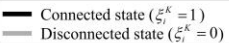
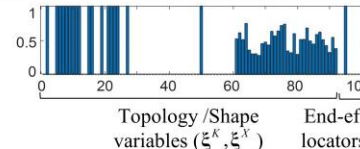
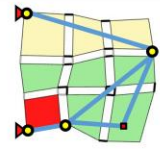
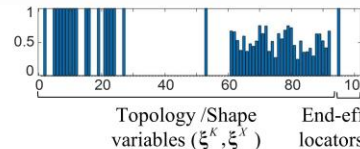
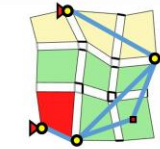
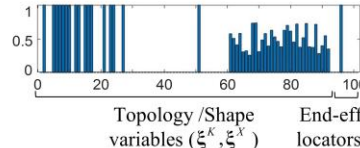
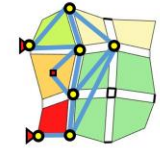
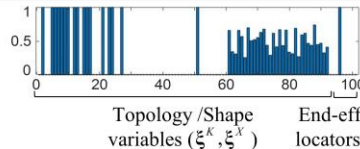

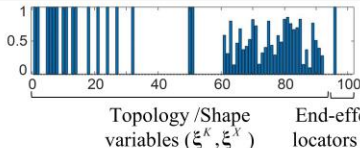
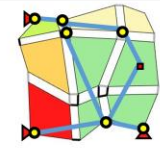
Examples of randomly generated mechanisms			Mechanism type
			
(a)	 <p>Topology /Shape variables (ξ^K, ξ^X) End-effector locators (\mathbf{P}^E)</p> 	<ul style="list-style-type: none">• $(1 - \bar{\eta}) = 0.0006 < 0.01$→ Fully rotatable(4-bar mechanism)	
(b)	 <p>Topology /Shape variables (ξ^K, ξ^X) End-effector locators (\mathbf{P}^E)</p> 	<ul style="list-style-type: none">• $(1 - \bar{\eta}) = 0.24 > 0.01$→ Not fully rotatable	
(c)	 <p>Topology /Shape variables (ξ^K, ξ^X) End-effector locators (\mathbf{P}^E)</p> 	<ul style="list-style-type: none">• $(1 - \bar{\eta}) = 0.004 < 0.01$→ Fully rotatable(6-bar mechanism)	
(d)	 <p>Topology /Shape variables (ξ^K, ξ^X) End-effector locators (\mathbf{P}^E)</p> 	<ul style="list-style-type: none">• $(1 - \bar{\eta}) = 0.4802 > 0.01$→ Not fully rotatable	
(e)	 <p>Topology /Shape variables (ξ^K, ξ^X) End-effector locators (\mathbf{P}^E)</p> 	<ul style="list-style-type: none">• $(1 - \bar{\eta}) = 0.9713 > 0.01$→ Not fully rotatable	

Fig. A.2 Examples of the generated mechanisms using randomly generated variables ξ^K , ξ^X and \mathbf{r}_Q based on the SBM. The end-effector locator (\mathbf{P}_E) in the figure is used to indicate the location of the block to which the end-effector is attached.

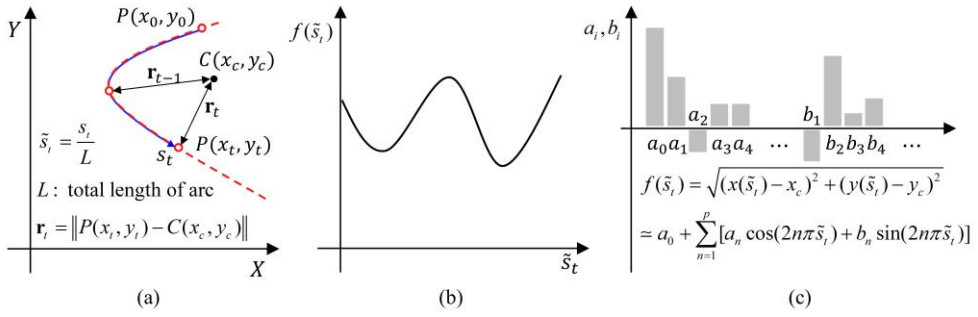


Fig. A.3 Description of a given target path using the Fourier coefficients of the central distance function $f(\tilde{s}_t)$. (a) Analysis needed to calculate the central distance function $f(\tilde{s}_t)$, (b) sketch of the centroid distance function of a typical path using the dimensionless arc length \tilde{s}_t , and (c) Fourier descriptors of the centroid distance function.

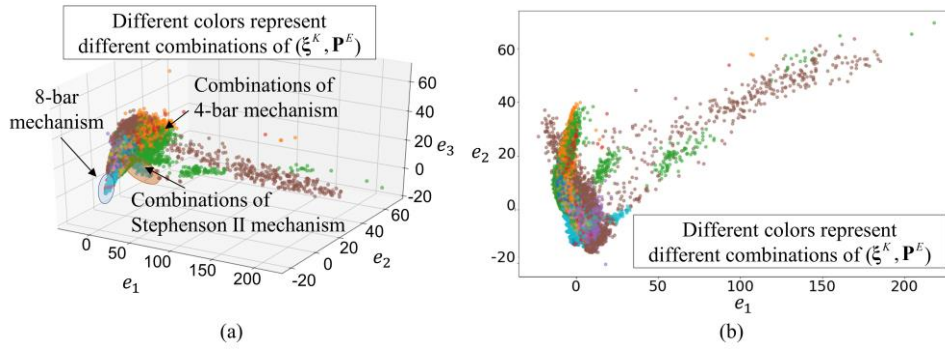


Fig. A.4 Visualization of the mechanism dataset by dimension reduction by means of a Principal Component Analysis (PCA) using the path data (FFT descriptors) and topology of the mechanism. The spaces of (a) three major component axes and (b) two major component axes are used to visualize. Dots of the same color have an identical $[\xi^K, \mathbf{P}^E]$ in both figures

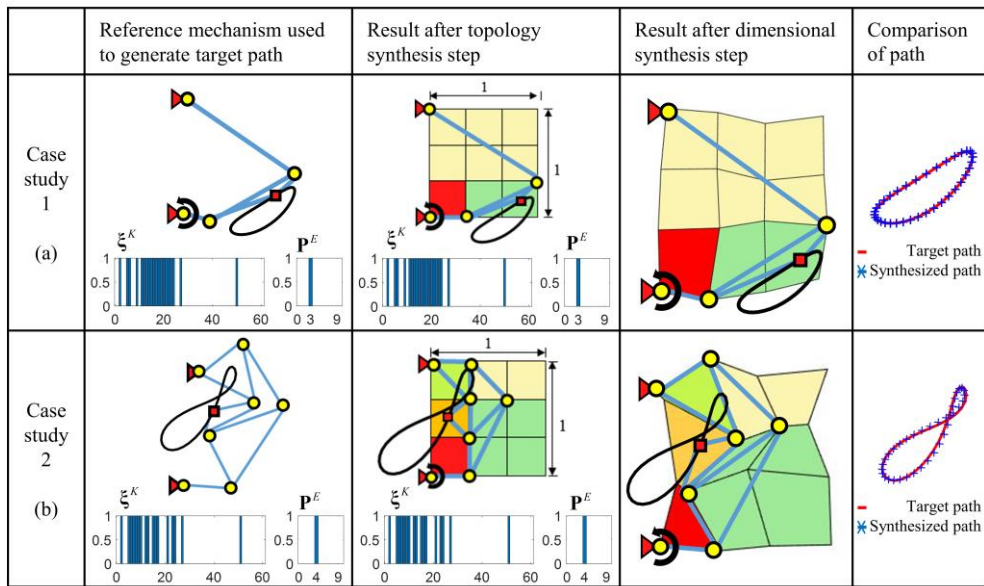


Fig. A.5 Test problems using known mechanisms to generate the target paths: (a) Case Study 1 using a 4-bar mechanism and (b) Case Study 2 utilizing a 6-bar mechanism.

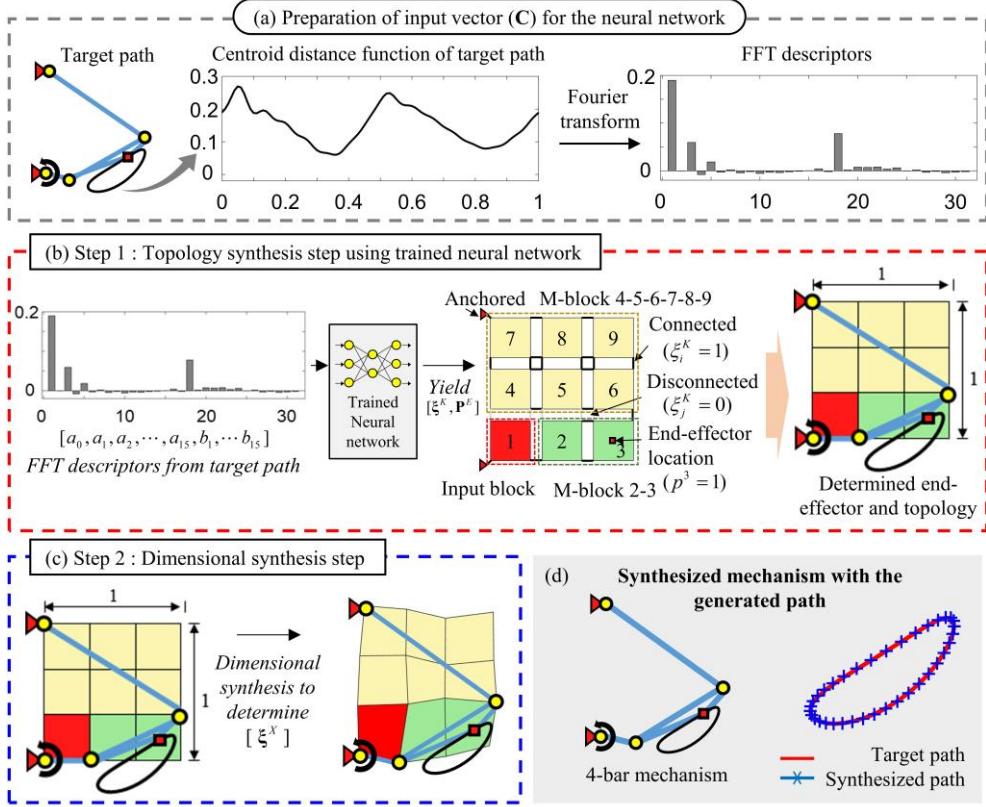


Fig. A.6 Detailed procedures of the proposed synthesis method for Case Study 1. (a) Procedure to compute the Fourier descriptor vector \mathbf{C} (with $p = 15$) of the target path, (b) topology synthesis step to determine ξ^K and \mathbf{P}^E , (c) dimensional synthesis step to determine ξ^X , and (d) the synthesized mechanism with the generated path.

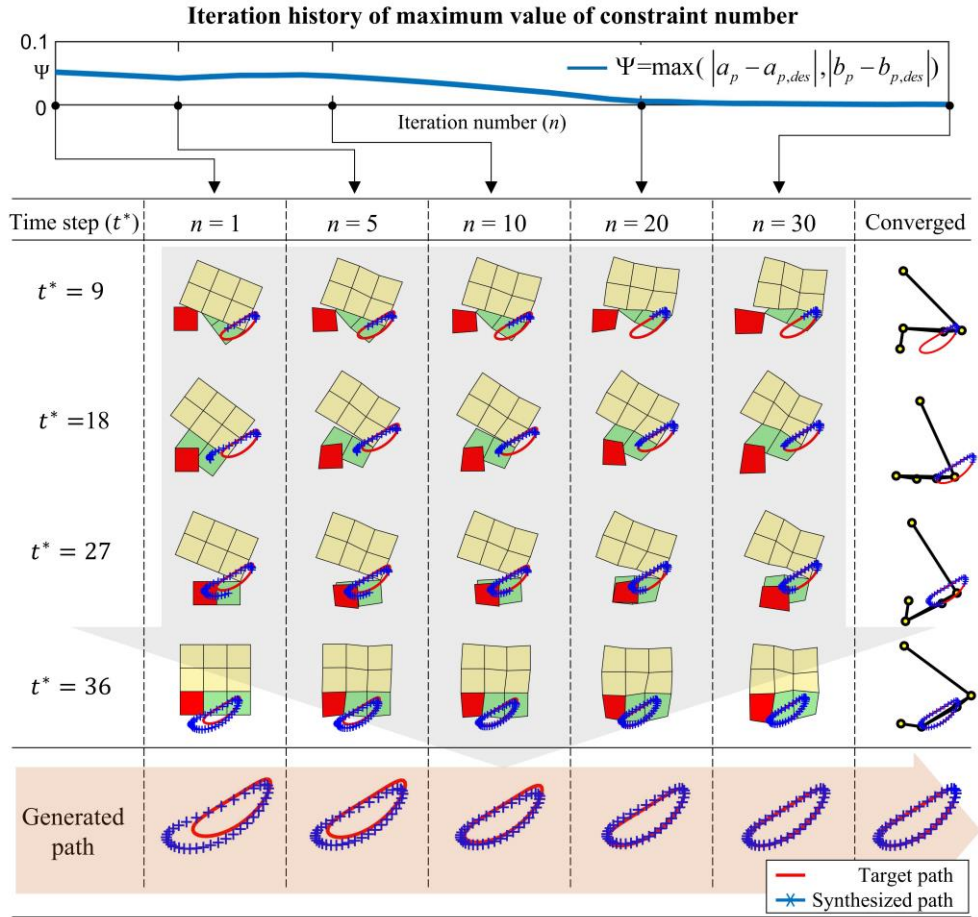


Fig. A.7 Evolution history of the dimensional synthesis step for Case Study 1.

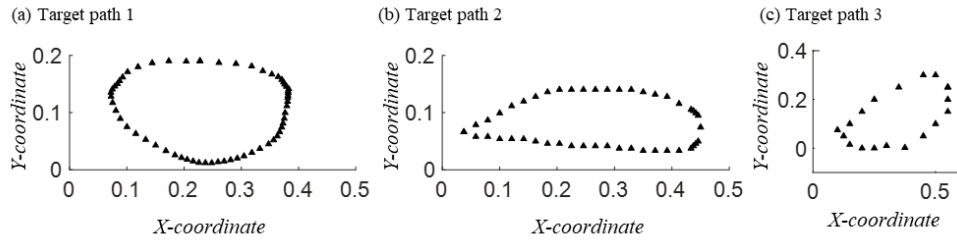


Fig. A.8 Paths considered for general mechanism synthesis: (a) Target path 1 (the path describing the trajectory of a finger in the reference frame of a swimmer over his/her full stroke cycle), (b) target path 2 (the path describing the anteroposterior and dorsoventral motion relative to a turtle's body throughout the limb cycle), and (c) target path 3 .

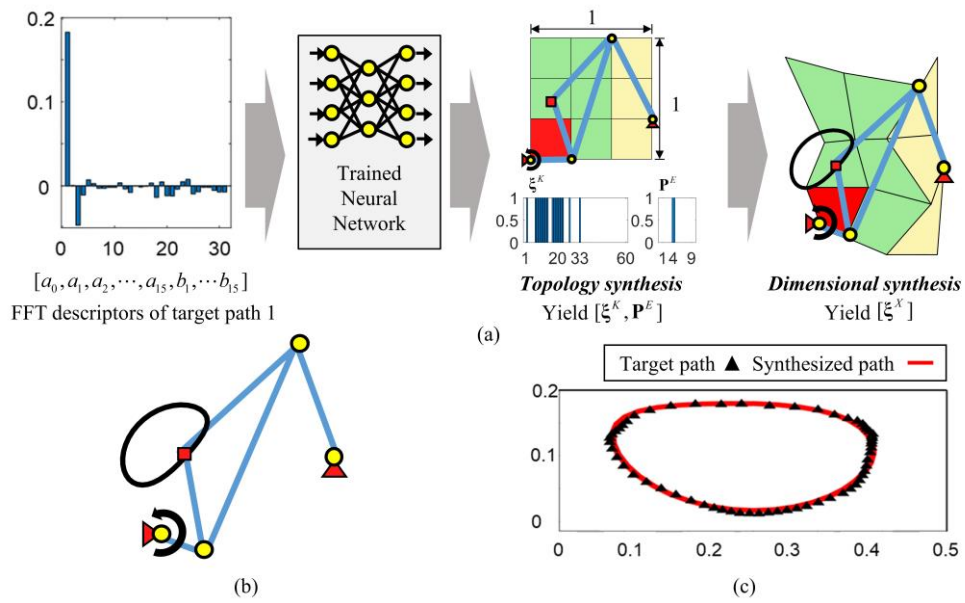


Fig. A.9 (a) Procedure to synthesize a mechanism generating Target path 1, (b) the synthesized mechanism (its end-effector location is indicated by the red square) and (c) comparison of the target path and the path generated by the synthesized mechanism.

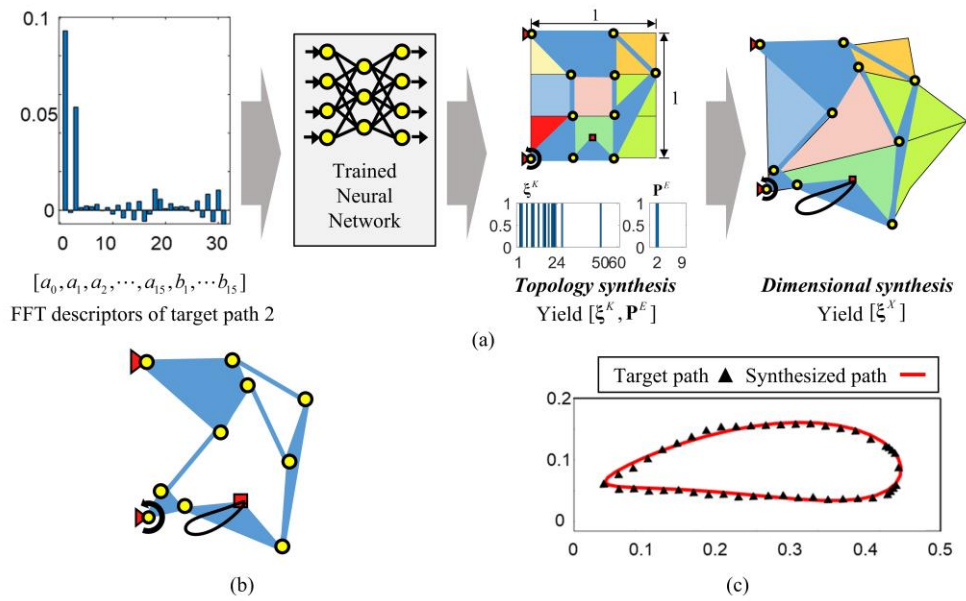


Fig. A.10 (a) Procedure to synthesize a mechanism generating Target path 2, (b) the synthesized mechanism (its end-effector location is indicated by the red square), and (c) comparison of the target path and the path generated by the synthesized mechanism.

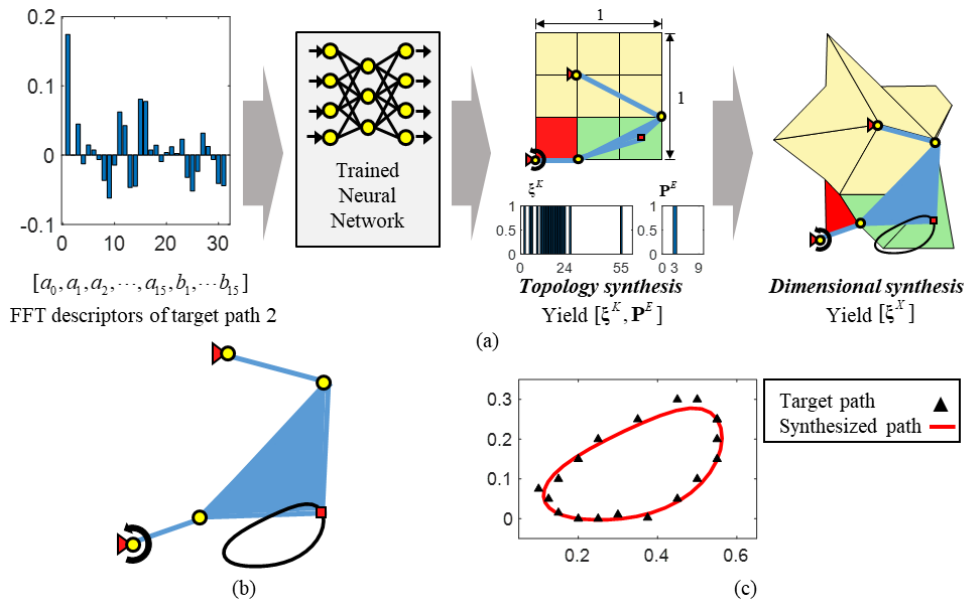


Fig. A.11 (a) Procedure to synthesize a mechanism generating Target path 3, (b) the synthesized mechanism (its end-effector location is indicated by the red square), and (c) comparison of the target path and the path generated by the synthesized mechanism

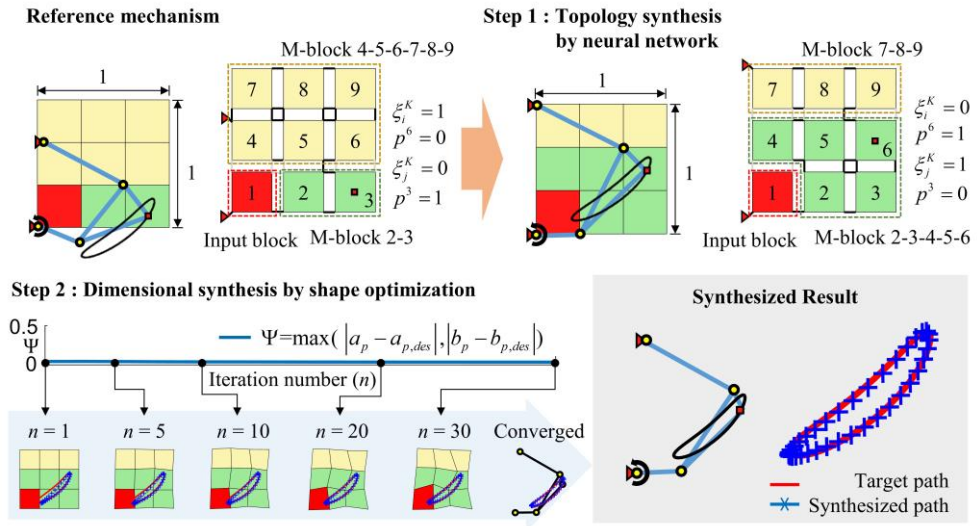


Fig. A.12 An illustrative example to show that (nearly) the same path can be obtained with different values of (ξ^K, \mathbf{P}^E) . The path generated by a reference mechanism is (nearly) recovered by a synthesized mechanism (having a different (ξ^K, \mathbf{P}^E) from that of the reference mechanism) with the developed approach.

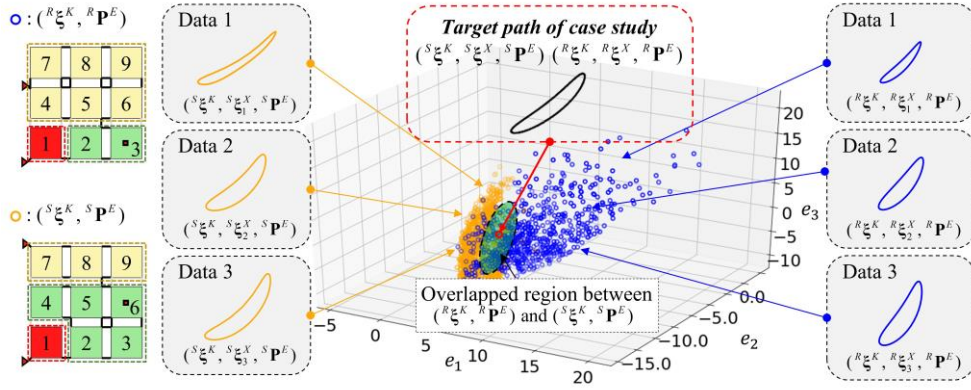


Fig. A.13 Mechanism data plotted on the three major principal axes used in Fig. 6.

Blue filled dots: mechanisms having $({}^R \xi^K, {}^R \mathbf{P}^E)$ with various values of ξ^X .

Orange open dots: mechanisms having $({}^S \xi^K, {}^S \mathbf{P}^E)$ with various values of ξ^X .

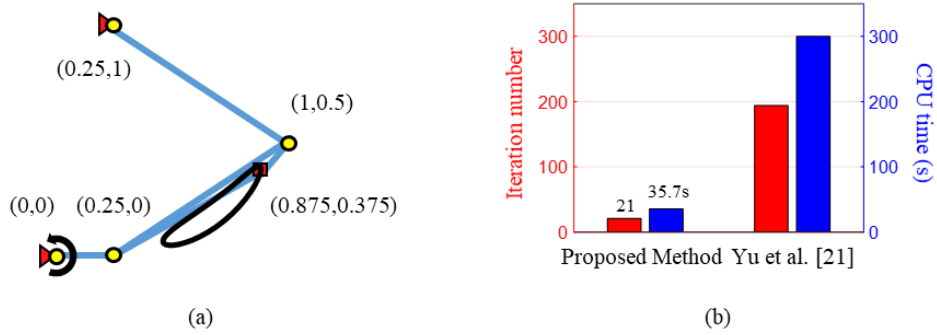


Fig. A.14 (a) The target mechanism and the generated path at its end-effector (this problem is taken from Ref.) and (b) comparison of the proposed big data approach and the gradient-based method given in Ref. in terms of computational cost.

REFERENCES

- [1] C. Felner, and O. Sigmund, "Topology optimization of rigid body mechanisms," *Technical University of Denmark, Lyngby, Denmark*, 2003.
- [2] A. Kawamoto, M. P. Bendsøe, and O. Sigmund, "Articulated mechanism design with a degree of freedom constraint," *International Journal for Numerical Methods in Engineering*, vol. 61, no. 9, pp. 1520-1545, 2004.
- [3] K. Sedlaczek, and P. Eberhard, "Topology optimization of large motion rigid body mechanisms with nonlinear kinematics," *Journal of computational and nonlinear dynamics*, vol. 4, no. 2, 2009.
- [4] M. Ohsaki, and S. Nishiwaki, "Generation of link mechanism by shape-topology optimization of trusses considering geometrical nonlinearity," *Journal of Computational Science and Technology*, vol. 3, no. 1, pp. 46-53, 2009.
- [5] G. H. Yoon, and J. C. Heo, "Constraint force design method for topology optimization of planar rigid-body mechanisms," *Computer-Aided Design*, vol. 44, no. 12, pp. 1277-1296, 2012.
- [6] J. C. Heo, and G. H. Yoon, "Size and configuration syntheses of rigid-link mechanisms with multiple rotary actuators using the constraint force design method," *Mechanism and Machine Theory*, vol. 64, pp. 18-38, 2013.
- [7] Y. Y. Kim, G.-W. Jang, J. H. Park, J. S. Hyun, and S. J. Nam, "Automatic synthesis of a planar linkage mechanism with revolute joints by using

- spring-connected rigid block models,” 2007.
- [8] S. W. Kang, S. I. Kim, and Y. Y. Kim, “Topology optimization of planar linkage systems involving general joint types,” *Mechanism and Machine Theory*, vol. 104, pp. 130-160, 2016.
 - [9] S. W. Kang, and Y. Y. Kim, “Unified topology and joint types optimization of general planar linkage mechanisms,” *Structural and Multidisciplinary Optimization*, vol. 57, no. 5, pp. 1955-1983, 2018.
 - [10] S. Jun Nam, G.-W. Jang, and Y. Young Kim, “The spring-connected rigid block model based automatic synthesis of planar linkage mechanisms: numerical issues and remedies,” 2012.
 - [11] S. I. Kim, and Y. Y. Kim, “Topology optimization of planar linkage mechanisms,” *International Journal for Numerical Methods in Engineering*, vol. 98, no. 4, pp. 265-286, 2014.
 - [12] J. Yu, S. M. Han, and Y. Y. Kim, “Simultaneous shape and topology optimization of planar linkage mechanisms based on the spring-connected rigid block model,” *Journal of Mechanical Design*, vol. 142, no. 1, 2020.
 - [13] S. M. Han, S. In Kim, and Y. Y. Kim, “Topology optimization of planar linkage mechanisms for path generation without prescribed timing,” *Structural and Multidisciplinary Optimization*, vol. 56, no. 3, pp. 501-517, 2017.
 - [14] S. M. Han, and Y. Y. Kim, “Topology optimization of linkage mechanisms simultaneously considering both kinematic and compliance characteristics,”

- Journal of Mechanical Design*, vol. 143, no. 6, pp. 061704, 2021.
- [15] N. H. Yim, J. Lee, J. Kim, and Y. Y. Kim, "Big data approach for the simultaneous determination of the topology and end-effector location of a planar linkage mechanism," *Mechanism and Machine Theory*, vol. 163, pp. 104375, 2021.
 - [16] C. Zhang, P. R. Norton, and T. Hammonds, "Optimization of parameters for specified path generation using an atlas of coupler curves of geared five-bar linkages," *Mechanism and machine theory*, vol. 19, no. 6, pp. 459-466, 1984.
 - [17] D. Dooner, "A geared 2-dof mechanical function generator," 1999.
 - [18] S. B. Nokleby, and R. P. Podhorodeski, "Optimization-based synthesis of Grashof geared five-bar mechanisms." pp. 1125-1134.
 - [19] L. Beiner, "A three-gear linkage for generating dwell motions," *J. Mech. Des.*, vol. 123, no. 4, pp. 637-640, 2001.
 - [20] G. R. Pennock, and H. Sankaranarayanan, "Path curvature of a geared seven-bar mechanism," *Mechanism and Machine Theory*, vol. 38, no. 12, pp. 1345-1361, 2003.
 - [21] J. Liu, S. Chang, and D. Mundo, "Study on the use of a non-circular gear train for the generation of Figure-8 patterns," *Proceedings of the Institution of Mechanical Engineers, Part C: Journal of Mechanical Engineering Science*, vol. 220, no. 8, pp. 1229-1236, 2006.
 - [22] D.-Z. Chen, W.-B. Shieh, and Y.-C. Yeh, "Kinematic characteristics and

classification of geared mechanisms using the concept of kinematic fractionation,” 2008.

- [23] D. Mundo, G. Gatti, and D. Dooner, “Optimized five-bar linkages with non-circular gears for exact path generation,” *Mechanism and Machine Theory*, vol. 44, no. 4, pp. 751-760, 2009.
- [24] J. Buśkiewicz, “Use of shape invariants in optimal synthesis of geared five-bar linkage,” *Mechanism and Machine Theory*, vol. 45, no. 2, pp. 273-290, 2010.
- [25] S. Coros, B. Thomaszewski, G. Noris, S. Sueda, M. Forberg, R. W. Sumner, W. Matusik, and B. Bickel, “Computational design of mechanical characters,” *ACM Transactions on Graphics (TOG)*, vol. 32, no. 4, pp. 1-12, 2013.
- [26] R. Sandhya, M. Kadam, G. Balamurugan, and H. Rangavittal, "Synthesis and analysis of geared five bar mechanism for ornithopter applications." pp. 16-19.
- [27] V. Venkata Kamesh, K. Mallikarjuna Rao, and A. Balaji Srinivasa Rao, “An innovative approach to detect isomorphism in planar and geared kinematic chains using graph theory,” *Journal of Mechanical Design*, vol. 139, no. 12, 2017.
- [28] A. Kawamoto, “Path-generation of articulated mechanisms by shape and topology variations in non-linear truss representation,” *International journal for numerical methods in engineering*, vol. 64, no. 12, pp. 1557-

1574, 2005.

- [29] A. Kawamoto, M. P. Bendsøe, and O. Sigmund, “Planar articulated mechanism design by graph theoretical enumeration,” *Structural and Multidisciplinary Optimization*, vol. 27, pp. 295-299, 2004.
- [30] S. I. Kim, S. W. Kang, Y. S. Yi, J. Park, and Y. Y. Kim, “Topology optimization of vehicle rear suspension mechanisms,” *International Journal for Numerical Methods in Engineering*, vol. 113, no. 8, pp. 1412-1433, 2018.
- [31] B. S. Kim, and H. H. Yoo, “Unified synthesis of a planar four-bar mechanism for function generation using a spring-connected arbitrarily sized block model,” *Mechanism and machine theory*, vol. 49, pp. 141-156, 2012.
- [32] B. S. Kim, and H. H. Yoo, “Unified mechanism synthesis method of a planar four-bar linkage for path generation employing a spring-connected arbitrarily sized rectangular block model,” *Multibody System Dynamics*, vol. 31, pp. 241-256, 2014.
- [33] M. P. Bendsøe, and O. Sigmund, “Material interpolation schemes in topology optimization,” *Archive of applied mechanics*, vol. 69, pp. 635-654, 1999.
- [34] K. Svanberg, “The method of moving asymptotes—a new method for structural optimization,” *International journal for numerical methods in engineering*, vol. 24, no. 2, pp. 359-373, 1987.

- [35] W. Chen, C. Xiong, and Y. Wang, "Analysis and synthesis of underactuated compliant mechanisms based on transmission properties of motion and force," *IEEE Transactions on Robotics*, vol. 36, no. 3, pp. 773-788, 2020.
- [36] S. J. Ball, I. E. Brown, and S. H. Scott, "Performance evaluation of a planar 3DOF robotic exoskeleton for motor assessment," *Journal of Medical Devices*, vol. 3, no. 2, 2009.
- [37] Y. Liu, Y. Gao, F. Xiao, and J. Zhao, "Research on the cable-pulley underactuated lower limb exoskeleton." pp. 577-583.
- [38] V. Krovi, G. Ananthasuresh, and V. Kumar, "Kinematic and kinetostatic synthesis of planar coupled serial chain mechanisms," *J. Mech. Des.*, vol. 124, no. 2, pp. 301-312, 2002.
- [39] X. Nie, and V. Krovi, "Fourier methods for kinematic synthesis of coupled serial chain mechanisms," *J. Mech. Des.*, vol. 127, no. 2, pp. 232-241, 2005.
- [40] B. Kim, and A. D. Deshpande, "Design of nonlinear rotational stiffness using a noncircular pulley-spring mechanism," *Journal of Mechanisms and Robotics*, vol. 6, no. 4, pp. 041009, 2014.
- [41] N. H. Yim, S. W. Kang, and Y. Y. Kim, "Topology optimization of planar gear-linkage mechanisms," *Journal of Mechanical Design*, vol. 141, no. 3, pp. 032301, 2019.
- [42] Y. Liu, and M. Y. Wang, "Optimal design of remote center compliance devices of rotational symmetry." pp. 161-169.

- [43] X. Zhou, H. Zhang, M. Feng, J. Zhao, and Y. Fu, “New remote centre of motion mechanism for robot-assisted minimally invasive surgery,” *Biomedical engineering online*, vol. 17, no. 1, pp. 1-16, 2018.
- [44] L.-J. Lai, and Z.-N. Zhu, “Modeling and analysis of a compliance model and rotational precision for a class of remote center compliance mechanisms,” *Applied Sciences*, vol. 6, no. 12, pp. 388, 2016.
- [45] L. Wu, G. Carbone, and M. Ceccarelli, “Designing an underactuated mechanism for a 1 active DOF finger operation,” *Mechanism and Machine Theory*, vol. 44, no. 2, pp. 336-348, 2009.
- [46] S. B. Backus, and A. M. Dollar, “An adaptive three-fingered prismatic gripper with passive rotational joints,” *IEEE Robotics and Automation Letters*, vol. 1, no. 2, pp. 668-675, 2016.
- [47] M. Ceccarelli, and M. Zottola, “Design and simulation of an underactuated finger mechanism for LARM Hand,” *Robotica*, vol. 35, no. 3, pp. 483-497, 2017.
- [48] W. Chen, C. Xiong, W. Chen, and S. Yue, “Mechanical adaptability analysis of underactuated mechanisms,” *Robotics and Computer-Integrated Manufacturing*, vol. 49, pp. 436-447, 2018.
- [49] C.-H. Liu, F.-M. Chung, Y. Chen, C.-H. Chiu, and T.-L. Chen, “Optimal design of a motor-driven three-finger soft robotic gripper,” *IEEE/ASME Transactions on Mechatronics*, vol. 25, no. 4, pp. 1830-1840, 2020.
- [50] K. C. Galloway, J. E. Clark, and D. E. Koditschek, “Variable stiffness legs

- for robust, efficient, and stable dynamic running,” *Journal of Mechanisms and Robotics*, vol. 5, no. 1, 2013.
- [51] S. Nansai, N. Rojas, M. R. Elara, and R. Sosa, "Exploration of adaptive gait patterns with a reconfigurable linkage mechanism." pp. 4661-4668.
 - [52] D. Fedorov, and L. Birglen, “Design of a self-adaptive robotic leg using a triggered compliant element,” *IEEE Robotics and Automation Letters*, vol. 2, no. 3, pp. 1444-1451, 2017.
 - [53] D. Fedorov, and L. Birglen, “Design of a compliant mechanical device for upper leg rehabilitation,” *IEEE Robotics and Automation Letters*, vol. 4, no. 2, pp. 870-877, 2019.
 - [54] A. Vaidya, and P. Padole, “A performance evaluation of four bar mechanism considering flexibility of links and joints stiffness,” *The open mechanical engineering Journal*, vol. 4, no. 1, 2010.
 - [55] H. Kobayashi, and R. Ozawa, “Adaptive neural network control of tendon-driven mechanisms with elastic tendons,” *Automatica*, vol. 39, no. 9, pp. 1509-1519, 2003.
 - [56] M. Plooij, and M. Wisse, "A novel spring mechanism to reduce energy consumption of robotic arms." pp. 2901-2908.
 - [57] J. Serón, J. L. Martínez, A. Mandow, A. J. Reina, J. Morales, and A. J. García-Cerezo, “Automation of the arm-aided climbing maneuver for tracked mobile manipulators,” *IEEE Transactions on Industrial Electronics*, vol. 61, no. 7, pp. 3638-3647, 2013.

- [58] G. Du, P. Zhang, and D. Li, "Human-manipulator interface based on multisensory process via Kalman filters," *IEEE Transactions on Industrial Electronics*, vol. 61, no. 10, pp. 5411-5418, 2014.
- [59] D. Eizicovits, and S. Berman, "Efficient sensory-grounded grasp pose quality mapping for gripper design and online grasp planning," *Robotics and Autonomous Systems*, vol. 62, no. 8, pp. 1208-1219, 2014.
- [60] M. Keshmiri, W.-F. Xie, and A. Mohebbi, "Augmented image-based visual servoing of a manipulator using acceleration command," *IEEE Transactions on Industrial Electronics*, vol. 61, no. 10, pp. 5444-5452, 2014.
- [61] P. Larochelle, "Synthesis of planar mechanisms for pick and place tasks with guiding positions," *Journal of Mechanisms and Robotics*, vol. 7, no. 3, pp. 031009, 2015.
- [62] M. M. Plecnik, D. W. Haldane, J. K. Yim, and R. S. Fearing, "Design exploration and kinematic tuning of a power modulating jumping monopod," *Journal of Mechanisms and Robotics*, vol. 9, no. 1, pp. 011009, 2017.
- [63] J.-W. Kim, T. Seo, and J. Kim, "A new design methodology for four-bar linkage mechanisms based on derivations of coupler curve," *Mechanism and Machine Theory*, vol. 100, pp. 138-154, 2016.
- [64] S. I. Kim, D. Shin, S. M. Han, S. W. Kang, S. Kwon, Y.-S. Yi, and Y. Y. Kim, "A novel space-constrained vehicle suspension mechanism

- synthesized by a systematic design process employing topology optimization,” *Structural and Multidisciplinary Optimization*, vol. 62, no. 3, pp. 1497-1517, 2020.
- [65] D. Dong, W. Ge, S. Liu, F. Xia, and Y. Sun, “Design and optimization of a powered ankle-foot prosthesis using a geared five-bar spring mechanism,” *International Journal of Advanced Robotic Systems*, vol. 14, no. 3, pp. 1729881417704545, 2017.
- [66] R. Altenburger, D. Scherly, and K. S. Stadler, “Design of a passive, iso-elastic upper limb exoskeleton for gravity compensation,” *Robomech Journal*, vol. 3, no. 1, pp. 1-7, 2016.
- [67] D. Aukes, B. Heyneman, V. Duchaine, and M. R. Cutkosky, "Varying spring preloads to select grasp strategies in an adaptive hand." pp. 1373-1379.
- [68] G. Carbone, and M. Ceccarelli, "Design of LARM hand: problems and solutions." pp. 298-303.
- [69] S. Chen, S. A. Billings, and P. Grant, “Non-linear system identification using neural networks,” *International journal of control*, vol. 51, no. 6, pp. 1191-1214, 1990.
- [70] A. Vasiliu, and B. Yannou, “Dimensional synthesis of planar mechanisms using neural networks: application to path generator linkages,” *Mechanism and Machine Theory*, vol. 36, no. 2, pp. 299-310, 2001.
- [71] N. Khan, I. Ullah, and M. Al-Grafi, “Dimensional synthesis of mechanical

- linkages using artificial neural networks and Fourier descriptors,” *Mechanical Sciences*, vol. 6, no. 1, pp. 29-34, 2015.
- [72] G. Galán-Marín, F. J. Alonso, and J. M. Del Castillo, “Shape optimization for path synthesis of crank-rocker mechanisms using a wavelet-based neural network,” *Mechanism and Machine Theory*, vol. 44, no. 6, pp. 1132-1143, 2009.
- [73] S. Acharyya, and M. Mandal, “Performance of EAs for four-bar linkage synthesis,” *Mechanism and Machine Theory*, vol. 44, no. 9, pp. 1784-1794, 2009.
- [74] E. Mezura-Montes, E. A. Portilla-Flores, and B. Hernández-Ocaña, “Optimum synthesis of a four-bar mechanism using the modified bacterial foraging algorithm,” *International Journal of Systems Science*, vol. 45, no. 5, pp. 1080-1100, 2014.
- [75] G. Asaeikheybari, A. S. Lafmejani, A. Kalhor, and M. T. Masouleh, "Dimensional synthesis of a four-bar linkage mechanism via a pso-based cooperative neural network approach." pp. 906-911.
- [76] S. H. Kafash, and A. Nahvi, “Optimal synthesis of four-bar path generator linkages using Circular Proximity Function,” *Mechanism and Machine Theory*, vol. 115, pp. 18-34, 2017.
- [77] S. Deshpande, and A. Purwar, “Computational creativity via assisted variational synthesis of mechanisms using deep generative models,” *Journal of Mechanical Design*, vol. 141, no. 12, 2019.

- [78] S. Deshpande, and A. Purwar, "An image-based approach to variational path synthesis of linkages," *Journal of Computing and Information Science in Engineering*, vol. 21, no. 2, 2021.
- [79] K.-L. Ting, and Y.-W. Liu, "Rotatability laws for N-bar kinematic chains and their proof," 1991.
- [80] J.-H. Shyu, and K.-L. Ting, "Invariant link rotatability of N-bar kinematic chains," 1994.
- [81] I. Ullah, and S. Kota, "Optimal synthesis of mechanisms for path generation using Fourier descriptors and global search methods," 1997.
- [82] J. Buśkiewicz, R. Starosta, and T. Walczak, "On the application of the curve curvature in path synthesis," *Mechanism and Machine Theory*, vol. 44, no. 6, pp. 1223-1239, 2009.
- [83] J. Wu, Q. Ge, F. Gao, and W. Guo, "On the extension of a Fourier descriptor based method for planar four-bar linkage synthesis for generation of open and closed paths," 2011.
- [84] X. Li, S. Wei, Q. Liao, and Y. Zhang, "A novel analytical method for four-bar path generation synthesis based on Fourier series," *Mechanism and Machine Theory*, vol. 144, pp. 103671, 2020.
- [85] V. Nair, and G. E. Hinton, "Rectified linear units improve restricted boltzmann machines." pp. 807-814.
- [86] R. C. Cohen, P. W. Cleary, B. R. Mason, and D. L. Pease, "The role of the hand during freestyle swimming," *Journal of biomechanical engineering*,

vol. 137, no. 11, 2015.

- [87] A. R. Rivera, G. Rivera, and R. W. Blob, "Forelimb kinematics during swimming in the pig-nosed turtle, *Carettochelys insculpta*, compared with other turtle taxa: rowing versus flapping, convergence versus intermediacy," *Journal of Experimental Biology*, vol. 216, no. 4, pp. 668-680, 2013.
- [88] J. Cabrera, A. Simon, and M. Prado, "Optimal synthesis of mechanisms with genetic algorithms," *Mechanism and machine theory*, vol. 37, no. 10, pp. 1165-1177, 2002.
- [89] F. Peñuñuri, R. Peón-Escalante, C. Villanueva, and D. Pech-Oy, "Synthesis of mechanisms for single and hybrid tasks using differential evolution," *Mechanism and Machine theory*, vol. 46, no. 10, pp. 1335-1349, 2011.

ABSTRACT (KOREAN)

이종 기계 요소를 고려한 기구 위상 최적설계 방법론 개발

임 능 환

서울대학교 대학원

기계항공공학부

기구 위상 최적 설계는 초기 설계안이 없어도 다양한 위상과 치수의 기구를 합성할 수 있는 장점을 가지고 있습니다. 이러한 이유로 기구 위상 최적 설계 방법은 일반적인 기계장치를 설계함에 있어 창의적인 결과를 얻을 수 있었습니다. 일반적인 기계장치의 경우 주로 강체 링크와 조인트로 구성되어 있지만, 현재 로봇 메커니즘의 경우 민첩성 및 적응성과 같은 로봇 성능을 구현하거나 개선하기 위하여 다양한 이종 기구 요소와 탄성체 요소가 적극적으로 사용되고 있습니다. 그러나 기존 기구 위상 최적 설계 기법의 경우 강체 링크와 조인트로 구성된 기구만 합성 가능하기에, 다양한 이종 요소와 탄성체 요소에 대한 고려가 필요한 로봇 메커니즘에 적용하는 데는 한계점이 존재했습니다. 이에 이번 학위

논문에서는 위상 최적 설계 기반의 다중 강체-탄성체 기구 요소 통합 설계 기술을 제안하려 합니다.

다중 강체-탄성체 기구 요소 통합 설계를 제안하기 위해서는 다음 두 가지 문제를 해결해야 합니다. 첫 번째는 다양한 기구 요소의 위상과 치수를 표현할 수 있는 모델링이 필요하며, 두 번째는 이를 합성하기 위한 최적화 알고리즘을 정식화해야 합니다. 이 때, 통합 설계 기술의 대상은 하나의 구동기로 구성된 1자유도 메커니즘의 경로 생성 문제로 제한합니다. 1자유도 메커니즘의 경우 적은 구동기를 사용하기 때문에 저렴하며, 적은 무게를 갖기 때문에 로봇 메커니즘 적용에 적합합니다.

기구 위상설계 방법을 적용하기 위해서는 다양한 기구요소의 위상과 치수를 하나의 모델링으로 표현할 수 있는 모델링이 필요합니다. 이전 강체 링크지 기구의 기구 위상설계 방법론의 경우 설계 공간을 강체 블록과 강체 블록 간을 연결하는 스프링으로 이산화하여 표현하였습니다. 이때 각각의 강체 블록은 강체 링크를 의미하며, 연결되어 있는 스프링의 강성 조합으로 링크지 기구의 위상과 치수를 표현하였습니다. 본 학위 논문에서는 이산화된 강체 스프링 블록 모델을 기반으로 다양한 기구 요소의 위상과 치수를 표현하고자 하며, 적은 설계 변수로 다양한 기구의 위상과 치수를 표현하기 위하여 강체 블록의 모양과 강체 블록의 질량 중심까지 고려할 수 있는 형상 강체 스프링 블록 모델을 새롭게 제안

합니다.

다양한 기구의 구성 요소를 다루기 위해서는 새로운 통합 기구 요소 모델링이 필요합니다. 이번 학위논문에서 제안하는 다중 기구요소 통합 모델링의 가장 핵심 아이디어는 각각의 기구 설계 공간을 적층하는 방법입니다. 이를 위해, 기어요소와 풀리요소에 해당되는 기어블록과 풀리블록을 새롭게 정의하고, 강체블록의 질량중심을 서로 연결한 스프링 요소를 정의하였습니다. 각각의 블록들을 가지고 기구 요소에 해당되는 기구 설계 공간을 정의하며, 이를 링크지 설계 공간과 적층하여 사용합니다. 이때, 기어블록과 풀리블록은 링크지 설계 공간의 강체블록들과 스프링으로 연결되어 사용됩니다. 이러한 다중 기구 적층 모델을 사용하면, 다양한 기구의 위상과 치수를 연속 설계 변수를 통해 표현할 수 있습니다.

다양한 기구요소를 다루기 위해서는 새로운 통합 기구 요소 모델링이 필요합니다. 이 학위 논문에서 제안하는 다중 기구요소 통합 모델링의 가장 핵심 아이디어는 각각의 기구 설계 공간을 적층하는 방법입니다. 제안하는 다중 기구 요소 모델링의 경우 앞서 제시한 스프링 강체블록 모델에 기반하기 때문에 각각의 기구요소를 강체블록으로 적절하게 표현하는 것이 필요합니다. 이를 위해, 강체 이중 기구요소인 기어요소와 풀리요소에 해당되는 블록인 기어블록과 풀리블록을 새롭게 정의하고, 강체블록의 질량 중심을 서로 연결한 스프링 요소를 정의하였습니다. 기어

블록은 입력 운동에 따라 특정 기어비를 가지고 회전하며, 폴리블록은 다른 강체블록들과 특정 각도 관계를 가지고 회전하는 블록을 의미합니다. 마찬가지로 스프링 요소의 경우도 늘어나거나 줄어드는 거리에 비례하는 탄성력을 갖는 기구요소를 의미합니다. 이렇게 정의된 각각의 블록들을 가지고 기구요소에 해당되는 기구 설계 공간을 정의하며, 각각의 기구 설계 공간은 링크지 설계 공간과 적층하여 사용됩니다. 이때, 기어블록과 폴리블록은 링크지 설계 공간의 강체블록들과 4개의 꼭지점이 길이가 0인 스프링으로 연결되어 사용됩니다. 연결된 스프링이 최대 강성을 가지게 된다면, 해당 강체블록은 링크가 아닌 기어 요소 역할을 하게 되며, 연결된 스프링이 최소 강성 값을 갖게 되면 해당 강체블록은 그대로 링크의 역할을 유지하게 됩니다. 폴리 요소도 이와 마찬가지로입니다. 스프링 요소의 경우, 스프링 자체의 강성 값이 직접적인 기구의 구성을 의미하도록 모델링하였습니다. 이러한 다중 기구 적층 모델을 사용한다면, 블록의 모양과 다양한 종류의 스프링의 강성값을 나타내는 연속 설계 변수를 통하여 다양한 기구의 위상과 치수를 표현할 수 있습니다.

제안하는 통합설계 기술은, 앞서 제안한 통합 기구 요소 모델링에 적합한 최적화 정식화가 새롭게 필요하기에, 최적화 알고리즘을 기반으로 합니다. 기구의 운동은 비선형성을 가지고 있기 때문에, 기구를 합성하는 데에는 민감도 기반의 최적화 알고리즘이 전역 최적화보다 효율적입니다.

이를 위해 연속 설계 변수로 표현된 블록의 모양과 스프링의 강성 값과 관련된 목적함수와 제한함수를 새롭게 정의하였습니다. 목적함수로는 기존의 링크지 기구 위상설계 방법에서 사용한 일전달 효율 함수를 사용하였으며, 제한함수로는 엔드이펙터에서의 생성경로와 목적경로와의 유클리디안 차이를 사용하였습니다. 또한, 주변 환경 변화에 대한 고려가 필요한 강체-탄성체 기구 합성 문제의 경우, 목적함수로 일전달효율함수에서 변형된 에너지기반의 함수를 새롭게 정의하여 사용하였습니다.

이 방법론은 다양한 위상과 치수의 기어-링크지 기구, 폴리-링크지 기구, 스프링-링크지 기구가 효율적으로 합성됨을 다양한 기구 예제를 통해 확인하였습니다. 더 나아가, 주변 환경 변화의 크기가 0인 경우를 기존 완전 구동 기구 합성 문제와 같기 때문에, 본 학위 논문에서 나누어 설명한 강체-탄성체 기구 요소 통합설계기술과 다중 강체 기구 요소 통합기술을 동시에 통합하여 확장할 수 있습니다. 더불어, 본 방법론은 기어, 폴리, 스프링 등 이중 기구 요소까지 확장하여 적용할 수 있습니다.

주요어: 기구 설계, 기구 위상최적 설계, 이중 기구요소의 기구 설계, 스프링-링크지 메커니즘.

학 번 : 2017-26804

ACKNOWLEDGEMENTS

This research was supported by the National Research Foundation of Korea (NRF) Grant No. 2016R1A2B3010231 funded by the Ministry of Science and ICT (MSIT), Korea, contracted through Institute of Advanced Machines and Design (IAMD) at Seoul National University in Korea. Also, this research was supported by the by Samsung Research Funding Center of Samsung Electronics under project No. SRFC-IT1901-02.